Supporting Information

Tuning Ligand Effects and Probing the Inner-Workings of Bond Activation Steps: Generation of Ruthenium Complexes with Tailor-made Properties

Fritz Weisser,[†] Sebastian Plebst,[‡] Stephan Hohloch, [†] Margarethe van der Meer, [†] Sinja Manck, [†] Felix Führer, [†] Vanessa Radtke, [†] Daniel Leichnitz, [†] and Biprajit Sarkar*,[†]

[†] Institut für Chemie und Biochemie, Anorganische Chemie, Freie Universität Berlin, Fabeckstraße 34-36, D-14195, Berlin, Germany

[‡] Institut für Anorganische Chemie, Universität Stuttgart, Pfaffenwaldring 55, D-70569, Stuttgart, Germany

Content

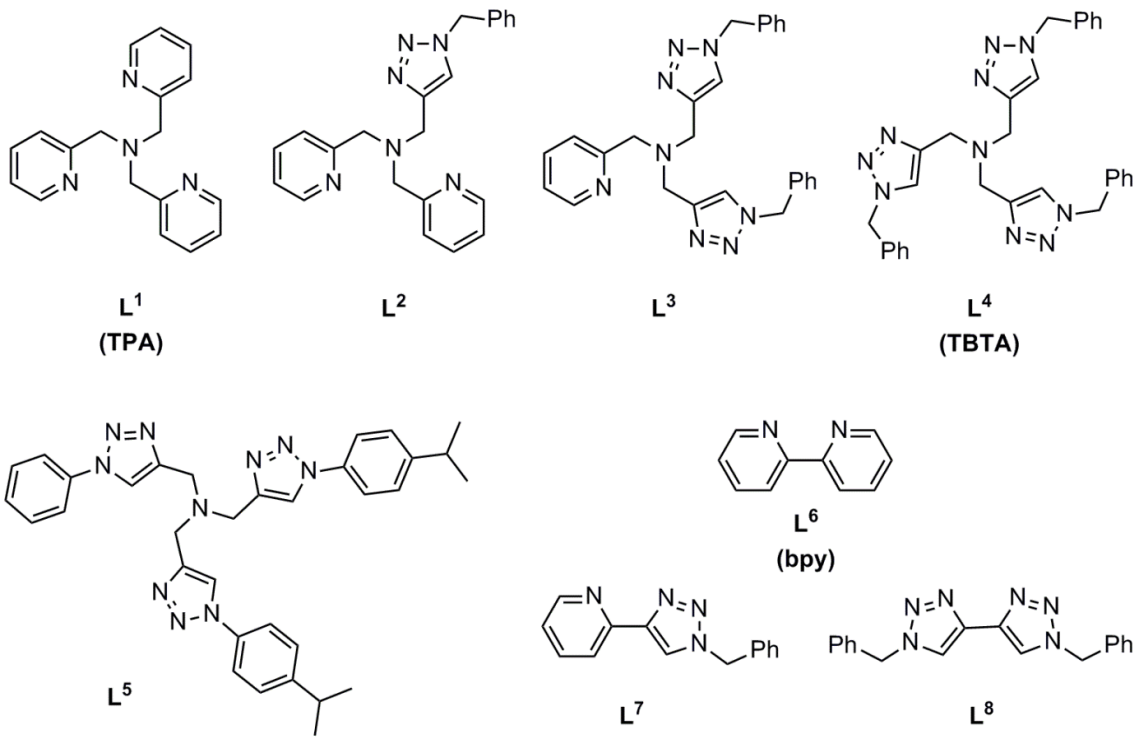

Scheme S1. Ligands used in this work.

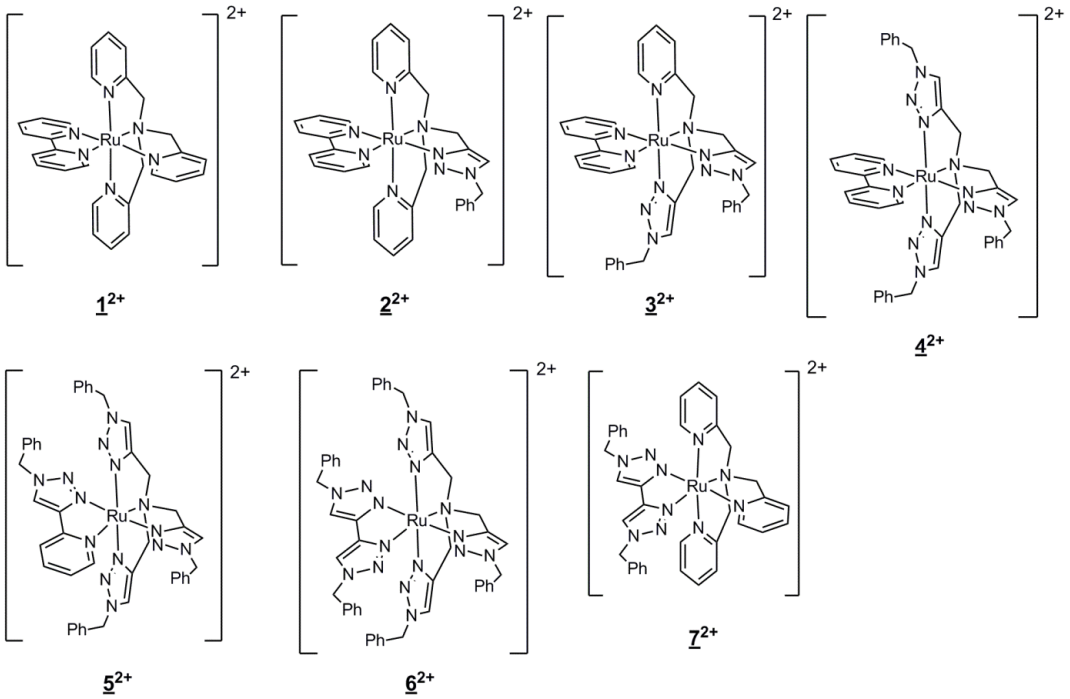

Scheme S2. Complexes $\mathbf{1}^{2+}$–$\mathbf{7}^{2+}$ (each complexes has two PF_6^- counterions).

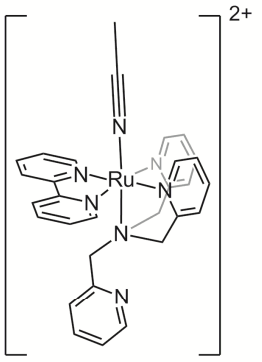

[1(CH$_3$CN)]$^{2+}$

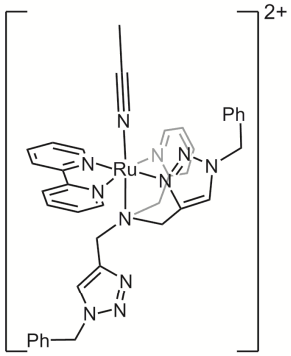

[3(CH$_3$CN)]$^{2+}$

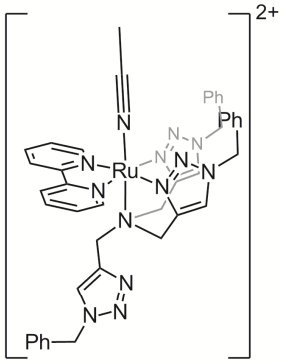

[4(CH$_3$CN)]$^{2+}$

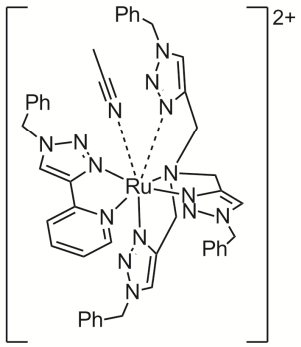

or

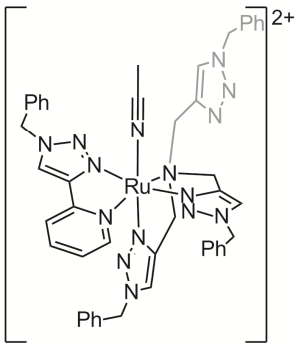

or

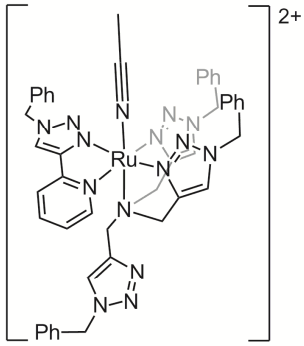

[5(CH$_3$CN)]$^{2+}$

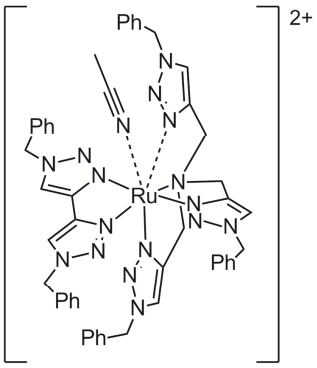

or

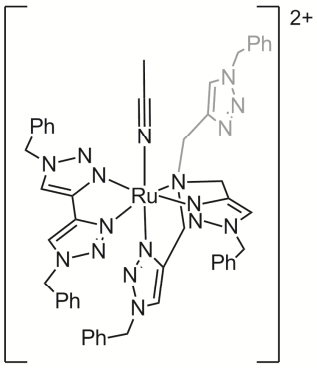

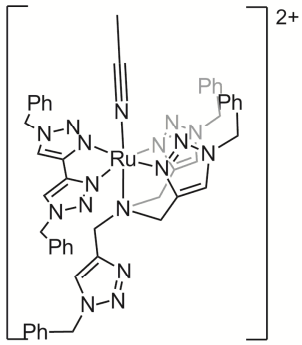

[6a(CH$_3$CN)]$^{2+}$ **[6b(CH$_3$CN)]$^{2+}$**

Scheme S3. Acetonitrile adducts of complexes **1**$^{2+}$ and **3**$^{2+}$–**6**$^{2+}$.

Syntheses

Schemes S1–S3 show the ligands used in this work, the synthesized complexes, and the corresponding acetonitrile adducts. Schemes S4 and S5 show the synthesis of L^5 and the general synthesis of the complexes $\mathbf{1}^{2+}$–$\mathbf{8}^{2+}$, respectively.

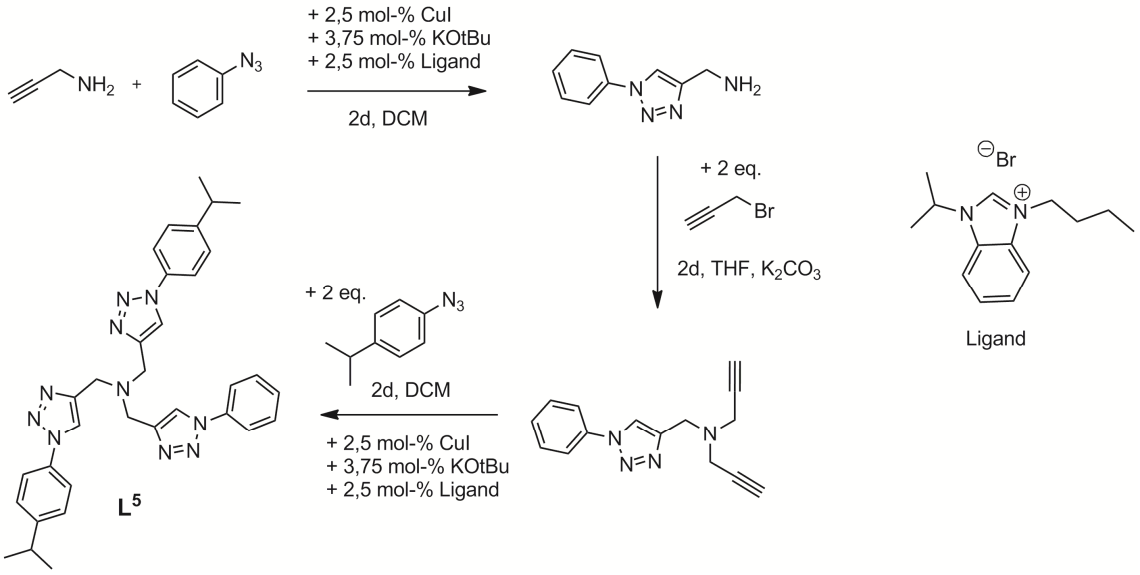

Scheme S4. Synthesis of ligand L^5.

***N,N*-bis[(4-isopropylphen-1-yl-1*H*-1,2,3-triazol-4-yl)methyl]-*N*-[(phen-1-yl-1*H*-1,2,3-triazol-4-yl)methyl]amine (L^5):** Propargyl amine (280 mg, 5 mmol) and phenylazide[1] (740 mg, 6 mmol) were mixed in a Schlenk flask in DCM (20 mL). 1-Butyl-3-isopropyl-1H-benzo[d]imidazol-3-iumbromid[2] (37 mg, 2.5 mol-%), CuI (24 mg, 2.5 mol-%), and KO^{t}Bu (24 mg, 3.75 mol-%) were added, and the mixture was stirred for 2 d at room temperature. A $H_2EDTANa_2$ (ca. 0.5 g) solution in aqueous ammonia (ca. 5%, 15 mL) was added to stop the reaction. The aqueous phase was extracted with DCM (3× 15 mL), and the combined organic phases were washed with distilled water and dried over Na_2SO_4. The solvent was removed under reduced pressure, and the resulting residue was purified by column chromatography on basic aluminum oxide by slowly changing the eluent from DCM (phenylazide) to ethyl acetate and finally methanol (product). The product (1-phenyl-1*H*-1,2,3-triazol-4-yl)methanamine was obtained as a light yellow solid (748 mg, 86% yield). ^{1}H NMR (400 MHz, acetone-d_6): δ = 8.38 (s, 1H, Ph–*triazole*), 7.90–7.85 (m, 2H, *Ph*–triazole), 7.58–7.52 (m, 2H, *Ph*–triazole), 7.46–7.41 (m, 1H, *Ph*–triazole), 4.53 (s, 2H, triazole–CH_2–N_{amine}).

(1-Phenyl-1*H*-1,2,3-triazol-4-yl)methanamine (510 mg, 2.9 mmol), propargylbromide (9.0 mmol, 80 wt-% in toluene, 1.0 mL), and K_2CO_3 (25 mmol, 3.46 g) were mixed in dry THF (20 mL) in a Schlenk flask and stirred at room temperature for 1 d. After addition of another portion of propargylbromide (0.3 mL), the mixture was stirred for another day. The mixture was then filtered under an inert gas atmosphere, washed with dry DCM, and the filtrate was concentrated by removing the volatiles in a vacuum to obtain crude *N*-[(1-phenyl-1*H*-1,2,3-triazol-4-yl)methyl]-*N*,*N*-bis(prop-2-yn-1-yl)amine. The resulting brown oil was used for the subsequent Click reaction without further purification. ^{1}H NMR (400 MHz, chloroform-d): δ = 7.98 (s, 1H, Ph–*triazole*), 7.75–7.71 (m, 2H, *Ph*–triazole), 7.55–7.49 (m, 2H, *Ph*–triazole), 7.45–7.40 (m, 1H, *Ph*–triazole), 3.95 (s, 2H, triazole–CH_2–N_{amine}), 3.52 (d, J = 2.4 Hz, 4H, alkyne–CH_2–N_{amine}), 2.28 (t, J = 2.4 Hz, 2H, *H*–alkyne–CH_2) ppm.

The crude *N*-[(1-phenyl-1*H*-1,2,3-triazol-4-yl)methyl]-*N*,*N*-bis(prop-2-yn-1-yl)amine was dissolved in DCM (15 mL), and 4-isopropylphenylazide (987 mg, 6.1 mmol), 1-butyl-3-isopropyl-1H-benzo[d]imidazol-3-iumbromid (37 mg, 2.5 mol-%), CuI (24 mg, 2.5 mol-%), and KO^{t}Bu (24 mg, 3.75 mol-%) were added. The mixture was stirred for 2 d at room temperature. The subsequent work-up was identical to that applied in the first Click step. The crude product was purified by column chromatography on basic aluminium oxide by starting with pure DCM as the eluent to wash out the

remaining azide. The desired product L^5 was obtained with a DCM/ethyl acetate mixture (1:1) as the eluent [1.21 g, 73% yield with respect to (1-phenyl-1*H*-1,2,3-triazol-4-yl)methanamine]. ^{1}H NMR (400 MHz, chloroform-d): δ = 8.26 (s, 1H, Ph–*triazole*), 8.21 (s, 2H, iPr–Ph–*triazole*), 7.79–7.74 (m, 2H, *Ph*–triazole), 7.69–7.64 (m, 4H, iPr–*Ph*–triazole), 7.54–7.50 (m, 2H, *Ph*–triazole), 7.45–7.39 (m, 1H, *Ph*–triazole), 7.38–7.33 (m, 4H, iPr–*Ph*–triazole), 3.95 (s, 6H, triazole–CH_2–N_{amine}), 2.97 (hept, *J* = 6.9 Hz, 2H, *iPr*–Ph), 1.28 (d, *J* = 6.9 Hz, 12H, *iPr*–Ph) ppm.

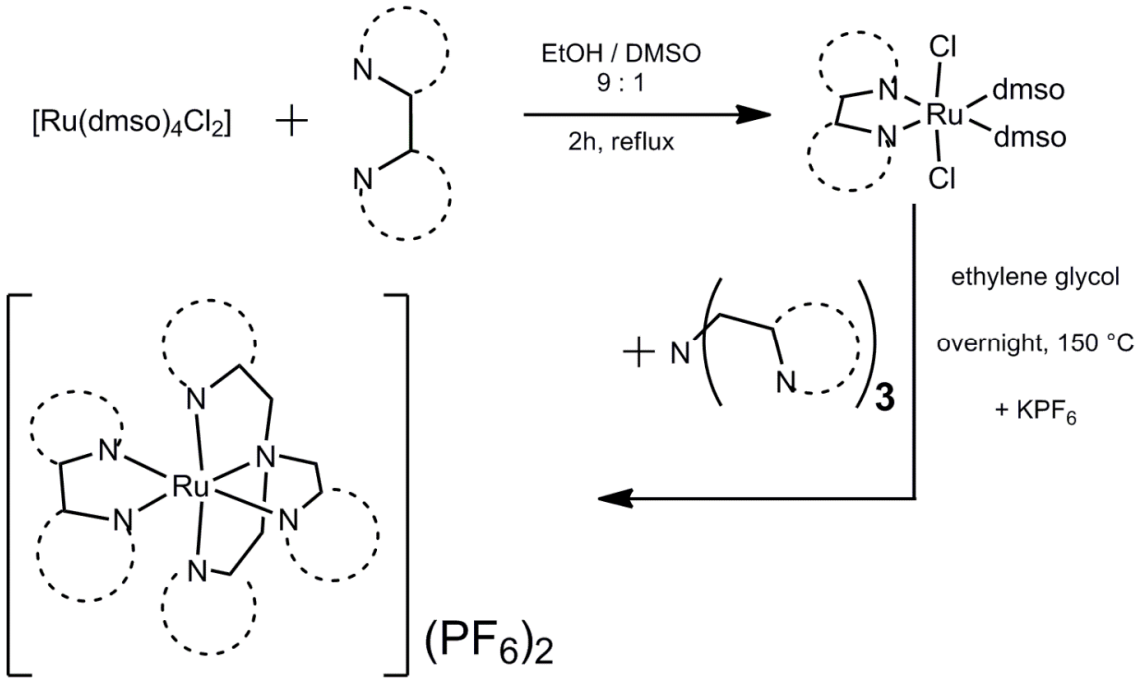

Scheme S5. General synthetic route for complexes $\mathbf{1}^{2+}$–$\mathbf{8}^{2+}$.

[Ru(L^1)(bpy)](PF_6)$_2$ {1(PF_6)$_2$}: [Ru(bpy)(dmso)$_2$Cl$_2$] (81 mg, 0.17 mmol), TPA (L^1) (50 mg, 0.17 mmol), and KPF_6 (80 mg, 0.43 mmol) were heated overnight at 150 °C in ethylene glycol (10 mL), which was purged with nitrogen prior to the reaction. After the mixture had cooled down to room temperature, water (20 mL) and excess KPF_6 (312 mg, 1.7 mmol) were added to induce precipitation of the product. The orange precipitate was filtered off and redissolved in acetone/DCM (1:1, 15 mL). The organic phase was washed three times with water (5 mL) and dried over Na_2SO_4. The solvents were removed under reduced pressure, and the resulting crude solid was purified by cholumn chromatography on aluminum oxide. After starting with pure DCM, the eluent was slowly changed to DCM/methanol (98:2) to extract the product. Evaporation of the solvent under reduced pressure yielded the pure product (116 mg, 82% yield). ^{1}H NMR (400 MHz, acetone-d_6): δ = 9.90 (d, *J* = 5.7 Hz, 1H, *bpy*), 9.49 (d, *J* = 5.8 Hz, 1H, py_{eq}), 9.37 (d, *J* = 5.8 Hz, 1H, *bpy*), 8.78 (d, *J* = 8.4 Hz, 1H, *bpy*), 8.66 (d, *J* = 8.4 Hz, 1H, *bpy*), 8.34 (t, *J* = 7.8 Hz, 1H, py_{eq}), 8.08 (t, *J* = 7.4 Hz, 1H, *bpy*), 8.03 (t, *J* = 8.1 Hz, 1H, *bpy*), 7.96 (d, *J* = 5.6 Hz, 2H, py_{ax}), 7.78 (t, *J* = 7.7 Hz, 1H, *bpy*), 7.72 (t, *J* = 7.8 Hz, 2H, py_{ax}), 7.57 (t, *J* = 7.4 Hz, 1H, *bpy*), 7.55–7.50 (m, 3H, py_{eq} + py_{ax}), 7.40 (t, *J* = 7.4 Hz, 1H, py_{eq}), 7.12 (t, *J* = 6.74 Hz, 2H, py_{ax}), 5.87 (d, *J* = 17.1 Hz, 2H, CH_2(ax)), 5.42 (d, *J* = 17.2 Hz, 2H, CH_2(ax)), 5.01 (s, 2H, CH_2(eq)) ppm. ^{1}H NMR (400 MHz, acetonitrile-d_3) δ = 9.53 (d, *J* = 5.9 Hz, 1H, *bpy*), 9.01 (d, *J* = 5.9 Hz, 1H, py_{eq}), 8.98 (d, *J* = 5.6 Hz, 1H, *bpy*), 8.46 (d, *J* = 8.1 Hz, 1H, *bpy*), 8.35 (d, *J* = 8.4 Hz, 1H, *bpy*), 8.19 (t, *J* = 8.0 Hz, 1H, *bpy*), 7.94–7.86 (m, 2H, *bpy* + py_{eq}), 7.67–7.61 (m, 3H, py_{ax} + py_{eq}), 7.58 (t, *J* = 7.8 Hz, 2H, py_{ax}), 7.44 (t, *J* = 5.7 Hz, 1H, *bpy*), 7.32–7.27 (m, 3H, py_{ax} + *bpy*), 7.25 (t, *J* = 7.4 Hz, 1H, py_{eq}), 6.96 (t, *J* = 5.9 Hz, 2H, py_{ax}), 5.40 (d, *J* = 17.2 Hz, 2H, CH_2(ax)), 5.04 (d, *J* = 17.1 Hz, 1H, CH_2(ax)), 4.63 (s, 2H, CH_2(eq)) ppm. $C_{28}H_{26}N_6P_2F_{12}Ru$: calcd. C 40.15, H 3.13, N 10.03; found C 40.28, H 4.09, N 10.07. UV/Vis (DCM): λ [nm] (ε [M^{-1} cm^{-1}]) = 249 (28210), 295 (31010), 370 (13880), 425 (11930), 452 (10090) sh.

[Ru(L^2)(bpy)](PF_6)$_2$ {2(PF_6)$_2$}: The complex was prepared analogously to **1**(PF_6)$_2$. [Ru(bpy)(dmso)$_2$Cl$_2$] (97 mg, 0.20 mmol), L^2 (74 mg, 0.20 mmol), and KPF_6 (92 mg, 0.50 mmol)

yielded pure **2**$(PF_6)_2$ after column chromatography (143 mg, 78% yield). ^{1}H NMR (400 MHz, acetonitrile-d_3): δ = 10.65 (d, *J* = 5.8 Hz, 1H, *bpy*), 9.09 (d, *J* = 5.7 Hz, 1H, *bpy*), 8.44 (d, *J* = 8.4 Hz, 1H, *bpy*), 8.34 (d, *J* = 7.9 Hz, 1H, *bpy*), 8.13 (dd, *J* = 8.1, 7.5 Hz, 1H, *bpy*), 7.92 (dd, *J* = 8.1, 7.4 Hz, 1H, *bpy*), 7.83 (dd, *J* = 7.3, 5.8 Hz, 1H, *bpy*), 7.68 (s, 1H, *triazole*), 7.57 (td, *J* = 7.8, 1.6 Hz, 2H, py_{ax}), 7.50 (dd, *J* = 7.5, 5.8 Hz, 1H, *bpy*), 7.47 (dd, *J* = 5.6, 1.6 Hz, 2H, py_{ax}), 7.34–7.25 (m, 5H, *Ph*–CH_2–triazole + py_{ax}), 7.03–6.98 (m, 2H, *Ph*–CH_2–triazole), 6.95 (dd, *J* = 7.8, 5.6 Hz, 2H, py_{ax}), 5.57 (s, 2H, Ph–CH_2–triazole), 5.42 (d, *J* = 16.7 Hz, 2H, CH_2(ax)–N_{amine}), 5.03 (d, *J* = 16.7 Hz, 2H, CH_2(ax)–N_{amine}), 4.38 (s, 2H, CH_2(eq)–N_{amine}) ppm. ^{1}H NMR (400 MHz, acetone-d_6): δ = 10.87 (d, *J* = 5.8 Hz, 1H, *bpy*), 9.60 (d, *J* = 5.5 Hz, 1H, *bpy*), 8.75 (d, *J* = 8.1 Hz, 1H, *bpy*), 8.65 (d, *J* = 8.3 Hz, 1H, *bpy*), 8.28 (d, *J* = 8.1 Hz, 1H, *bpy*), 8.12 (s, 1H, *triazole*), 8.06 (dd, *J* = 8.8, 7.4 Hz, 1H, *bpy*), 7.97 (dd, *J* = 7.4, 5.9, 1H, *bpy*), 7.76–7.68 (m, 4H, py_{ax}), 7.64 (dd, *J* = 7.4, 5.8 Hz, 1H, *bpy*), 7.54 (d, *J* = 8.0, 2H, py_{ax}), 7.34–7.27 (m, 3H, *Ph*–CH_2–triazole), 7.15–7.07 (m, 4H, py_{ax} + *Ph*–CH_2–triazole), 5.89 (d, *J* = 16.8 Hz, 2H, CH_2(ax)–N_{amine}), 5.78 (s, 2H, Ph–CH_2–triazole), 5.42 (d, *J* = 16.7 Hz, 2H, CH_2(ax)–N_{amine}), 4.80 (s, 2H, CH_2(eq)–N_{amine}) ppm. $C_{32}H_{30}N_8P_2F_{12}Ru\cdot1.5H_2O$: calcd. C 40.69, H 3.48, N 11.86; found C 40.70, H 3.23, N 11.81. UV/Vis (DCM): λ [nm] (ε [M^{-1} cm^{-1}]) = 249 (23760), 295 (33400), 337 (12050) sh, 384 (14370), 457 (8760).

[Ru(L^3)(bpy)]$(PF_6)_2$ {3$(PF_6)_2$}: The complex was prepared analogously to **1**$(PF_6)_2$. However, after addition of water and excess KPF_6, precipitation was not complete, and the precipitate was to fine to be filtered off completely. The ethylene glycol/water phase was therefore extracted with acetone/DCM (1:1, 15 mL) three times. The combined organic phases were washed with water (15 mL) once and dried over Na_2SO_4. After evaporation of the solvents under reduced pressure, the resulting orange crude product was purified by column chromatography analogously to **1**$(PF_6)_2$. [Ru(bpy)$(dmso)_2Cl_2$] (97 mg, 0.15 mmol), L^3 (68 mg, 0.15 mmol), and KPF_6 (80 mg, 0.43 mmol) yielded pure **3**$(PF_6)_2$ (127 mg, 85% yield). ^{1}H NMR (400 MHz, acetone-d_6): δ = 10.83 (d, *J* = 5.6 Hz, 1H, *bpy*), 9.50 (d, *J* = 5.6 Hz, 1H, *bpy*), 8.66 (d, *J* = 8.2 Hz, 1H, *bpy*), 8.59 (d, *J* = 8.2 Hz, 1H, *bpy*), 8.21 (dd, *J* = 8.9, 7.7 Hz, 1H, *bpy*), 8.12 (s, 1H, $triazole_{eq}$), 8.08 (s, 1H, $triazole_{ax}$), 8.04 (dd, *J* = 8.5, 7.7 Hz, 1H, *bpy*), 7.89 (dd, *J* = 7.3, 5.7 Hz, 1H, *bpy*), 7.73 (d, *J* = 5.6 Hz, 1H, py_{ax}), 7.68 (dd, *J* = 8.0, 7.7 Hz, 1H, py_{ax}), 7.60 (dd, *J* = 8.0, 6.0 Hz, 1H, *bpy*), 7.47 (d, *J* = 8.0 Hz, 1H, py_{ax}), 7.38–7.19 (m, 8H, *Ph*–CH_2–$triazole_{eq/ax}$), 7.10–7.03 (m, 3H, py_{ax} + *Ph*–CH_2–$triazole_{eq}$), 5.83 (d, *J* = 16.9 Hz, 1H, py–CH_2(ax)–N_{amine}), 5.80 (d, *J* = 14.8 Hz, 1H, Ph–CH_2–$triazole_{eq}$), 5.72 (d, *J* = 14.9 Hz, 1H, Ph–CH_2–$triazole_{eq}$), 5.49 (d, *J* = 15.8 Hz, 1H, $triazole_{ax}$–CH_2(ax)–N_{amine}), 5.42 (s, 2H, Ph–CH_2–$triazole_{ax}$), 5.36 (d, *J* = 16.9 Hz, 1H, py–CH_2(ax)–N_{amine}), 5.21 (d, *J* = 16.0 Hz, 1H, $triazole_{ax}$–CH_2(ax)–N_{amine}), 4.79 (d, *J* = 17.1 Hz, 1H, $triazole_{eq}$–CH_2(eq)–N_{amine}), 4.60 (d, *J* = 17.0 Hz, 1H, $triazole_{eq}$–CH_2(eq)–N_{amine}) ppm.^{1}H NMR (400 MHz, acetonitrile-d_3): δ = 10.62 (d, *J* = 5.9 Hz, 1H, *bpy*), 9.03 (d, *J* = 5.6 Hz, 1H, *bpy*), 8.41 (d, *J* = 8.2 Hz, 1H, *bpy*), 8.33 (d, *J* = 8.2 Hz, 1H, *bpy*), 8.11 (dd, *J* = 8.2, 7.5 Hz, 1H, *bpy*), 7.93 (dd, *J* = 8.4, 7.6 Hz, 1H, *bpy*), 7.77 (dd, *J* = 7.3, 5.7 Hz, 1H, *bpy*), 7.73 (s, 1H, $triazole_{ax}$), 7.70 (s, 1H, $triazole_{eq}$), 7.55 (dd, *J* = 8.0, 7.8 Hz, 1H, py_{ax}), 7.51–7.47 (m, 2H, *bpy*, py_{ax}), 7.33–7.22 (m, 7H, py_{ax} + *Ph*–CH_2–$triazole_{eq/ax}$), 7.13–7.09 (m, 2H, *Ph*–CH_2–$triazole_{ax}$), 6.98–6.94 (m, 2H, *Ph*–CH_2–$triazole_{eq}$), 6.92 (dd, *J* = 7.8, 5.8 Hz, 1H, py_{ax}), 5.63 (d, *J* = 15.0 Hz, 1H, Ph–CH_2–$triazole_{eq}$), 5.51 (d, *J* = 15.0 Hz, 1H, Ph–CH_2–$triazole_{eq}$), 5.40 (d, *J* = 16.7 Hz, 1H, py–CH_2(ax)–N_{amine}), 5.24 (s, 2H, Ph–CH_2–$triazole_{ax}$), 5.06 (d, *J* = 15.8 Hz, 1H, $triazole_{ax}$–CH_2(ax)–N_{amine}), 5.01 (d, *J* = 16.8, 1H, py–CH_2(ax)–N_{amine}), 4.87 (d, *J* = 16.0 Hz, 1H, $triazole_{ax}$–CH_2(ax)–N_{amine}), 4.42 (d, *J* = 16.9 Hz, 1H, $triazole_{eq}$–CH_2(eq)–N_{amine}), 4.24 (d, *J* = 16.9 Hz, 1H, $triazole_{eq}$–CH_2(eq)–N_{amine}) ppm. $C_{36}H_{34}N_{10}P_2F_{12}Ru\cdot1.1H_2O$: calcd. C 42.49, H 3.59, N 13.77; found C 42.54, H 3.48, N 13.71. UV/Vis (DCM): λ [nm] (ε [M^{-1} cm^{-1}]) = 250 (16140), 293 (33030), 334 (11690), 367 (10530) sh, 450 (6810).

[Ru(L^4)(bpy)]$(PF_6)_2$ {4$(PF_6)_2$}: The complex was prepared analogously to **3**$(PF_6)_2$. [Ru(bpy)$(dmso)_2Cl_2$] (97 mg, 0.20 mmol), L^4 (106 mg, 0.20 mmol), and KPF_6 (92 mg, 0.50 mmol) yielded **4**$(PF_6)_2$. Because evaporation of the solvent from the eluted product fraction only yielded the product as an oily solid, **4**$(PF_6)_2$ was precipitated by adding a concentrated solution of the complex in acetone to an excess volume of Et_2O, which afforded an orange powder (166 mg, 77% yield). ^{1}H NMR (400 MHz, acetone-d_6): δ = 10.84 (d, *J* = 5.7 Hz, 1H, *bpy*), 9.43 (d, *J* = 5.7 Hz, 1H, *bpy*), 8.64 (d, *J* = 8.2 Hz, 1H, *bpy*), 8.59 (d, *J* = 8.1 Hz, 1H, *bpy*), 8.21 (dd, *J* = 8.0, 7.8 Hz, 1H, *bpy*), 8.09 (s, 1H, $triazole_{eq}$), 8.08 (s, 2H, $triazole_{ax}$), 8.07 (dd, 1H, *bpy*), 7.84 (dd, *J* = 7.4, 5.8 Hz, 1H, *bpy*), 7.59 (dd, *J* = 7.3, 5.7 Hz, 1H, *bpy*), 7.43–7.38 (m, 5H, *Ph*–CH_2–triazole), 7.29–7.21 (m, 6H, *Ph*–CH_2–triazole), 7.04–6.98 (m, 4H, *Ph*–CH_2–triazole), 5.75 (s, 2H, Ph–CH_2–$triazole_{eq}$), 5.48 (d, *J* = 16.1 Hz, 2H, $triazole_{ax}$–CH_2–N_{amine}), 5.40 (s, 4H, Ph–CH_2–$triazole_{ax}$), 5.19 (d, *J* = 16.2 Hz, 2H, $triazole_{ax}$–CH_2–N_{amine}), 4.63 (s, 2H, $triazole_{eq}$–CH_2–N_{amine}) ppm. ^{1}H NMR (400 MHz, acetonitrile-d_3): δ = 10.61 (d, *J* = 5.8 Hz, 1H, *bpy*), 8.96 (d, *J* = 5.3 Hz, 1H, *bpy*), 8.37 (d, *J* = 8.1 Hz, 1H, *bpy*), 8.30 (d, *J* = 9.2 Hz, 1H, *bpy*), 8.08 (d, *J* = 8.2 Hz, 1H, *bpy*), 7.93 (dd, *J* = 8.3, 7.6 Hz, 1H, *bpy*), 7.72 (dd, 1H, *bpy*), 7.72 (s, 1H, $triazole_{eq}$), 7.69

(s, 2H, *triazole*$_{ax}$), 7.48 (dd, *J* = 7.4, 5.7 Hz, 1H, *bpy*), 7.42–7.35 (m, 3H, *Ph*–CH_2–triazole), 7.34–7.20 (m, 8H, *Ph*–CH_2–triazole), 6.97–6.88 (m, 4H, *Ph*–CH_2–triazole), 5.57 (s, 2H, Ph–C*H*$_2$–triazole$_{eq}$), 5.22 (s, 4H, Ph–C*H*$_2$–triazole$_{ax}$), 5.05 (d, *J* = 16.0 Hz, 2H, triazole$_{ax}$–C*H*$_2$–N$_{amine}$), 4.84 (d, *J* = 16.1 Hz, 2H, triazole$_{ax}$–C*H*$_2$–N$_{amine}$), 4.28 (s, 2H, triazole$_{eq}$–C*H*$_2$–N$_{amine}$) ppm. $C_{40}H_{38}N_{12}P_2F_{12}Ru \cdot Et_2O$: calcd. C 45.88, H 4.20, N 14.59; found C 46.34, H 4.65, N 15.27. UV/Vis (DCM): λ [nm] (ε [M^{-1} cm^{-1}]) = 245 (10830), 255 (10040) sh, 292 (29980), 326 (11800) sh, 446 (4920).

[Ru(L^4)(L^7)](PF$_6$)$_2$ {5(PF$_6$)$_2$}: [Ru(dmso)$_4$Cl$_2$] (0.5 mmol, 242 mg) and L^7 (0.5 mmol, 118 mg) were heated at reflux for 2 h in an ethanol/DMSO mixture (9:1, 10 mL). The mixture was allowed to cool down, and crude [Ru(L^7)(dmso)$_2$Cl$_2$] was filtered off as a yellow precipitate and washed with cold ethanol. The crude product was used without further purification (152 mg, 54% yield). ^{1}H NMR (400 MHz, DMSO-d6): δ = 9.51 (d, *J* = 5.9 Hz, 1H, *py*–triazole), 8.47 (s, 1H, py–*triazole*), 7.39 (d, *J* = 7.3 Hz 1H, *py*–triazole), 7.27 (t, *J* = 7.3 Hz, 1H, *py*–triazole), 6.76 (t, *J* = 7.3 Hz, 1H, *py*–triazole), 6.67–6.56 (m, 5H, *Ph*–CH_2–triazole), 5.08 (s, 2H, Ph–C*H*$_2$–triazole), 2.59 (s, 12H, Ru–*dmso*) ppm. MS (+ESI): *m*/*z* = 588.9678 [M + Na]$^+$.

The target complex was prepared analogously to **3**(PF$_6$)$_2$. [Ru(L^7)(dmso)$_2$Cl$_2$] (56 mg, 0.10 mmol), L^4 (53 mg, 0.10 mmol), and KPF_6 (46 mg, 0.25 mmol) afforded pure **5**(PF$_6$)$_2$ (85 mg, 73% yield) as a yellow solid after column chromatography. ^{1}H NMR (400 MHz, acetone-d$_6$): δ = 10.59 (d, *J* = 5.9 Hz, 1H, *py*–triazole), 9.07 (s, 1H, py–*triazole*), 8.28 (d, *J* = 8.0 Hz, 1H, *py*–triazole), 8.17 (td, *J* = 7.8, 1.5 Hz, 1H, *py*–triazole), 8.13 (s, 2H, *triazole*$_{ax}$), 8.07 (s, 1H, *triazole*$_{eq}$), 7.79 (dd, *J* = 7.4, 5.7 Hz, 1H, *py*–triazole), 7.47–7.25 (m, 16H, *Ph*–CH_2–triazole), 7.10–7.03 (m, 4H, *Ph*–CH_2–triazole), 5.86 (s, 2H, Ph–C*H*$_2$–triazole), 5.78 (s, 2H, Ph–C*H*$_2$–triazole), 5.49 (d, *J* = 14.9 Hz, 2H, triazole$_{ax}$–C*H*$_2$–N$_{amine}$), 5.45 (s, 4H, Ph–C*H*$_2$–triazole$_{ax}$), 5.22 (d, *J* = 14.8 Hz, 2H, triazole$_{ax}$–C*H*$_2$–N$_{amine}$), 4.61 (s, 2H, triazole$_{eq}$–C*H*$_2$–N$_{amine}$) ppm. ^{1}H NMR (400 MHz, acetonitrile-d$_3$) δ = 10.33 (d, *J* = 5.7 Hz, 1H, *py*–triazole), 8.50 (s, 1H, py–*triazole*), 8.04–7.94 (m, 2H, *py*–triazole), 7.71 (s, 2H, *triazole*$_{ax}$), 7.67 (s, 1H, *triazole*$_{eq}$), 7.63 (dd, *J* = 7.0, 5.7 Hz, 1H, *py*–triazole), 7.42–7.21 (m, 16H, *Ph*–CH_2–triazole), 6.97–6.91 (m, 4H, *Ph*–CH_2–triazole), 5.60 (s, 2H, Ph–C*H*$_2$–triazole), 5.55 (s, 2H, Ph–C*H*$_2$–triazole), 5.24 (s, 4H, Ph–C*H*$_2$–triazole$_{ax}$), 5.18 (d, *J* = 14.7 Hz, 2H, triazole$_{ax}$–C*H*$_2$–N$_{amine}$), 4.85 (d, *J* = 14.8 Hz, 2H, triazole$_{ax}$–C*H*$_2$–N$_{amine}$), 4.23 (s, 2H, triazole$_{eq}$–C*H*$_2$–N$_{amine}$) ppm. $C_{44}H_{42}N_{14}P_2F_{12}Ru \cdot 0.7H_2O$: calcd. C 45.15, H 3.74, N 16.75; found C 45.30, H 3.89, N 16.60. UV/Vis (DCM): λ [nm] (ε [M^{-1} cm^{-1}]) = 236 (13570), 274 (25460), 320 (15410), 386 (7630).

[Ru(L^4)(L^8)](PF$_6$)$_2$ {6(PF$_6$)$_2$}: [Ru(dmso)$_4$Cl$_2$] (0.5 mmol, 242 mg) and L^8 (0.5 mmol, 158 mg) were heated at reflux for 2 h in an ethanol/DMSO mixture (9:1, 10 mL). The mixture was allowed to cool down, and crude [Ru(L^8)(dmso)$_2$Cl$_2$] was filtered off as a light yellow precipitate and washed with cold ethanol. The crude product was used without further purification (202 mg, 63% yield). ^{1}H NMR (400 MHz, DMSO-d6): δ = 7.97 (s, 2H, Ph–CH_2–*triazole*), 6.64–6.53 (m, 10H, *Ph*–CH_2–triazole), 5.02 (s, 4H, Ph–C*H*$_2$–triazole) ppm. MS (+ESI): *m*/*z* = 667.0032 [M + Na]$^+$.

The target complex was prepared analogously to **3**(PF$_6$)$_2$. [Ru(L^8)(dmso)$_2$Cl$_2$] (64 mg, 0.10 mmol), L^4 (53 mg, 0.10 mmol), and KPF_6 (46 mg, 0.25 mmol) afforded **6**(PF$_6$)$_2$. Because evaporation of the solvent from the eluted product fraction only yielded the product as an oily solid, **6**(PF$_6$)$_2$ was precipitated by adding a concentrated solution of the complex in acetone to an excess volume of Et_2O, which afforded an almost colorless powder (83 mg, 67% yield). ^{1}H NMR (400 MHz, acetone-d$_6$): δ = 8.73 (s, 1H, *triazole*–triazole), 8.63 (s, 1H, triazole–*triazole*), 8.09 (s, 2H, *triazole*$_{ax}$), 7.92 (s, 1H, *triazole*$_{eq}$), 7.55–7.51 (m, 2H, *Ph*–CH_2–triazole), 7.49–7.23 (m, 19H, *Ph*–CH_2–triazole), 7.09–7.04 (m, 4H, *Ph*–CH_2–triazole), 6.04 (s, 2H, Ph–C*H*$_2$–triazole), 5.78 (s, 2H, Ph–C*H*$_2$–triazole), 5.67 (s, 2H, Ph–C*H*$_2$–triazole), 5.43 (d, *J* = 15.0 Hz, 2H, triazole$_{ax}$–C*H*$_2$–N$_{amine}$), 5.43 (s, 4H, Ph–C*H*$_2$–triazole$_{ax}$), 5.18 (d, *J* = 14.8 Hz, 2H, triazole$_{ax}$–C*H*$_2$–N$_{amine}$), 4.59 (s, 2H, triazole$_{eq}$–C*H*$_2$–N$_{amine}$) ppm. ^{1}H NMR (400 MHz, acetonitrile-d$_3$): δ = 8.38 (s, 1H, *triazole*–triazole), 8.20 (s, 1H, triazole–*triazole*), 7.71 (s, 2H, *triazole*$_{ax}$), 7.59 (s, 1H, *triazole*$_{eq}$), 7.45–7.22 (m, 19H, *Ph*–CH_2–triazole), 7.22–7.16 (m, 2H, *Ph*–CH_2–triazole), 6.99–6.95 (m, 4H, *Ph*–CH_2–triazole), 5.83 (s, 2H, Ph–C*H*$_2$–triazole), 5.57 (s, 2H, Ph–C*H*$_2$–triazole), 5.47 (s, 2H, Ph–C*H*$_2$–triazole), 5.26 (s, 4H, Ph–C*H*$_2$–triazole$_{ax}$), 5.16 (d, *J* = 14.3 Hz, 2H, triazole$_{ax}$–C*H*$_2$–N$_{amine}$), 4.84 (d, *J* = 14.7 Hz, 2H, triazole$_{ax}$–C*H*$_2$–N$_{amine}$), 4.26 (s, 2H, triazole$_{eq}$–C*H*$_2$–N$_{amine}$) ppm. $C_{48}H_{46}N_{16}P_2F_{12}Ru \cdot Et_2O$: calcd. C 47.60, H 4.30, N 17.08; found C 48.10, H 4.35, N 17.58. UV/Vis (DCM): λ [nm] (ε [M^{-1} cm^{-1}]) = 233 (30630), 325 (25180).

[Ru(L^1)(L^8)](PF$_6$)$_2$ {7(PF$_6$)$_2$}: The target complex was prepared analogously to **6**(PF$_6$)$_2$. [Ru(L^8)(dmso)$_2$Cl$_2$] (64 mg, 0.10 mmol), L^1 (29 mg, 0.10 mmol), and KPF_6 (46 mg, 0.25 mmol) afforded **7**(PF$_6$)$_2$. Because evaporation of the solvent from the eluted product fraction only yielded the product

as an oily solid, **6**$(PF_6)_2$ was precipitated by adding a concentrated solution of the complex in acetone to an excess volume of Et_2O, which afforded a yellow powder (90 mg, 90% yield). ^{1}H NMR (400 MHz, acetone-d_6): δ = 10.29 (d, J = 5.7 Hz, 1H, py_{eq}), 8.89 (s, 1H, *triazole*–triazole), 8.70 (s, 1H, triazole–*triazole*), 7.93 (d, J = 5.5 Hz, 2H, py_{ax}), 7.81–7.73 (m, 3H, py_{ax} + py_{eq}), 7.69–7.65 (m, 2H, *Ph*–CH_2–triazole), 7.60 (d, J = 7.8 Hz, 2H, py_{ax}), 7.56–7.45 (m, 4H, *Ph*–CH_2–triazole + py_{eq}), 7.39–7.29 (m, 6H, *Ph*–CH_2–triazole), 7.12 (dd, J = 8.0, 5.3 Hz, 2H, py_{ax}), 6.14 (s, 2H, Ph–CH_2–triazole), 5.83 (d, J = 15.4 Hz, 2H, py_{ax}–CH_2–N_{amine}), 5.83 (s, 2H, Ph–CH_2–triazole), 5.41 (d, J = 15.3 Hz, 2H, py_{ax}–CH_2–N_{amine}), 5.13 (s, 2H, py_{eq}–CH_2–N_{amine}) ppm. ^{1}H NMR (400 MHz, acetonitrile-d_3): δ = 10.04 (d, J = 5.7 Hz, 1H, py_{eq}), 8.40 (s, 1H, *triazole*–triazole), 8.18 (s, 1H, triazole–*triazole*), 7.67 (d, J = 5.5 Hz, 2H, py_{ax}), 7.64–7.54 (m, 5H, py_{ax} + py_{eq} + *Ph*–CH_2–triazole), 7.52–7.44 (m, 3H, py_{eq} + *Ph*–CH_2–triazole), 7.37 (d, J = 8.0 Hz, 2H, py_{ax}), 7.34–7.26 (m, 4H, *Ph*–CH_2–triazole), 7.24–7.20 (m, 2H, *Ph*–CH_2–triazole), 7.13 (d, J = 7.8 Hz, 1H, py_{eq}), 6.97 (dd, J = 7.7, 5.6 Hz, 2H, py_{ax}), 5.91 (s, 2H, Ph–CH_2–triazole), 5.57 (s, 2H, Ph–CH_2–triazole), 5.52 (d, J = 15.5 Hz, 2H, py_{ax}–CH_2–N_{amine}), 5.03 (d, J = 15.4 Hz, 2H, py_{ax}–CH_2–N_{amine}), 4.71 (s, 2H, py_{eq}–CH_2–N_{amine}) ppm. $C_{36}H_{34}N_{10}P_2F_{12}Ru\cdot Et_2O\cdot H_2O$: C 44.08, H 4.25, N 12.85; found C 43.80, H 4.47, N 12.68. UV/Vis (DCM): λ [nm] (ε [M^{-1} cm^{-1}]) = 240 (18480), 286 (4670) sh, 378 (11400), 417 (5630) sh.

[Ru(L^5)(bpy)](PF$_6$)$_2$ {8(PF$_6$)$_2$}: The complex was prepared analogously to **3**$(PF_6)_2$. [Ru(bpy)(dmso)$_2$Cl$_2$] (97 mg, 0.20 mmol), L^5 (114 mg, 0.20 mmol), and KPF_6 (92 mg, 0.50 mmol) yielded pure **8**$(PF_6)_2$ (186 mg, 83% yield). The ratio of the two isomers **8a**$^{2+}$/**8b**$^{2+}$ after the first column chromatography was 70:30, which is close to the expected statistical distribution of 2:1 or 67:33. Attempts to separate the isomers by slow careful column chromatography, that is, collecting the eluted product in several test tubes and recording ^{1}H NMR spectra of the fraction in each test tube, only afforded a **8a**$^{2+}$/**8b**$^{2+}$ mixture of 60:40. However, when the compound was recrystallized from a concentrated solution in acetone by adding Et_2O and keeping the solution in the freezer (–20 °C), the first fraction of crystalline material showed a **8a**$^{2+}$/**8b**$^{2+}$ ratio of 28:72.

^{1}H NMR (700 MHz, chloroform-d, **8a**$^{2+}$/**8b**$^{2+}$ = 28:72): δ = 10.85 (d, J = 5.2 Hz, 1H, **a**/**b**, bpy), 9.46 (d, J = 5.8 Hz, 1H, **a**/**b** bpy), 8.40 (s, 0.28H, **a**, Ph–*triazole*, axial), 8.36 (d, J = 8.4 Hz, 1H, **a**/**b**, bpy), 8.34 (s, 1.72H, **a**/**b**, iPr–Ph–*triazole*, axial), 8.28 (d, J = 8.1 Hz, 1H, **a**/**b**, bpy), 8.21 (s, 0.72H, **b**, Ph–*triazole*, equatorial), 8.16 (s, 0.28H, **a**, iPr–Ph–*triazole*, equatorial), 8.11 (td, J = 7.8, 1.4 Hz, 1H, **a**/**b**, bpy), 7.89 (t, J = 7.7 Hz, 1H, **a**/**b**, bpy), 7.76 (d, J = 8.8 Hz, 1.44H, **b**, *Ph*–triazole, equatorial), 7.75–7.72 (m, 2H, **a**/**b**, bpy), 7.66 (d, J = 8.5 Hz, 0.56H, **a**, iPr–*Ph*–triazole, equatorial), 7.57 (dd, J = 8.6, 7.2 Hz, 1.44H, **b**, *Ph*–triazole, equatorial), 7.52 (d, J = 7.8 Hz, 0.56H, **a**, *Ph*–triazole, axial), 7.51 (t, J = 7.3 Hz, 0.72H, **b**, *Ph*–triazole, equatorial), 7.41 (d, J = 8.8 Hz, 3.44H, **a**/**b**, iPr–*Ph*–triazole, axial), 7.40 (d, J = 8.3 Hz, 0.56H, **a**, iPr–*Ph*–triazole, equatorial), 7.39 (t, J = 7.6 Hz, 0.56H, **a**, *Ph*–triazole, axial), 7.35 (t, J = 7.6 Hz, 0.28H, **a**, *Ph*–triazole, axial), 7.23 (d, J = 7.3 Hz, 3.44H, **a**/**b**, iPr–*Ph*–triazole, axial), 5.71 (d, J = 15.8 Hz, 2H, **a**/**b**, triazole–CH_2, axial), 5.40 (d, J = 15.8 Hz, 2H, **a**/**b**, triazole–CH_2, axial), 4.93 (s, 2H, **a**/**b**, triazole–CH_2, equatorial), 2.99 (hept, J = 7.1 Hz, 0.28H, **a**, *iPr*–Ph, equatorial), 2.88 (hept, J = 7.1 Hz, 1.72H, **a**/**b**, *iPr*–Ph, axial), 1.29 (d, J = 6.9 Hz, 1.68H, **a**, *iPr*–Ph, equatorial), 1.19 (d, J = 6.9 Hz, 1.68H, **a**, *iPr*–Ph, axial), 1.18 (d, J = 7.0 Hz, 8.64H, **b**, *iPr*–Ph, axial) ppm.
^{1}H NMR (700 MHz, chloroform-d, **8a**$^{2+}$/**8b**$^{2+}$ = 60:40): δ = 10.84 (t, J = 3.7 Hz, 1H, **a**/**b**, bpy), 9.37 (d, J = 5.5 Hz, 1H, **a**/**b** bpy), 8.37 (d, J = 8.1 Hz, 1H, **a**/**b**, bpy), 8.36 (s, 0.60H, **a**, Ph–*triazole*, axial), 8.31 (s, 1.60H, **a**/**b**, iPr–Ph–*triazole*, axial), 8.28 (d, J = 7.8 Hz, 1H, **a**/**b**, bpy), 8.16 (s, 0.40H, **b**, Ph–*triazole*, equatorial), 8.12 (s, 0.60H, **a**, iPr–Ph–*triazole*, equatorial), 8.12 (tdd, J = 7.8, 3.7, 1.4 Hz, 1H, **a**/**b**, bpy), 7.87 (t, J = 7.6 Hz, 1H, **a**/**b**, bpy), 7.75 (d, J = 7.1 Hz, 0.80H, **b**, *Ph*–triazole, equatorial), 7.75–7.72 (m, 1H, **a**/**b**, bpy), 7.69–7.66 (m, 1H, **a**/**b**, bpy), 7.65 (d, J = 8.6 Hz, 1.2H, **a**, iPr–*Ph*–triazole, equatorial), 7.56 (t, J = 8.6 Hz, 0.80H, **b**, *Ph*–triazole, equatorial), 7.50 (d, J = 8.6 Hz, 1.20H, **a**, *Ph*–triazole, axial), 7.49 (t, J = 7.9 Hz, 0.40H, **b**, *Ph*–triazole, equatorial), 7.40 (d, J = 8.6 Hz, 2.80H, **a**/**b**, iPr–*Ph*–triazole, axial), 7.39 (d, J = 8.6 Hz, 1.20H, **a**, iPr–*Ph*–triazole, equatorial), 7.38 (t, J = 8.6 Hz, 1.20H, **a**, *Ph*–triazole, axial), 7.33 (t, J = 7.2 Hz, 0.60H, **a**, *Ph*–triazole, axial), 7.22 (d, J = 8.9 Hz, 2.80H, **a**/**b**, iPr–*Ph*–triazole, axial), 5.63 (d, J = 15.8 Hz, 2H, **a**/**b**, triazole–CH_2, axial), 5.36 (d, J = 15.8 Hz, 2H, **a**/**b**, triazole–CH_2, axial), 4.88 (s, 2H, **a**/**b**, triazole–CH_2, equatorial), 2.99 (hept, J = 6.8 Hz, 0.60H, **a**, *iPr*–Ph, equatorial), 2.88 (hept, J = 7.1 Hz, 0.60H, **a**, *iPr*–Ph, axial), 2.87 (hept, J = 7.1 Hz, 0.80H, **b**, *iPr*–Ph, axial), 1.28 (d, J = 6.9 Hz, 3.60H, **a**, *iPr*–Ph, equatorial), 1.18 (d, J = 6.9 Hz, 3.60H, **a**, *iPr*–Ph, axial), 1.17 (d, J = 6.9 Hz, 4.80H, **b**, *iPr*–Ph, axial) ppm.
^{1}H NMR (400 MHz, acetonitrile-d_3, **8a**$^{2+}$/**8b**$^{2+}$ = 60:40): δ = 10.76 (d, J = 5.6 Hz, 1H, **a**/**b**, bpy), 9.14 (d, J = 5.7 Hz, 1H, **a**/**b**, bpy), 8.42 (d, J = 8.3 Hz, 1H, **a**/**b**, bpy), 8.36 (d, J = 8.0 Hz, 1H, **a**/**b**, bpy), 8.26–8.17 (m, 3H, **a**/**b**, triazole), 8.13 (t, J = 7.9 Hz, 1H, **a**/**b**, bpy), 7.97 (t, J = 7.8 Hz, 1H, **a**/**b**, bpy), 7.85–7.80 (m), 7.75–7.70 (m), 7.63–7.50 (m), 7.47–7.39 (m), 7.36–7.27 (m), 5.28 (d, J = 16.1 Hz, 2H, **a**/**b**, triazole–CH_2, axial), 5.06 (d, J = 16.0 Hz, 2H, **a**/**b**, triazole–CH_2, axial), 4.52 (s, 2H, **a**/**b**, triazole–CH_2,

equatorial), 2.99 (hept, *J* = 6.8 Hz, 0.28H, **a**, *iPr*–Ph, equatorial), 2.89 (hept, *J* = 6.9 Hz, 1.72H, **a**/**b**, *iPr*–Ph, axial), 1.23 (d, *J* = 6.9 Hz, 1.68H, **a**, *iPr*–Ph, equatorial), 1.15 (d, *J* = 6.9 Hz, 10.32H, **a**/**b**, *iPr*–Ph, axial) ppm.
^{1}H NMR (400 MHz, acetone-d_6, **8a**$^{2+}$/**8b**$^{2+}$ = 60:40): δ = 10.97 (d, *J* = 5.5 Hz, 1H, **a**/**b**, bpy), 9.62 (d, *J* = 5.5 Hz, 1H, **a**/**b** bpy), 8.75 (s, 0.60H, **a**, Ph–*triazole*, axial), 8.71 (d, *J* = 5.5 Hz, 1H, **a**/**b**, bpy), 8.70 (s, 1.40H, **a**/**b**, iPr–Ph–*triazole*, axial), 8.68 (s, 0.40H, **b**, Ph–*triazole*, equatorial), 8.65 (d, *J* = 8.5 Hz, 1H, **a**/**b**, bpy), 8.63 (s, 0.60H, **a**, iPr–Ph–*triazole*, equatorial), 8.28 (t, *J* = 8.0 Hz, 1H, **a**/**b**, bpy), 8.11 (t, *J* = 7.7 Hz, 1H, **a**/**b**, bpy), 7.97 (t, *J* = 6.4 Hz, 1H, **a**/**b**, bpy), 7.95 (d, *J* = 8.0 Hz, 0.80H, **b**, *Ph*–triazole, equatorial), 7.84 (d, *J* = 8.8 Hz, 1.2H, **a**, iPr–*Ph*–triazole, equatorial), 7.69 (t, *J* = 6.7 Hz, 1H, **a**/**b**, bpy), 7.62 (t, *J* = 7.4 Hz, 0.80H, **b**, *Ph*–triazole, equatorial), 7.58–7.53 (m, 1.2H, **a**, *Ph*–triazole, axial, 0.4H, **b**, *Ph*–triazole, axial), 7.49 (1.2H, **a**, iPr–*Ph*–triazole, equatorial), 7.47–7.40 (m, 1.2H, **a**, *Ph*–triazole, axial, 0.6H, **a**, *Ph*–triazole, axial), 7.46 (d, *J* = 8.7 Hz, 2.80H, **a**/**b**, iPr–*Ph*–triazole, axial), 7.33 (d, *J* = 8.7 Hz, 2.80H, **a**/**b**, iPr–*Ph*–triazole, axial), 5.72 (d, *J* = 16.4 Hz, 2H, **a**/**b**, triazole–CH_2, axial), 5.44 (d, *J* = 16.4 Hz, 2H, **a**/**b**, triazole–CH_2, axial), 4.91 (s, 2H, **a**/**b**, triazole–CH_2, equatorial), 3.00 (hept, *J* = 6.8 Hz, 0.60H, **a**, *iPr*–Ph, equatorial), 2.89 (hept, *J* = 6.9 Hz, 1.40H, **a**/**b**, *iPr*–Ph, axial), 1.24 (d, *J* = 6.9 Hz, 3.60H, **a**, *iPr*–Ph, equatorial), 1.15 (d, *J* = 6.9 Hz, 8.4H, **a**, *iPr*–Ph, axial) ppm.
$C_{43}H_{44}N_{12}P_2F_{12}Ru\cdot 0.2Et_2O$: C 46.36, H 4.09, N 14.81; found C 46.55, H 4.19, 14.98. UV/Vis (DCM): λ [nm] (ε [M^{-1} cm^{-1}]) = 245 (36164), 291 (35556), 347 (23196), 441 (7010).

[Ru(L^1)(bpy)(CD$_3$CN)](PF$_6$)$_2$ {[1(CD$_3$CN)](PF$_6$)$_2$}: A solution of **1**$(PF_6)_2$ in CD_3CN (0.7 mL, 5 mmol/L) was put in an NMR tube and heated in an oil bath at 80 °C for 2 days. After the solution had cooled down an ^{1}H NMR spectrum was recorded, which was identical to that of pure [**1**$(CD_3CN)]^{2+}$ known from the literature. ^{1}H NMR (400 MHz, acetonitrile-d_3): δ = 8.89 (d, *J* = 5.6 Hz, 2H, py_{coord}), 8.52–8.45 (m, 3H, py_{free} + *bpy*), 8.32 (d, *J* = 5.6 Hz, 2H, *bpy*), 8.10 (t, *J* = 7.9 Hz, 2H, *bpy*), 7.77 (t, *J* = 7.8 Hz, 2H, py_{coord}), 7.68 (t, *J* = 7.7 Hz, 1H, py_{free}), 7.53 (dd, *J* = 7.7, 5.5 Hz, 2H, *bpy*), 7.36–7.27 (m, 5H, py_{free} + py_{coord}), 7.07 (d, *J* = 7.8 Hz, 1H, py_{free}), 4.62 (d, *J* = 16.8 Hz, 2H, CH_2(coord.)), 4.12 (d, *J* = 16.8 Hz, 2H, CH_2(coord.)), 3.19 (s, 2H, CH_2(free)) ppm. UV/Vis (CH_3CN): λ [nm] (ε [M^{-1} cm^{-1}]) = 247 (25259), 286 (33304), 347 (11938), 427 (6951).

[Ru(L^3)(bpy)(CD$_3$CN)](PF$_6$)$_2$ {[3(CD$_3$CN)](PF$_6$)$_2$}: A solution of **3**$(PF_6)_2$ in CD_3CN (0.7 mL, 5 mmol/L) was put in an NMR tube and irradiated at 369 nm. The reaction was monitored by ^{1}H NMR, and after 16 h a maximum amount of 87% of the original complex had reacted to a new species, the ^{1}H NMR resonances of which could be attributed to [**3**$(CD_3CN)]^{2+}$ (see Discussion of the NMR results). ^{1}H NMR (400 MHz, acetonitrile-d_3): δ = 8.85 (d, *J* = 5.6 Hz, 1H, py_{coord}), 8.48 (d, *J* = 5.5 Hz, 1H, *bpy*), 8.46 (d, *J* = 5.3 Hz, 1H, *bpy*), 8.29 (dd, *J* = 5.7, 4.8 Hz, 2H, *bpy*), 8.12–8.06 (m, 2H, *bpy*), 7.79 (td, *J* = 7.8, 1.5 Hz, 1H, py_{coord}), 7.71 (s, 1H, *triazole*$_{coord}$), 7.64 (s, 1H, *triazole*$_{free}$), 7.54–7.49 (m, 2H, *bpy*), 7.36–7.29 (m, 8H, py_{coord} + *Ph*–CH_2–triazole), 7.22–7.18 (m, 2H, *Ph*–CH_2–triazole), 7.02–6.98 (m, 2H, *Ph*–CH_2–triazole), 5.61 (d, *J* = 15.3 Hz, 1H, Ph–CH_2–triazole$_{coord}$), 5.50 (d, *J* = 15.2 Hz, 1H, Ph–CH_2–triazole$_{coord}$), 5.47 (s, 2H, Ph–CH_2–triazole$_{free}$), 4.31 (d, *J* = 16.4 Hz, 1H, py–CH_2–N_{amine}), 4.23 (d, *J* = 16.5 Hz, 1H, triazole$_{coord}$–CH_2–N_{amine}), 3.98 (d, *J* = 16.5 Hz, 1H, py–CH_2–N_{amine}), 3.67 (d, *J* = 16.4 Hz, 1H, triazole$_{coord}$–CH_2–N_{amine}), 3.21 (d, *J* = 14.3 Hz, 1H, triazole$_{free}$–CH_2–N_{amine}), 3.13 (d, *J* = 14.2 Hz, 1H, triazole$_{free}$–CH_2–N_{amine}) ppm. UV/Vis (CH_3CN): λ [nm] (ε [M^{-1} cm^{-1}]) = 246 (15859), 252 (15588), 286 (32932), 326 (10633) sh, 424 (5960).

[Ru(L^4)(bpy)(CD$_3$CN)](PF$_6$)$_2$ {[4(CD$_3$CN)](PF$_6$)$_2$}: A solution of **4**$(PF_6)_2$ in CD_3CN (0.7 mL, 5 mmol/L) was put in an NMR tube and irradiated at 369 nm. The reaction was monitored by ^{1}H NMR, and after 4 h all of the original complex had reacted to a new species, the ^{1}H NMR resonances of which could be attributed to [**4**$(CD_3CN)]^{2+}$ (see Discussion of the NMR results). The complex was precipitated from the solution by adding Et_2O, and mass spectra were measured from a solution of [**4**$(CD_3CN)]^{2+}$ in DCM. ^{1}H NMR (400 MHz, acetonitrile-d_3) δ = 8.45 (d, *J* = 8.1 Hz, 2H, *bpy*), 8.10–8.02 (m, 4H, *bpy*), 7.82 (s, 2H, *triazole*$_{coord}$), 7.58 (s, 1H, *triazole*$_{free}$), 7.50 (dd, *J* = 7.6, 5.7 Hz, 2H, *bpy*), 7.44–7.38 (m, 6H, *Ph*–CH_2–triazole), 7.32–7.27 (m, 7H, *Ph*–CH_2–triazole), 7.20–7.15 (m, 2H, *Ph*–CH_2–triazole), 5.58 (s, 4H, Ph–CH_2–triazole$_{coord}$), 5.44 (s, 2H, Ph–CH_2–triazole$_{free}$), 4.12 (d, *J* = 16.9 Hz, 2H, triazole$_{coord}$–CH_2–N_{amine}), 3.66 (d, *J* = 16.1 Hz, 2H, triazole$_{coord}$–CH_2–N_{amine}), 3.15 (s, 2H, triazole$_{free}$–CH_2–N_{amine}) ppm. ^{1}H NMR (400 MHz, acetone-d_6): δ = 8.77 (dt, *J* = 8.3, 1.0 Hz, 2H, bpy), 8.36 (dd, *J* = 5.6, 1.5 Hz, 2H, bpy), 8.24 (s, 2H, *triazole*$_{coord}$), 8.22 (dd, *J* = 8.5, 7.9 Hz, 2H, bpy), 7.80 (s, 1H, *triazole*$_{free}$), 7.64 (dd, *J* = 7.6, 5.6 Hz, 2H, bpy), 7.46–7.40 (m, 6H, *Ph*–CH_2–triazole), 7.37 – 7.33 (m, 4H, *Ph*–CH_2–triazole), 7.30–7.26 (m, 3H, *Ph*–CH_2–triazole), 7.21–7.17 (m, 2H, *Ph*–CH_2–triazole), 5.78 (s, 4H, Ph–CH_2–triazole$_{coord}$), 5.50 (s, 2H, Ph–CH_2–triazole$_{free}$), 4.47 (d, *J* = 16.3 Hz, 2H, triazole$_{coord}$–CH_2–N_{amine}), 3.98 (d, *J* = 16.1 Hz, 2H, triazole$_{coord}$–CH_2–N_{amine}), 3.46 (s, 2H, triazole$_{free}$–CH_2–N_{amine}). MS (+ESI): *m*/*z*

= 977.2484 [Ru + L^4 + bpy + CD_3CN + PF_6]$^+$. UV/Vis (CH_3CN): λ [nm] (ε [M^{-1} cm^{-1}]) = 243 (10702), 252 (9868), 286 (30088), 316 (11513), 427 (4653).

[Ru(L^4)(L^7)(CD_3CN)](PF_6)$_2$ {[5(CD_3CN)](PF_6)$_2$}: A solution of **5**(PF_6)$_2$ in CD_3CN (0.7 mL, 5 mmol/L) was put in an NMR tube and irradiated at 369 nm. The reaction was monitored by ^{1}H NMR, and after 13 h a maximum amount of 68% of the original complex had reacted to a new species, the ^{1}H NMR resonances of which could be attributed to [**5**(CD_3CN)]$^{2+}$ (see Discussion of the NMR results). ^{1}H NMR (400 MHz, acetonitrile-d_3): δ = 9.97 (d, J = 5.7 Hz, 1H, *py*–triazole), 8.57 (s, 1H, py–*triazole*), 8.03 (dd, J = 8.1, 7.7 Hz, 1H, *py*–triazole), 8.02 (s, 1H, *triazole*), 7.98 (d, J = 8.1 Hz, 1H, *py*–triazole), 7.84 (s, 1H, *triazole*), 7.59 (dd, J = 7.4, 5.8 Hz, *py*–triazole), 7.57 (s, 1H, *triazole*), 7.44–7.20 (m, 18H, *Ph*–CH_2–triazole), 6.91–6.85 (m, 2H, *Ph*–CH_2–triazole), 5.67 (d, J = 15.0 Hz, 1H, Ph–CH_2–triazole), 5.66 (s, 2H, Ph–CH_2–triazole), 5.63 (s, 2H, Ph–CH_2–triazole), 5.61 (d, J = 15.0 Hz, 1H, triazole–CH_2–N_{amine}), 5.31 (d, J = 14.8 Hz, 1H, triazole–CH_2–N_{amine}), 5.16 (s, 2H, Ph–CH_2–triazole), 4.79 (d, J = 14.8 Hz, 1H, triazole–CH_2–N_{amine}), 4.66 (d, J = 15.6 Hz, 1H, triazole–CH_2–N_{amine}), 4.56 (d, J = 15.8 Hz, 1H, triazole–CH_2–N_{amine}), 3.80 (d, J = 16.0 Hz, 1H, triazole–CH_2–N_{amine}), 3.76 (d, J = 16.4 Hz, 1H, triazole–CH_2–N_{amine}) ppm.

[Ru(L^4)(L^8)(CD_3CN)](PF_6)$_2$ {[6(CD_3CN)](PF_6)$_2$}: A solution of **6**(PF_6)$_2$ in CD_3CN (0.7 mL, 5 mmol/L) was put in an NMR tube and irradiated at 369 nm. The reaction was monitored by ^{1}H NMR, and after 10 h a maximum amount of 92% of the original complex had reacted to two new species, the ^{1}H NMR resonances of which could be attributed to [**6a**(CD_3CN)]$^{2+}$ and [**6b**(CD_3CN)]$^{2+}$ (see Discussion of the NMR results). Complex [**6a**(CH_3CN)]$^{2+}$: ^{1}H NMR (400 MHz, acetonitrile-d_3) δ = 8.37 (s, 1H, *triazole*), 8.28 (s, 1H, *triazole*), 8.01 (s, 1H, *triazole*), 7.80 (s, 1H, *triazole*), 7.58 (s, 1H, *triazole*), 7.45–7.19 (m, 23H, *Ph*–CH_2–triazole), 6.93–6.86 (m, 2H, *Ph*–CH_2–triazole), 5.81 (d, J = 15.2 Hz, 1H, Ph–CH_2–triazole), 5.76 (d, J = 15.2 Hz, 1H, Ph–CH_2–triazole), 5.64 (s, 2H, Ph–CH_2–triazole), 5.62 (s, 2H, Ph–CH_2–triazole), 5.57 (s, 2H, Ph–CH_2–triazole), 5.28 (d, J = 15.0 Hz, 1H, triazole–CH_2–N_{amine}), 5.20 (d, J = 15.0 Hz, 1H, Ph–CH_2–triazole), 5.15 (d, J = 15.0 Hz, 1H, Ph–CH_2–triazole), 4.78 (d, J = 14.7 Hz, 1H, triazole–CH_2–N_{amine}), 4.66 (d, J = 15.8 Hz, 1H, triazole–CH_2–N_{amine}), 4.59 (d, J = 16.1 Hz, 1H, triazole–CH_2–N_{amine}), 3.80 (d, J = 16.2 Hz, 1H, triazole–CH_2–N_{amine}), 3.75 (d, J = 16.2 Hz, 1H, triazole–CH_2–N_{amine}) ppm.
Complex [**6b**(CH_3CN)]$^{2+}$: ^{1}H NMR (400 MHz, acetonitrile-d_3) δ = 8.33 (s, 2H, *triazole*–*triazole*), 7.86 (s, 2H, *triazole*$_{coord}$–CH_2–N_{amine}), 7.57 (s, 1H, *triazole*$_{free}$–CH_2–N_{amine}), 7.46–7.18 (m, 25H, *Ph*–CH_2–triazole), 5.66–5.55 (m, 4H, Ph–CH_2–tri–tri–CH_2–Ph) 5.59 (s, 4H, Ph–CH_2–triazole$_{coord}$), 5.49 (s, 2H, Ph–CH_2–triazole$_{free}$), 4.04 (d, J = 15.7 Hz, 2H, triazole$_{coord}$–CH_2–N_{amine}), 3.61 (d, J = 15.8 Hz, 2H, triazole$_{coord}$–CH_2–N_{amine}), 3.10 (s, 2H, triazole$_{free}$–CH_2–N_{amine}) ppm.

[Ru(L^5)(bpy)(CD_3CN)](PF_6)$_2$ {[8(CD_3CN)](PF_6)$_2$}: A solution of **8a**(PF_6)$_2$/**8b**(PF_6)$_2$ (28:72) in CD_3CN (0.7 mL, 5 mmol/L) was put in an NMR tube and irradiated at 369 nm. The reaction was monitored by ^{1}H NMR, and after 2 h all of the original complex molecules had reacted to two new species, the ^{1}H NMR resonances of which could be attributed to [**8a**(CD_3CN)]$^{2+}$/[**8b**(CD_3CN)]$^{2+}$ (80:20) (see Discussion of the NMR results). ^{1}H NMR (700 MHz, acetonitrile-d_3) δ = 8.59 (d, J = 8.2 Hz, 2H, **a**/**b**, bpy), 8.41 (s, 0.80H, **a**, Ph–*triazole*, coordinated), 8.38 (s, 1.20H, **a**/**b**, iPr–Ph–*triazole*, coordinated) 8.38–8.36 (m, 2H, **a**/**b**, bpy), 8.26 (s, 0.20H, **b**, Ph–*triazole*, de-coordinated), 8.22 (s, 0.80H, **a**, iPr–Ph–*triazole*, de-coordinated), 8.20–8.17 (m, 2H, **a**/**b**, bpy), 7.90–7.87, 7.81–7.77, 7.70–7.58, 7.54–7.51, 7.50–7.47 (5 multiplets, 15H, **a**/**b**, bpy, *Ph*–triazole, iPr–*Ph*–triazole), 4.43 (d, J = 16.3 Hz, 1.20H, **a**/**b**, iPr–Ph–triazole–CH_2, coordinated), 4.42 (d, J = 16.3 Hz, 0.80H, **a**, Ph–triazole–CH_2, coordinated), 3.99 (d, J = 16.3 Hz, 1.20H, **a**/**b**, iPr–Ph–triazole–CH_2, coordinated) , 3.98 (d, J = 16.3 Hz, 0.80H, **a**, Ph–triazole–CH_2, coordinated), 3.44 (s, 0.40H, **b**, Ph–triazole–CH_2, de-coordinated), 3.43 (s, 1.60H, **a**, iPr–Ph–triazole–CH_2, de-coordinated), 3.05 (hept, J = 6.8 Hz, 2H, **a**/**b**, *iPr*–Ph), 1.31–1.29 (d, J = 6.8 Hz, 2.40H, **b**, *iPr*–Ph, coordinated; d, J = 6.8 Hz, 4.80H, **a**, *iPr*–Ph, coordinated; d, J = 6.8 Hz, 4.80H, **a**, *iPr*–Ph, de-coordinated) ppm.

^{1}H NMR spectra

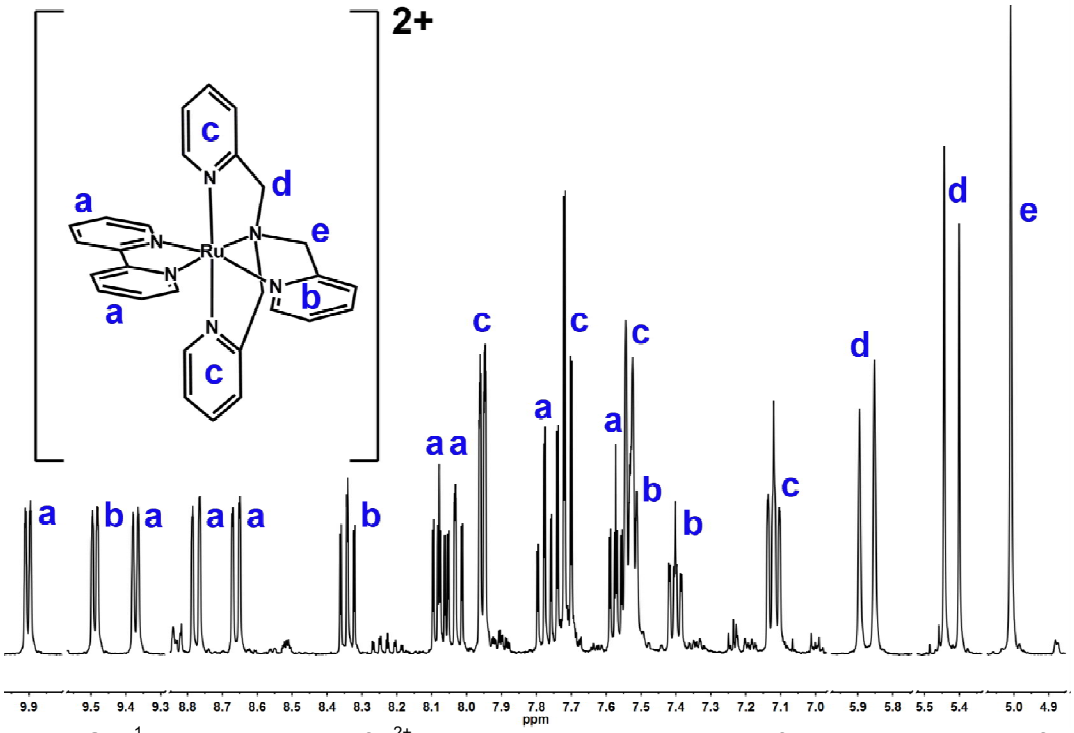

Figure S1. ^{1}H NMR spectrum of $\mathbf{1}^{2+}$ recorded in acetone-d_6. Parts of the spectrum are cut for better visibility of the signals.

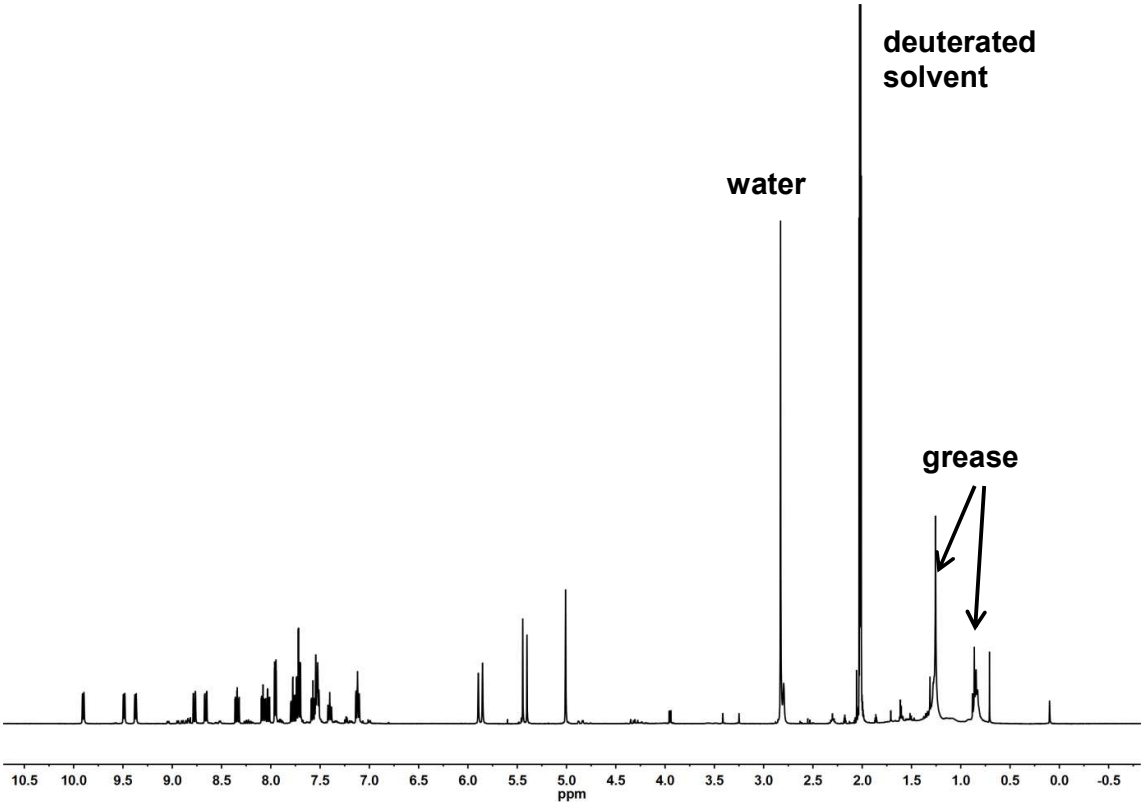

Figure S2. Full ^{1}H NMR spectrum of $\mathbf{1}^{2+}$ recorded in acetone-d_6. Solvent impurities are indicated.

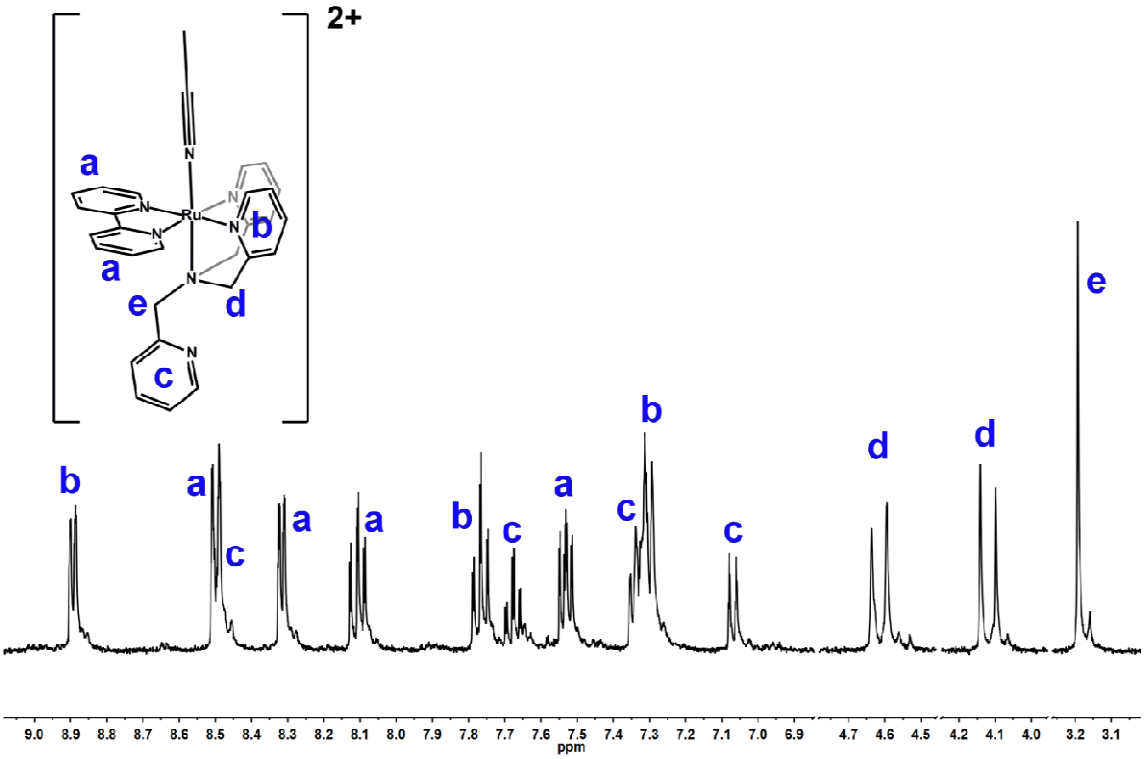

Figure S3. ^{1}H NMR spectrum of [**1**(CD$_3$CN)]$^{2+}$ recorded in acetonitrile-d$_3$. Parts of the spectrum are cut for better visibility of the signals.

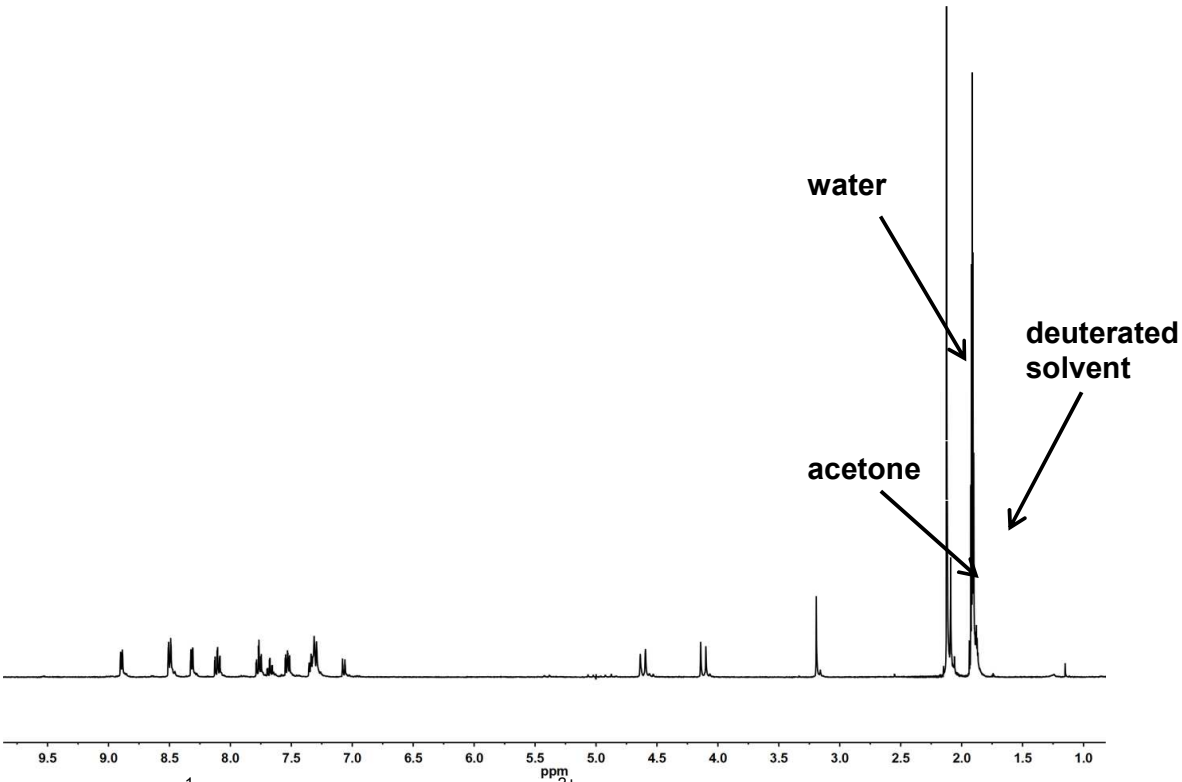

Figure S4. Full ^{1}H NMR spectrum of [**1**(CD$_3$CN)]$^{2+}$ recorded in acetonitrile-d$_3$. Solvent impurities are indicated.

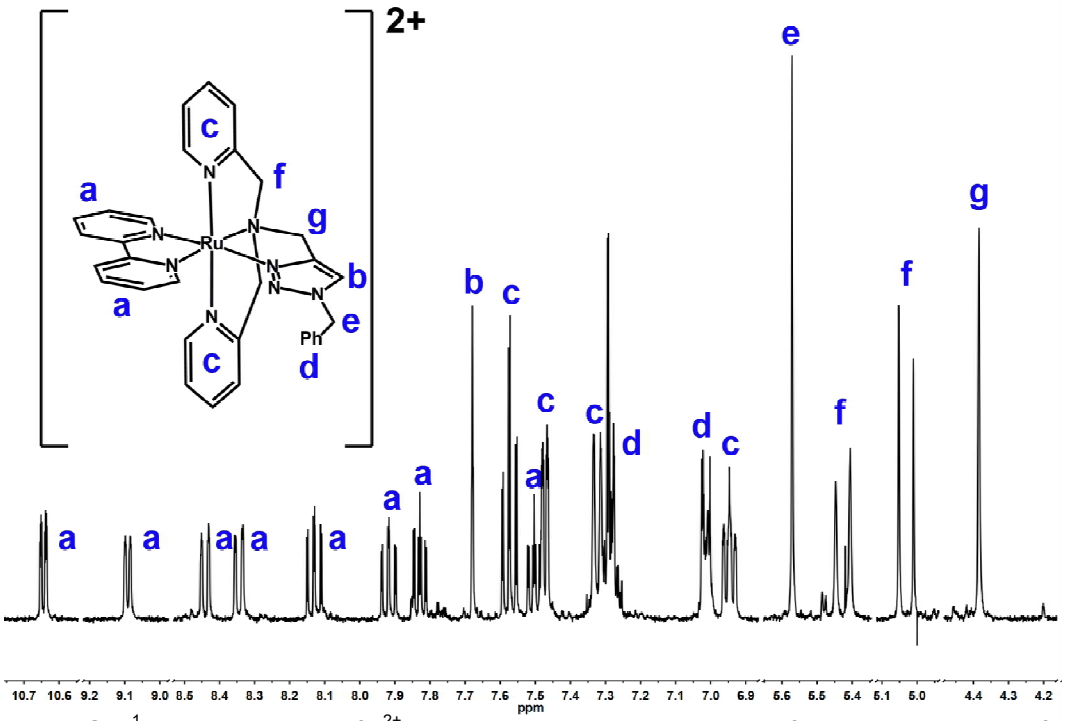

Figure S5. ^{1}H NMR spectrum of $\mathbf{2}^{2+}$ recorded in acetonitrile-d_3. Parts of the spectrum are cut for better visibility of the signals.

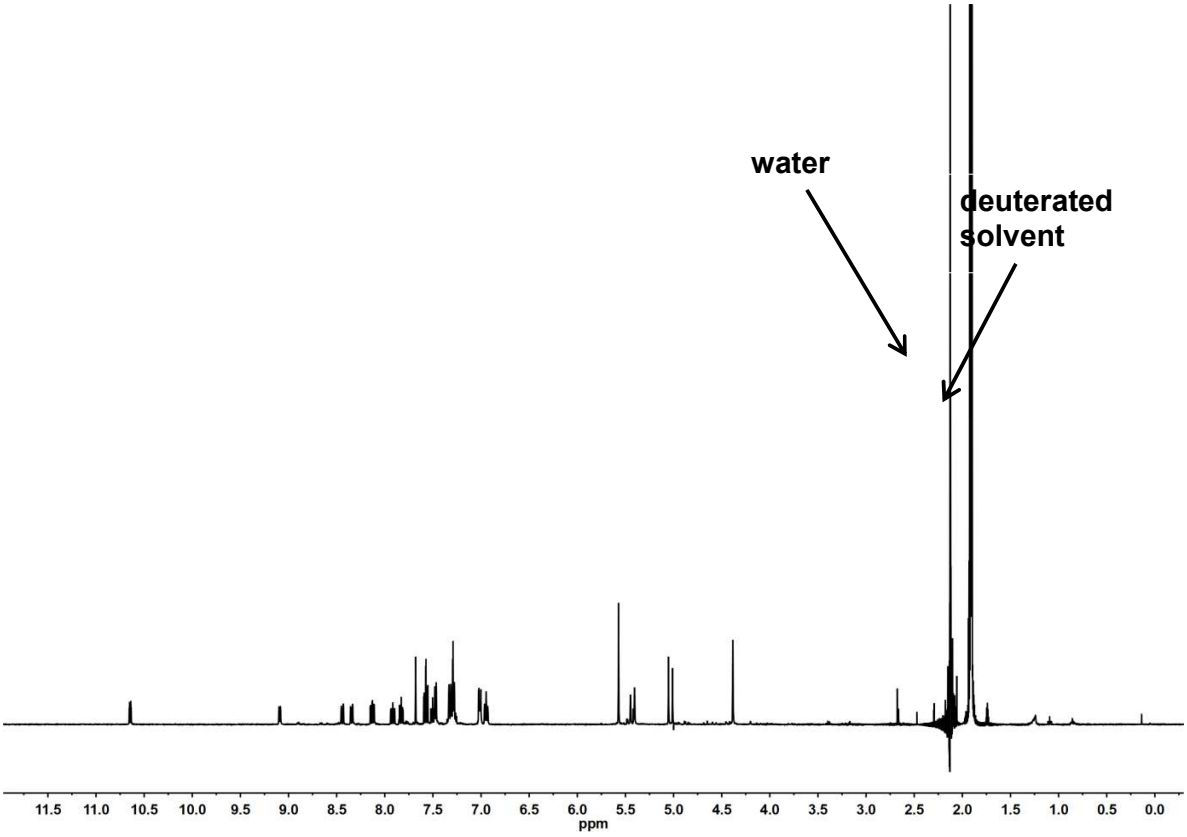

Figure S6. Full ^{1}H NMR spectrum of $\mathbf{2}^{2+}$ recorded in acetonitrile-d_3. Solvent impurities are indicated.

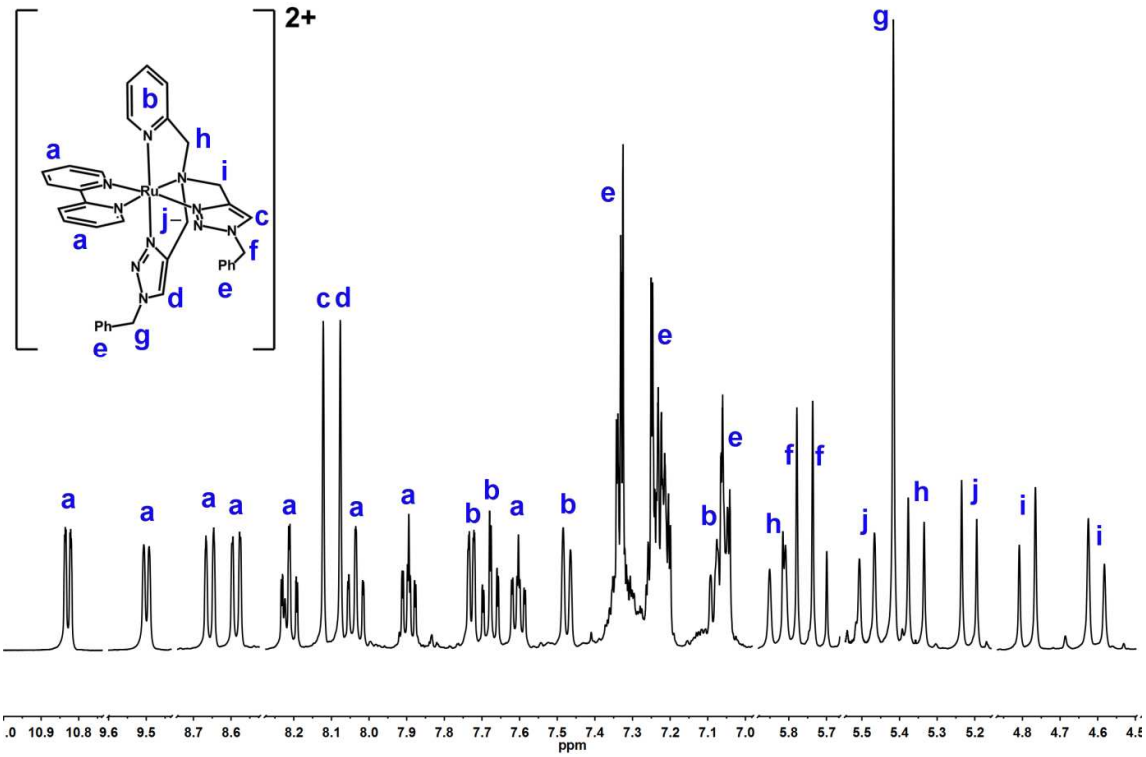

Figure S7. ^{1}H NMR spectrum of $\mathbf{3}^{2+}$ recorded in acetone-d_6. Parts of the spectrum are cut for better visibility of the signals.

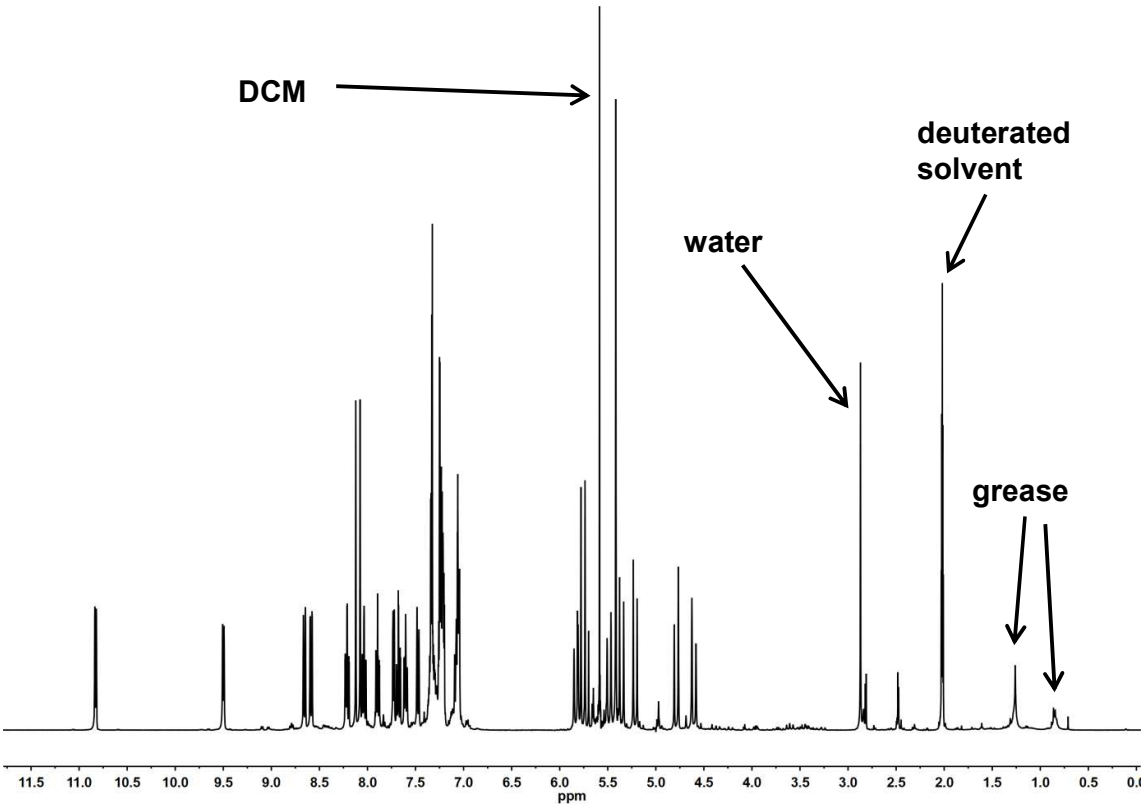

Figure S8. Full ^{1}H NMR spectrum of $\mathbf{3}^{2+}$ recorded in acetone-d_6. Solvent impurities are indicated.

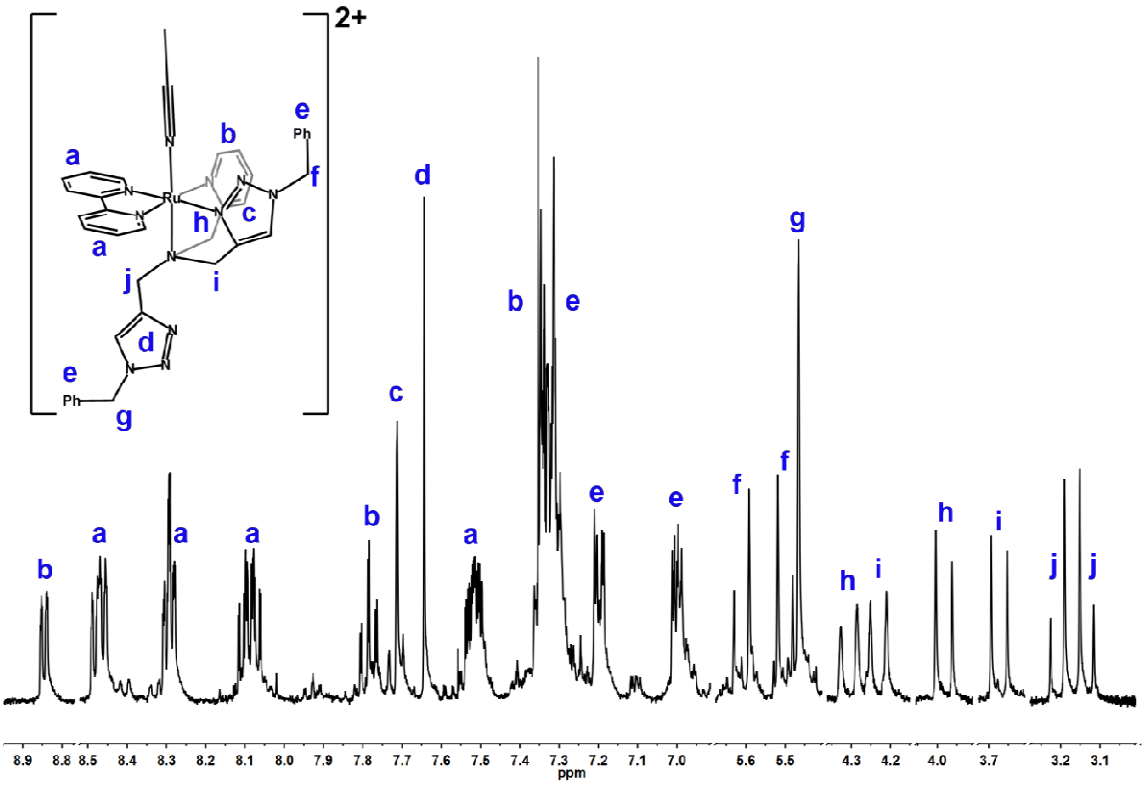

Figure S9. ^{1}H NMR spectrum of [**3**(CD_3CN)]$^{2+}$ recorded in acetonitrile-d_3. Parts of the spectrum are cut for better visibility of the signals.

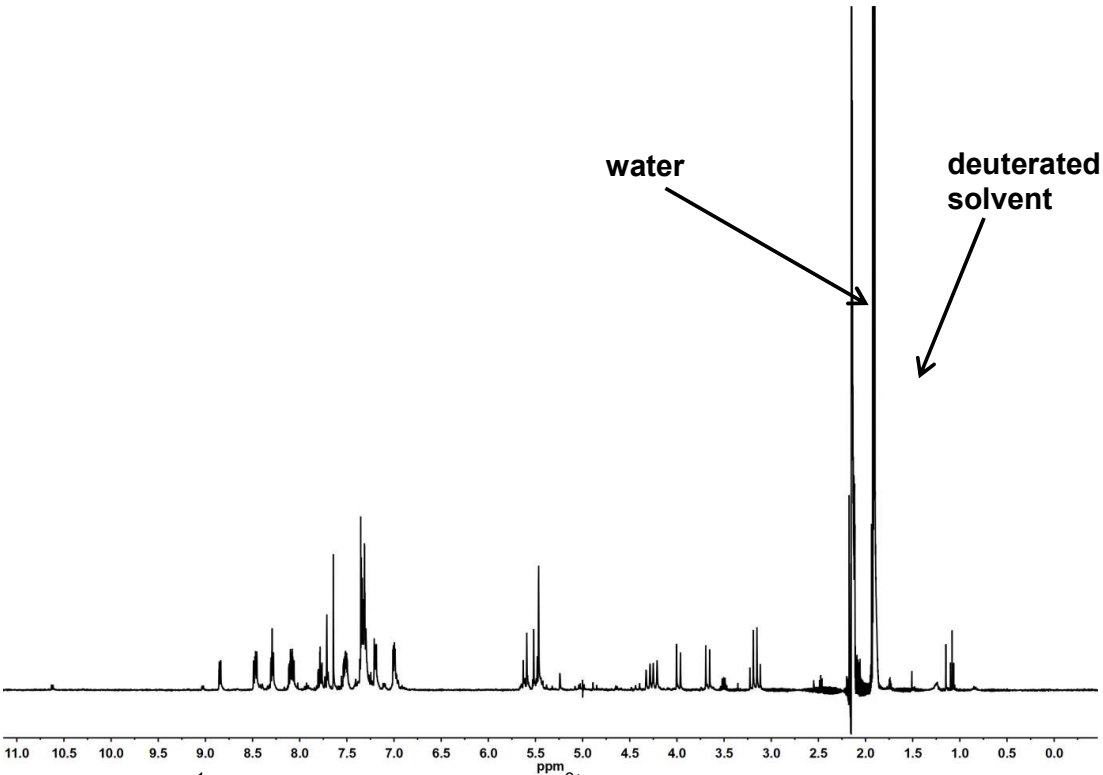

Figure S10. Full ^{1}H NMR spectrum of [**3**(CD_3CN)]$^{2+}$ recorded in acetonitrile-d_3. Solvent impurities are indicated.

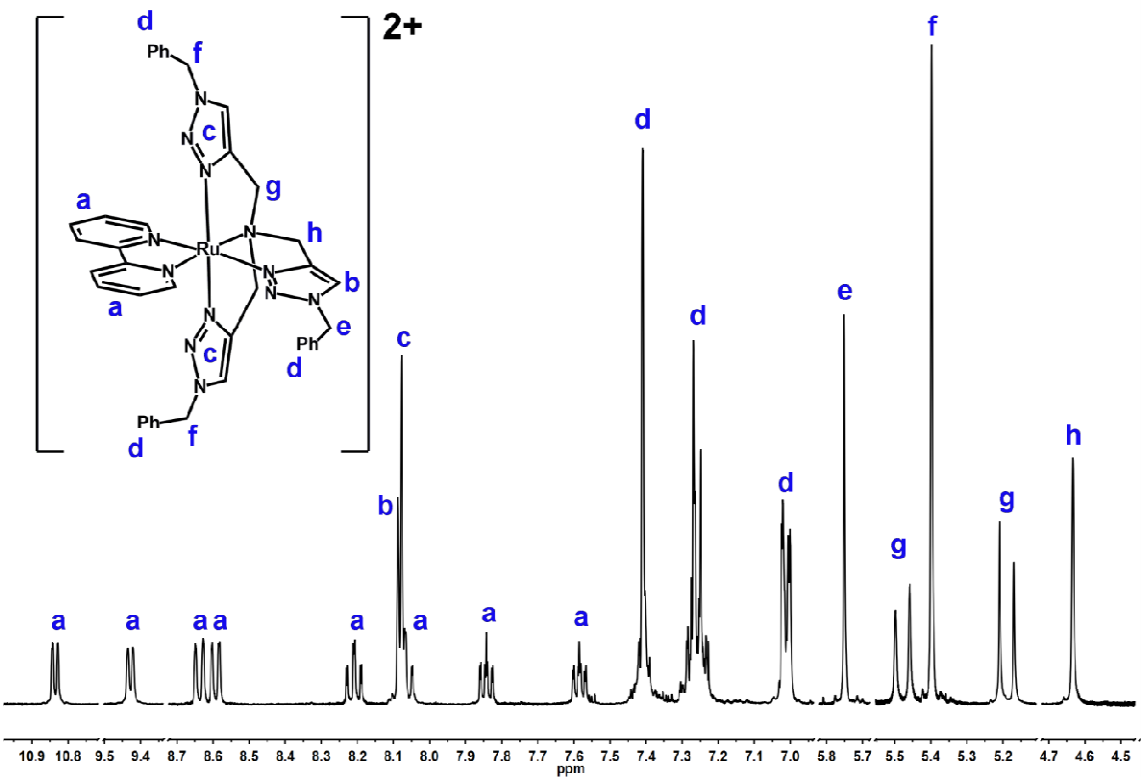

Figure S11. ^{1}H NMR spectrum of $\mathbf{4}^{2+}$ recorded in acetone-d_6. Parts of the spectrum are cut for better visibility of the signals.

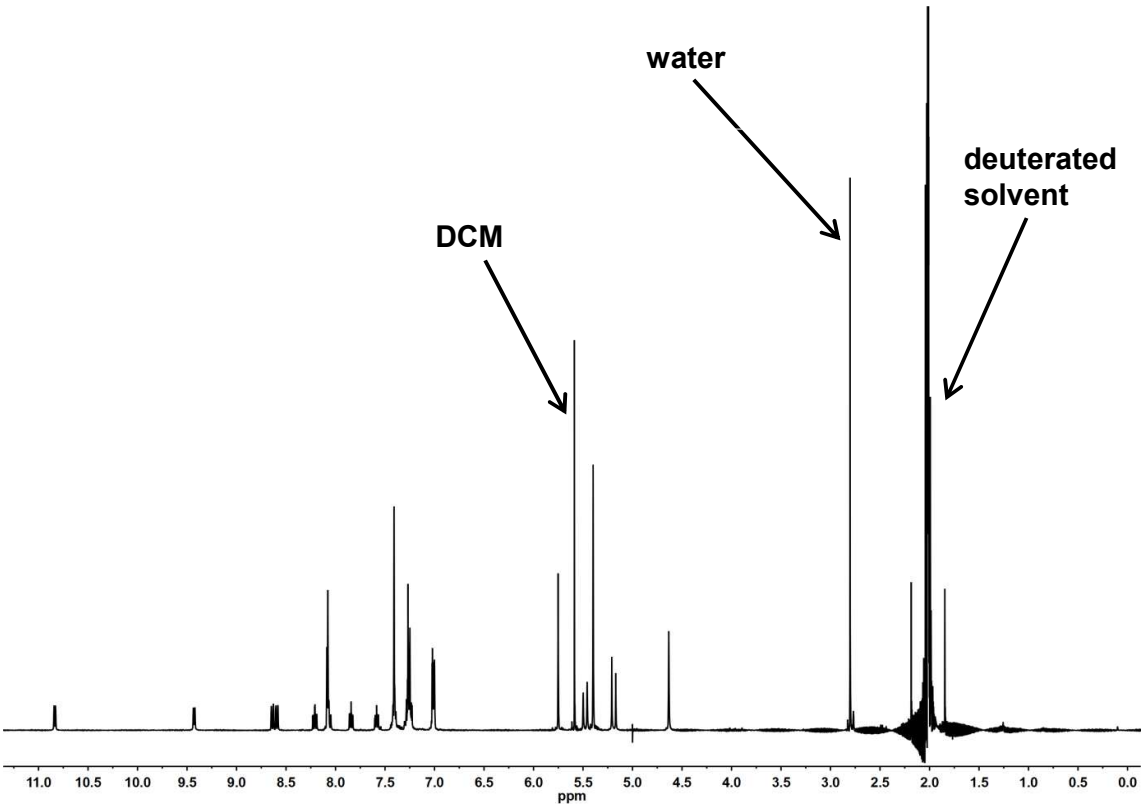

Figure S12. Full ^{1}H NMR spectrum of $\mathbf{4}^{2+}$ recorded in acetone-d_6. Solvent impurities are indicated.

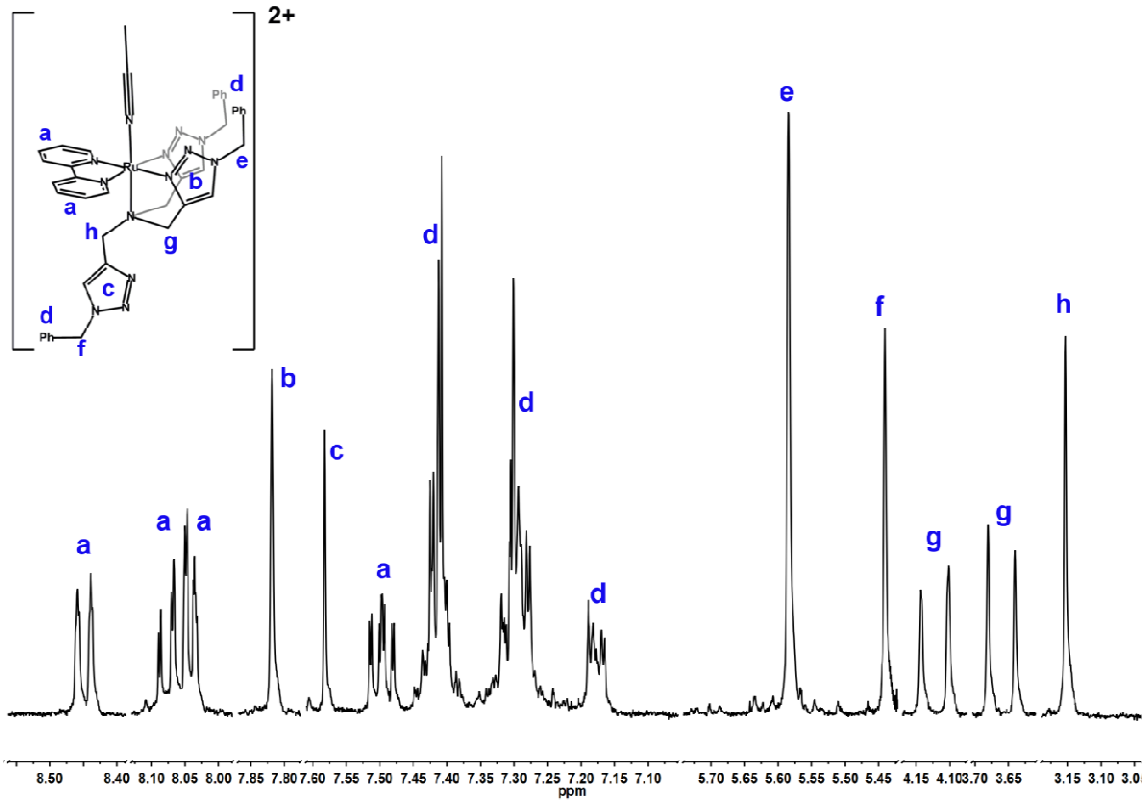

Figure S13. ^{1}H NMR spectrum of [**4**$(CD_3CN)]^{2+}$ recorded in acetonitrile-d_3. Parts of the spectrum are cut for better visibility of the signals.

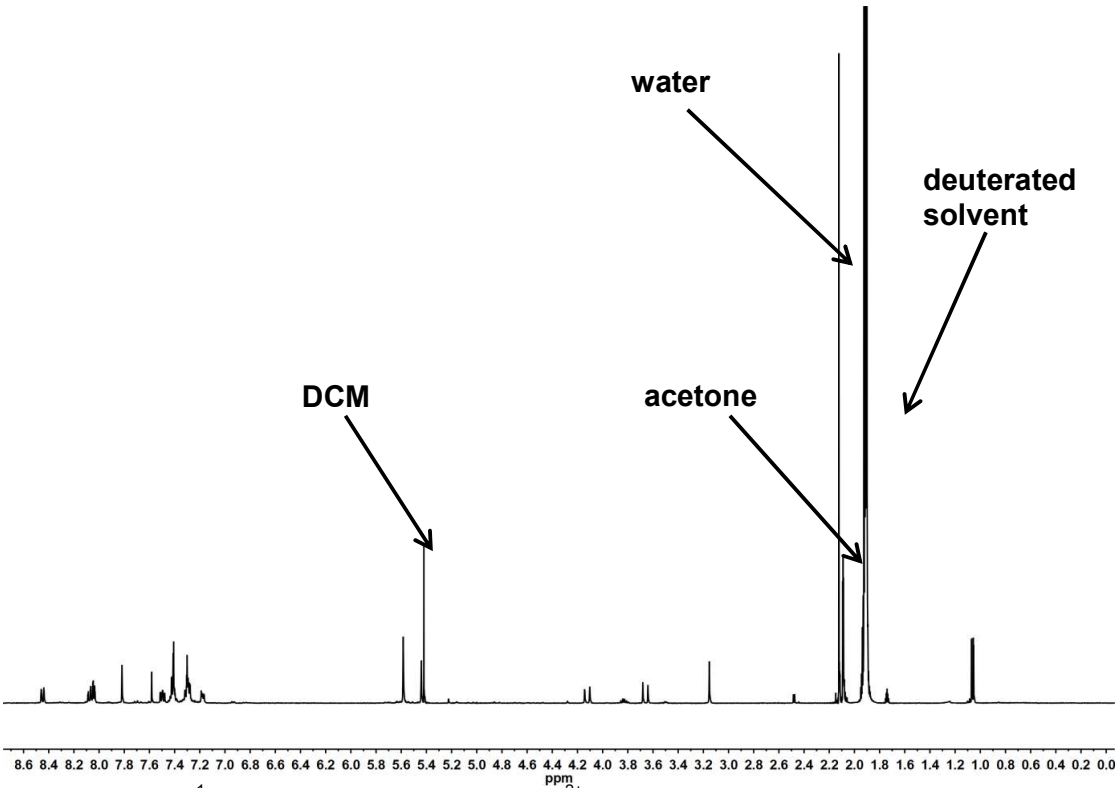

Figure S14. Full ^{1}H NMR spectrum of [**4**$(CD_3CN)]^{2+}$ recorded in acetonitrile-d_3. Solvent impurities are indicated.

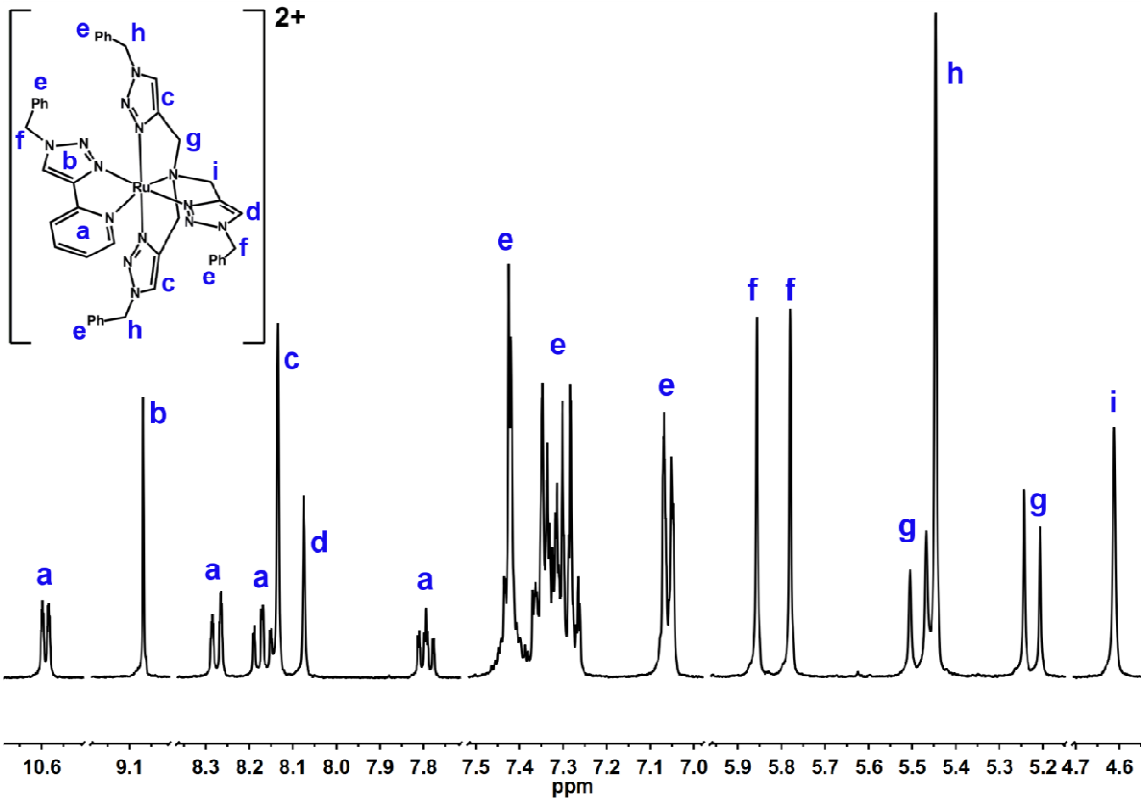

Figure S15. ^{1}H NMR spectrum of $\mathbf{5}^{2+}$ recorded in acetone-d_6. Parts of the spectrum are cut for better visibility of the signals.

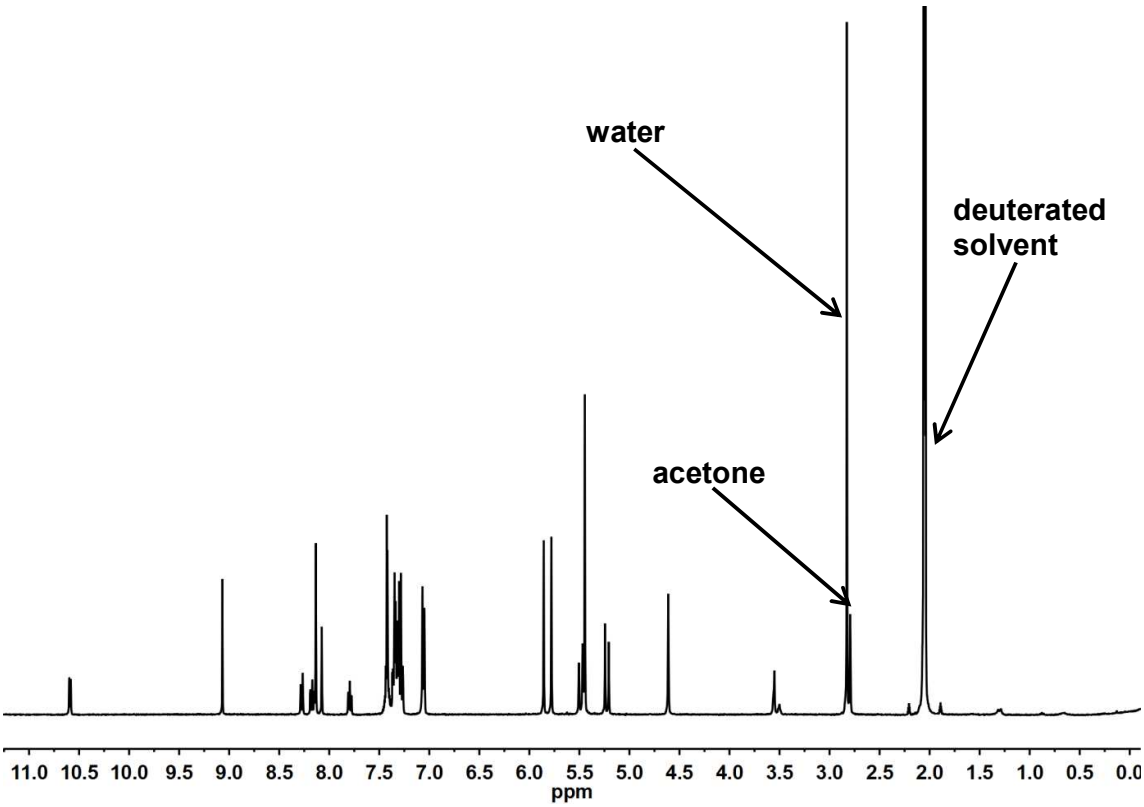

Figure S16. Full ^{1}H NMR spectrum of $\mathbf{5}^{2+}$ recorded in acetone-d_6. Solvent impurities are indicated.

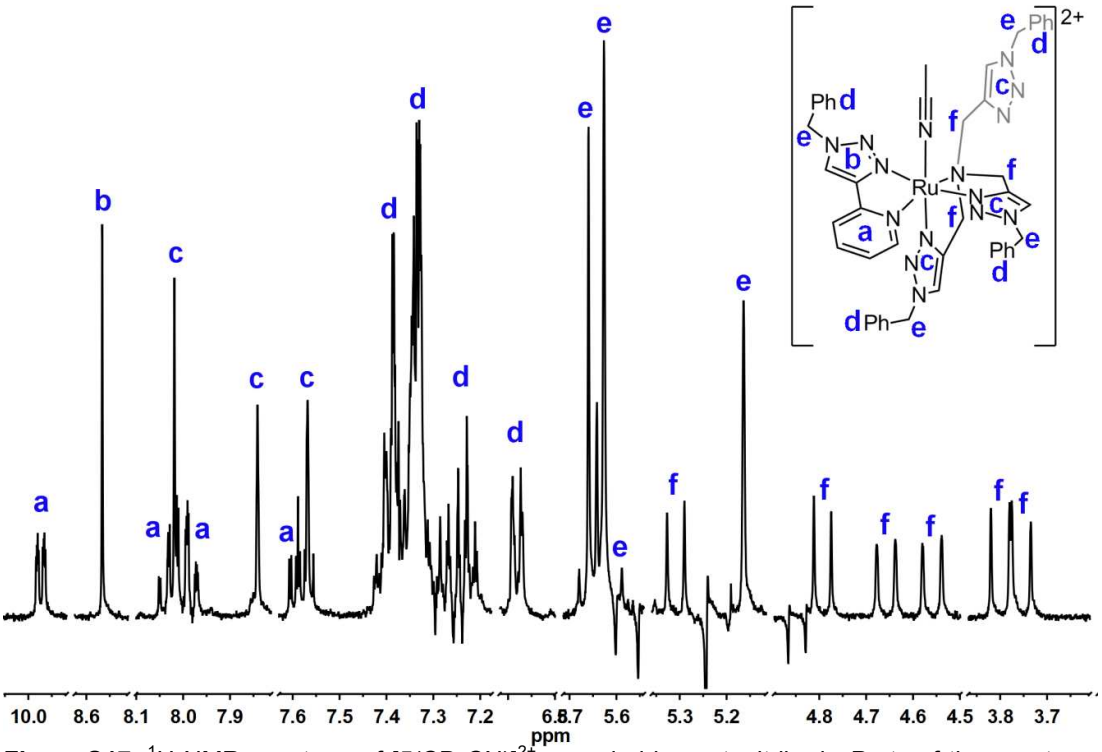

Figure S17. ^{1}H NMR spectrum of [**5**$(CD_3CN)]^{2+}$ recorded in acetonitrile-d_3. Parts of the spectrum are cut for better visibility of the signals. The conversion of $\mathbf{5}^{2+}$ to [**5**$(CD_3CN)]^{2+}$ was 68%, and the resonances of $\mathbf{5}^{2+}$ were subtracted to facilitate the assignment of resonances of [**5**$(CD_3CN)]^{2+}$.

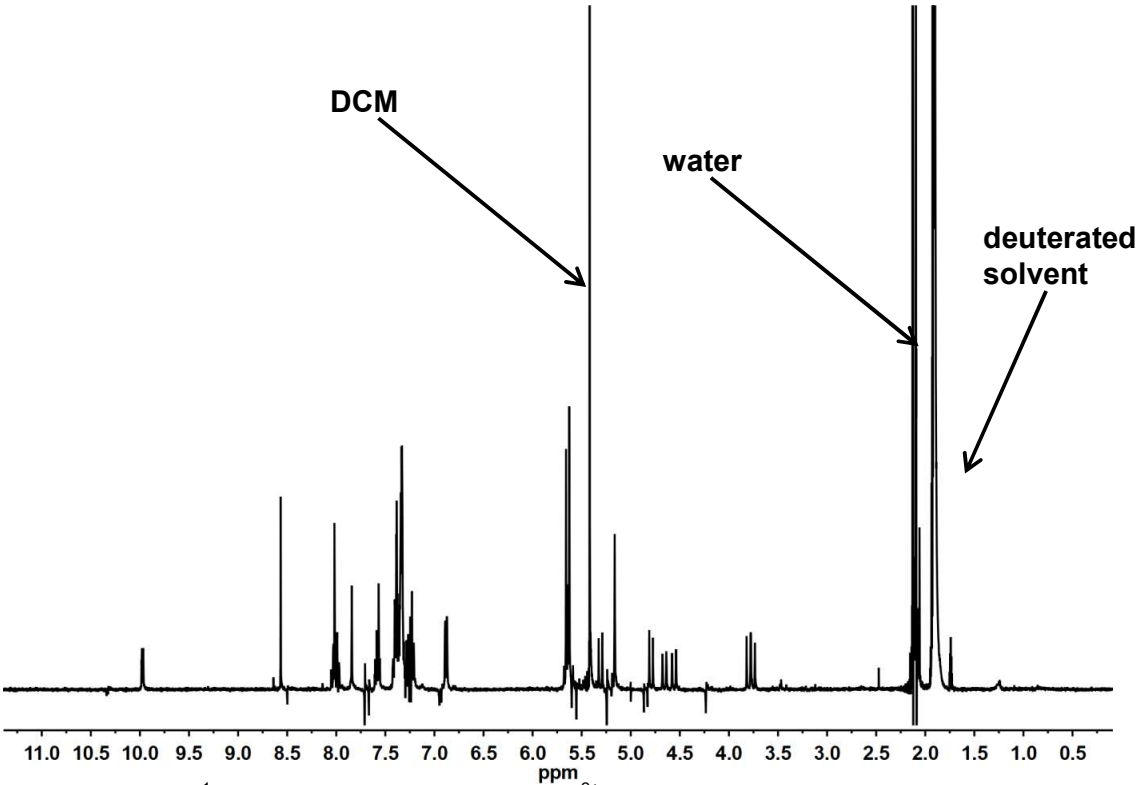

Figure S18. Full ^{1}H NMR spectrum of [**5**$(CD_3CN)]^{2+}$ recorded in acetonitrile-d_3. The resonances of remaining $\mathbf{5}^{2+}$ were subtracted to facilitate the assignment of resonances of [**5**$(CD_3CN)]^{2+}$. Solvent impurities are indicated.

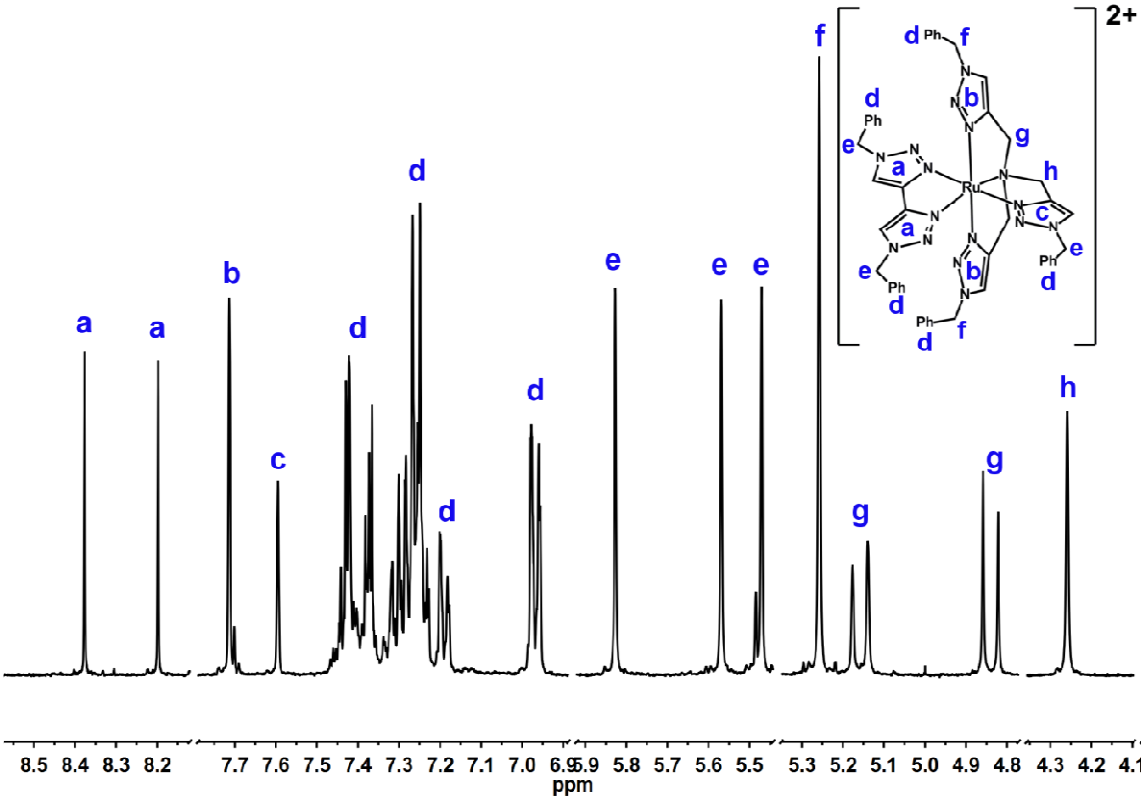

Figure S19. ^{1}H NMR spectrum of $\mathbf{6}^{2+}$ recorded in acetonitrile-d_3. Parts of the spectrum are cut for better visibility of the signals.

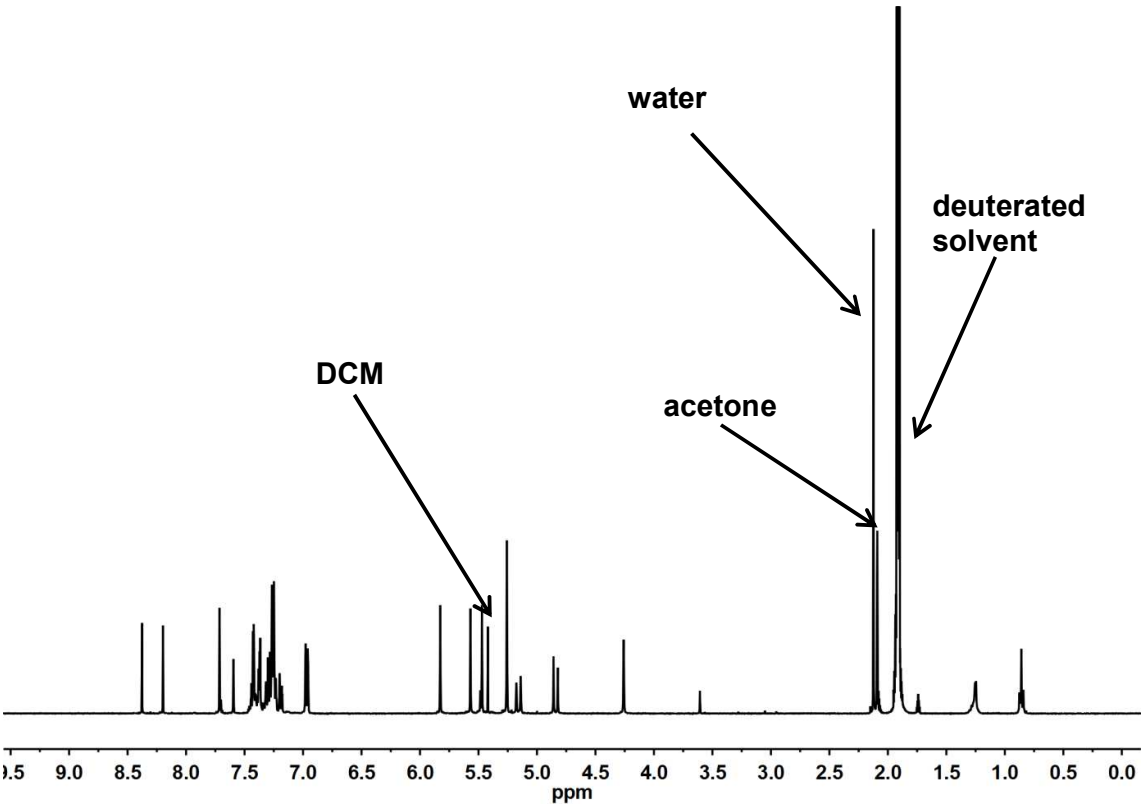

Figure S20. Full ^{1}H NMR spectrum of $\mathbf{6}^{2+}$ recorded in acetonitrile-d_3. Solvent impurities are indicated.

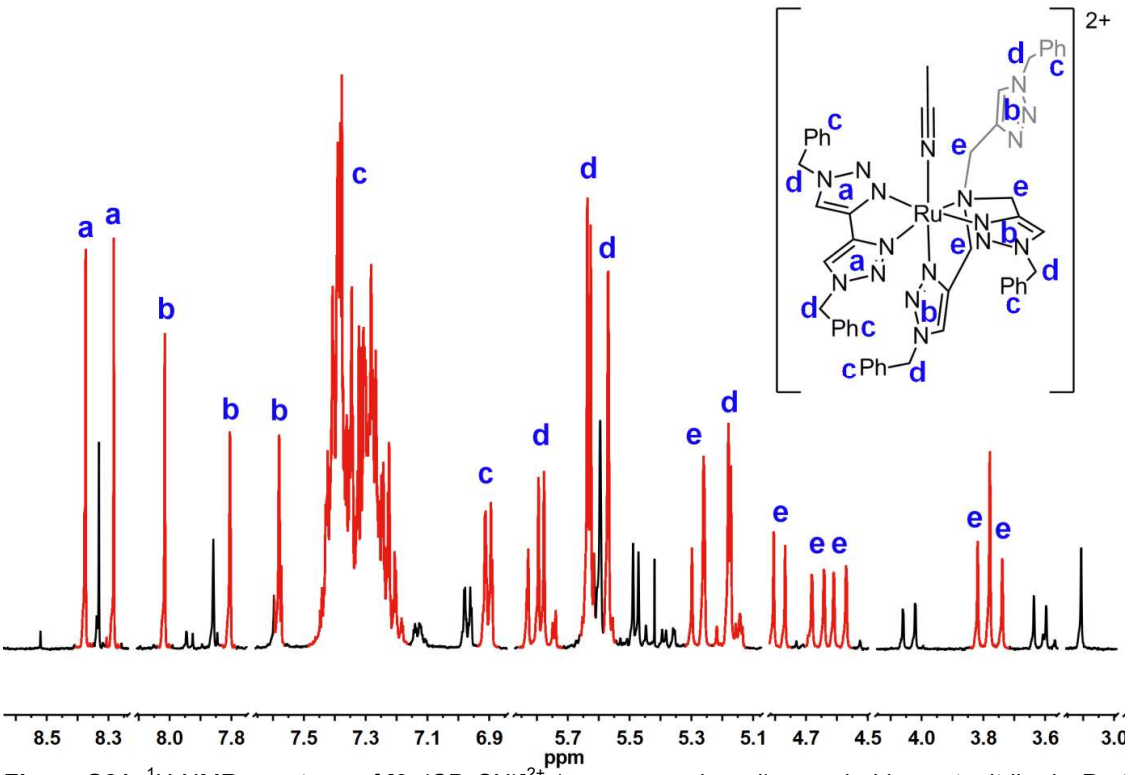

Figure S21. ^{1}H NMR spectrum of [**6a**$(CD_3CN)]^{2+}$ (resonances in red) recorded in acetonitrile-d_3. Parts of the spectrum are cut for better visibility of the signals. The conversion of $\mathbf{6}^{2+}$ to [**6a**$(CD_3CN)]^{2+}$ was ca. 74%.

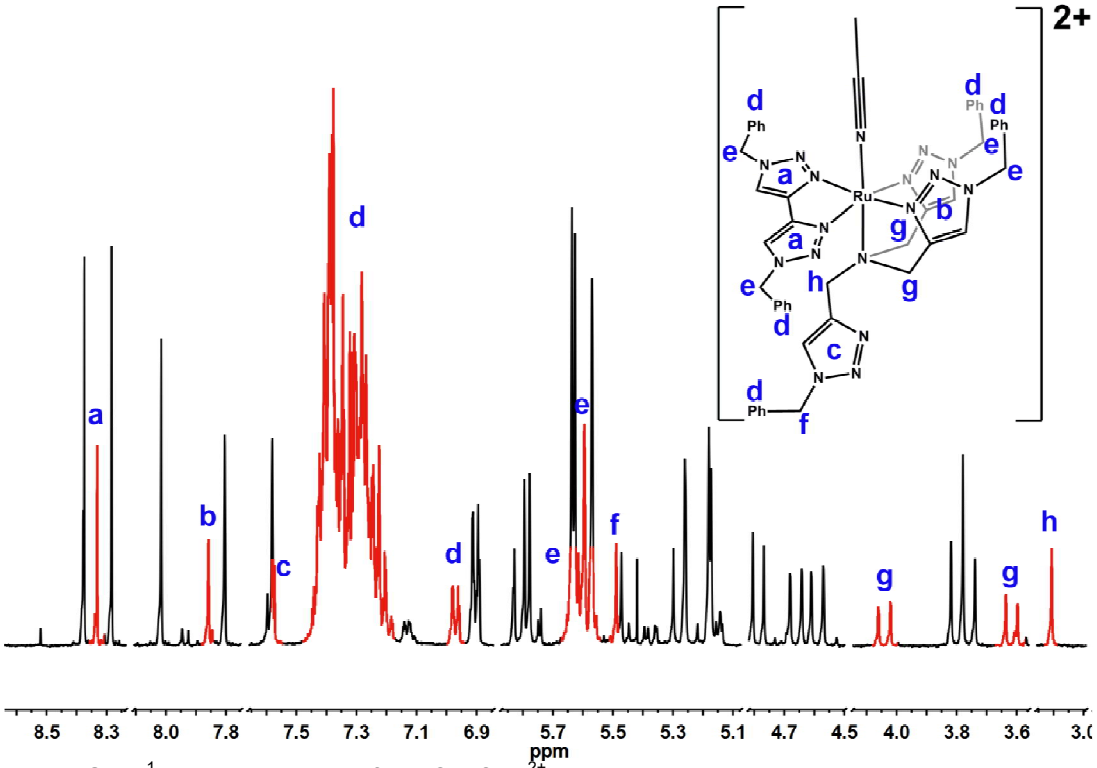

Figure S22. ^{1}H NMR spectrum of [**6b**$(CD_3CN)]^{2+}$ (resonances in red) recorded in acetonitrile-d_3. Parts of the spectrum are cut for better visibility of the signals. The conversion of $\mathbf{6}^{2+}$ to [**6b**$(CD_3CN)]^{2+}$ was ca. 8%.

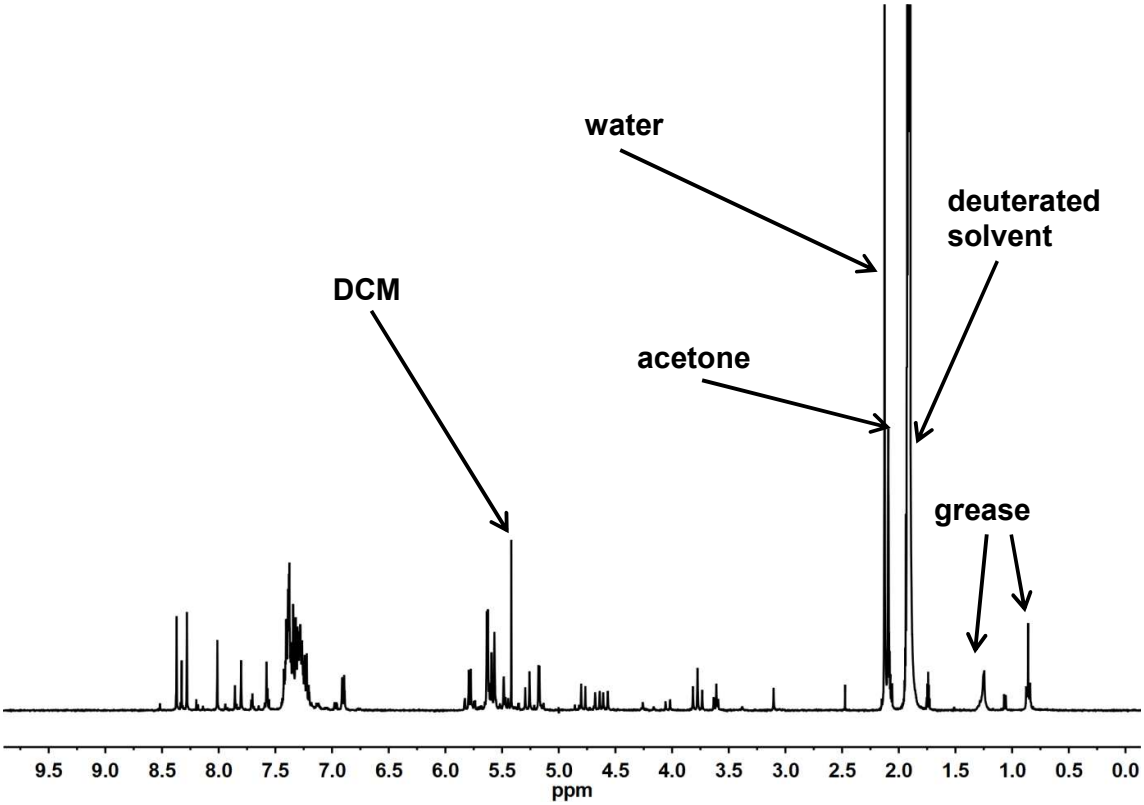

Figure S23. Full ^{1}H NMR spectrum of [**6a**$(CD_3CN)]^{2+}$ and [**6b**$(CD_3CN)]^{2+}$ recorded in acetonitrile-d_3. Solvent impurities are indicated.

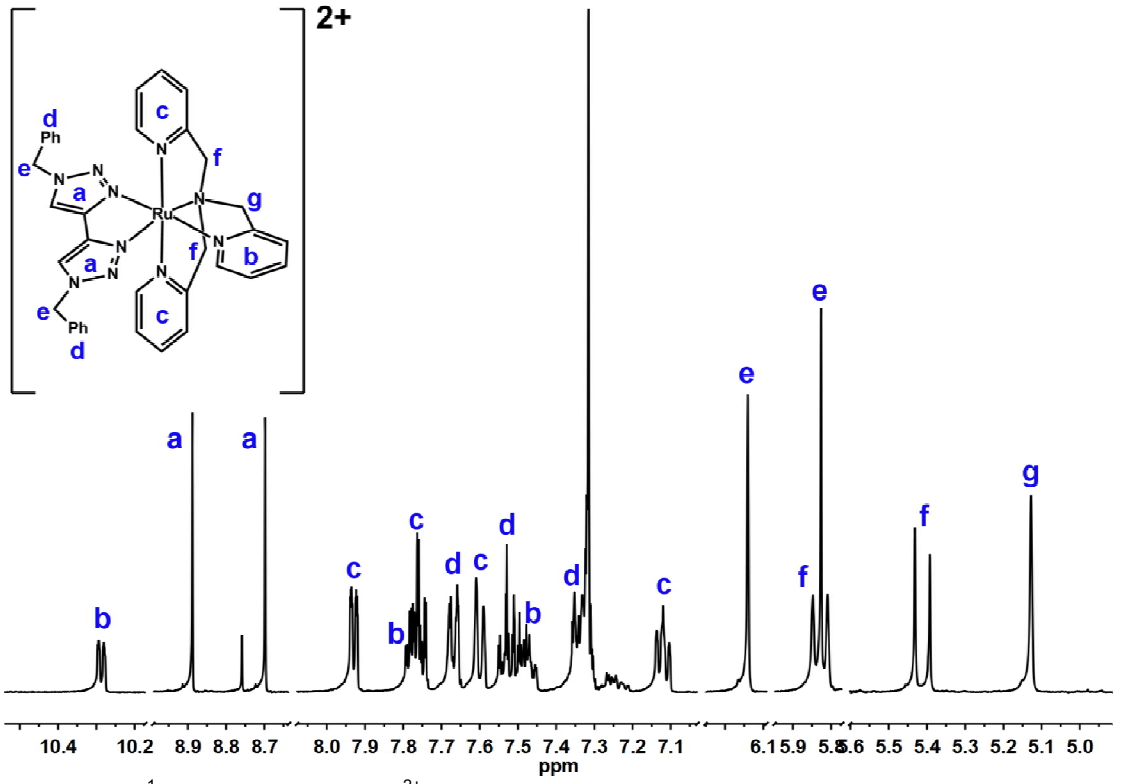

Figure S24. ^{1}H NMR spectrum of $\mathbf{7}^{2+}$ recorded in acetone-d_6. Parts of the spectrum are cut for better visibility of the signals.

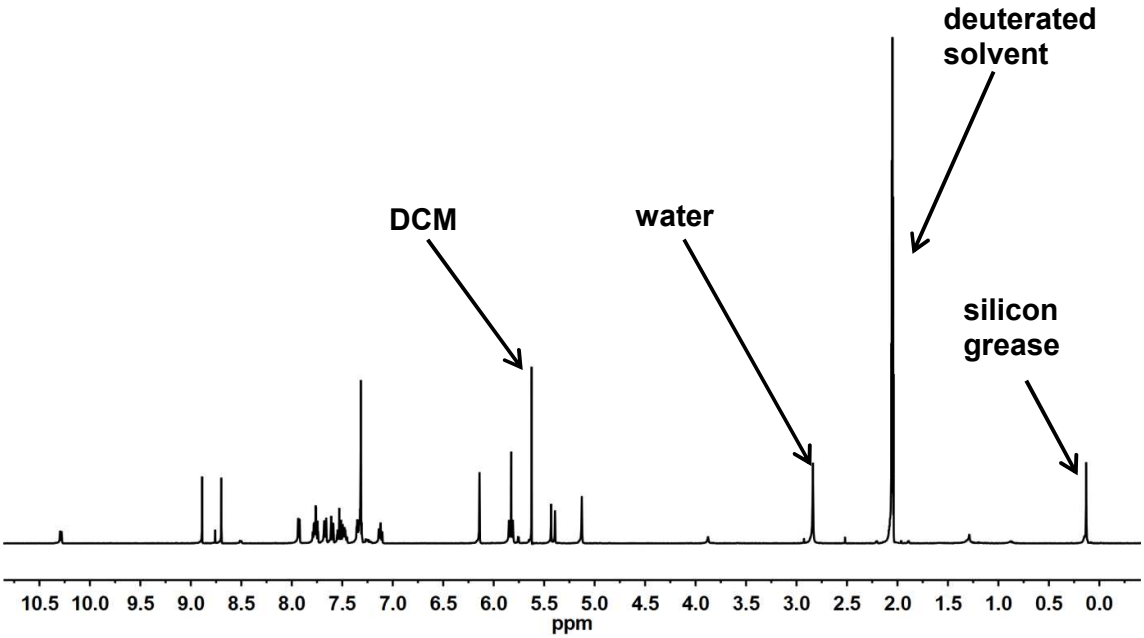

Figure S25. Full ^{1}H NMR spectrum of $\mathbf{7}^{2+}$ recorded in acetone-d_6. Solvent impurities are indicated.

Crystal Structures

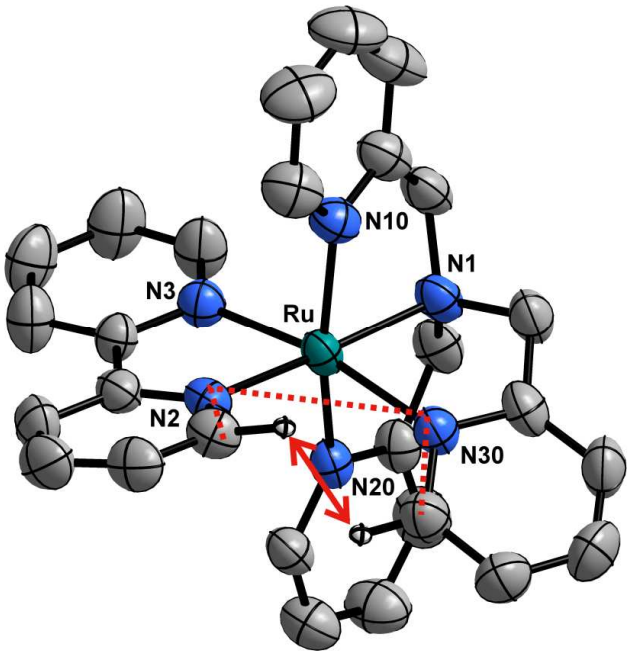

Figure S26. Perspective view of $\mathbf{1}^{2+}$.[3] The thermal ellipsoids are drawn at the 50% probability level. All but 2 H atoms, counterions, and crystal solvent molecules are omitted for clarity. The red dotted line indicates the torsion angle between the two adjacent pyridine rings in the equatorial plane. The double-headed red arrow indicates the steric repulsion between two C–H bonds in the equatorial plan.

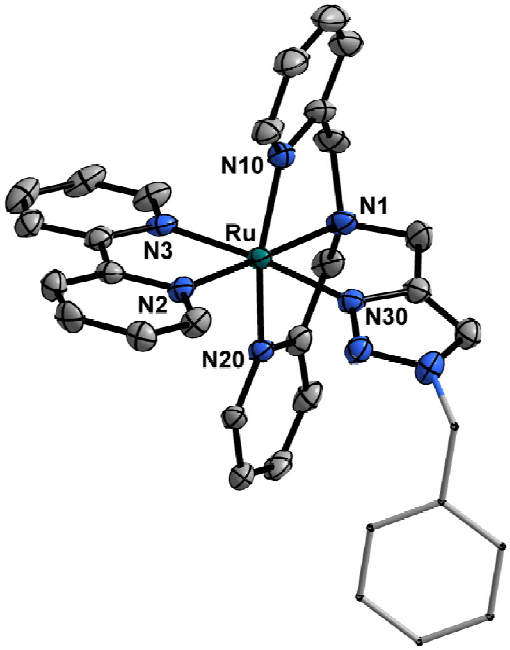

Figure S27. Perspective view of $\mathbf{2}^{2+}$. The thermal ellipsoids are drawn at the 50% probability level, and the benzyl moieties are drawn as stick models. H atoms, counterions, and crystal solvent molecules are omitted for clarity.

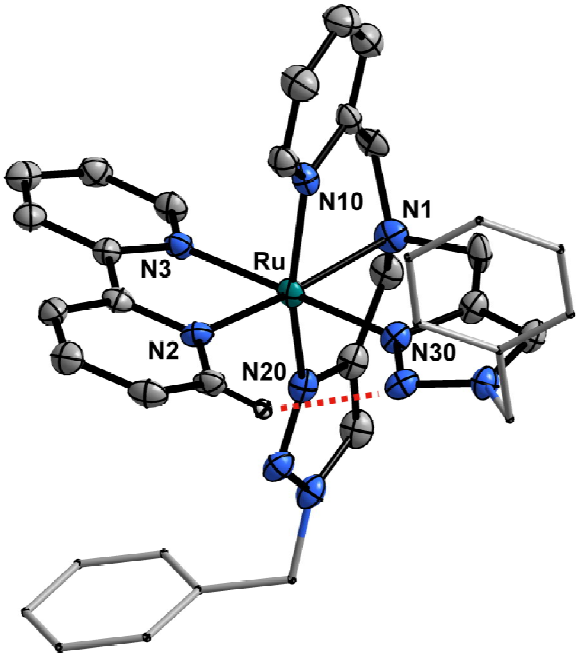

Figure S28. Perspective view of $\mathbf{3}^{2+}$. The thermal ellipsoids are drawn at the 50% probability level, and the benzyl moieties are drawn as stick models. All but 1 H atom, counterions, and crystal solvent molecules are omitted for clarity. The red dotted line indicates a short C–H···N contact.

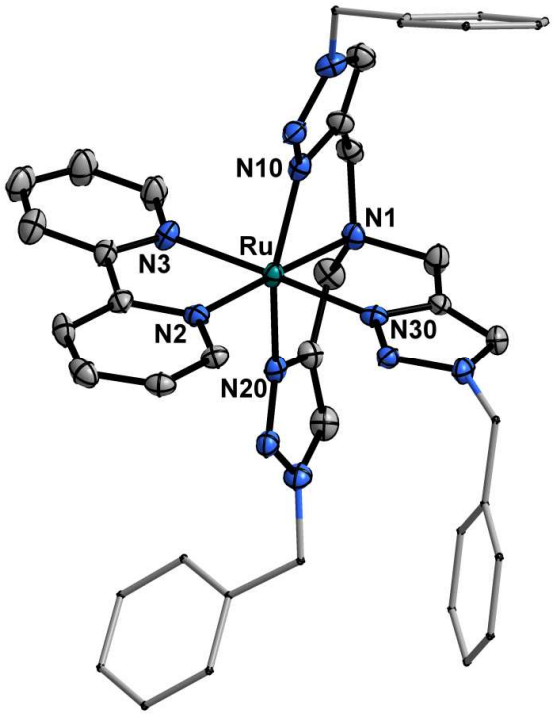

Figure S29. Perspective view of $\mathbf{4}^{2+}$. The thermal ellipsoids are drawn at the 50% probability level, and the benzyl moieties are drawn as stick models. H atoms, counterions, and crystal solvent molecules are omitted for clarity.

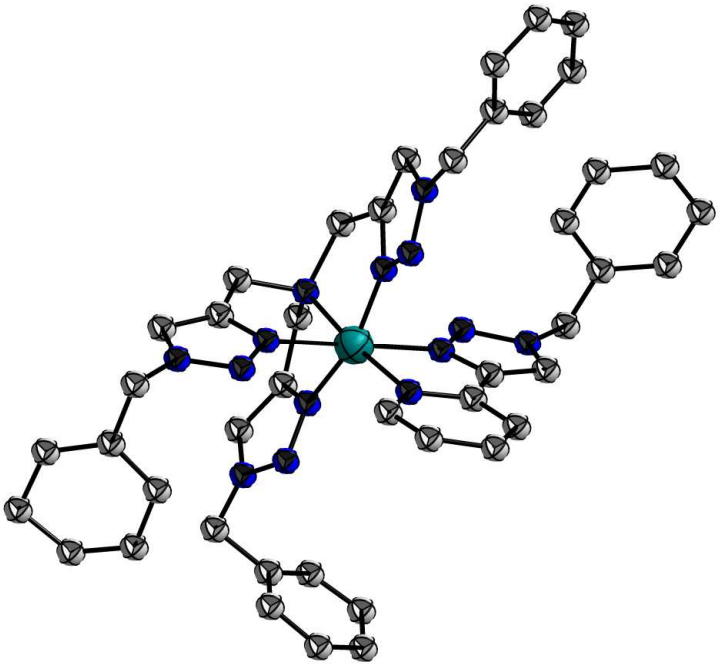

Figure S30. Perspective view of $\mathbf{5}^{2+}$ (ball-and-stick model). H atoms, counterions, and crystal solvent molecules are omitted for clarity.

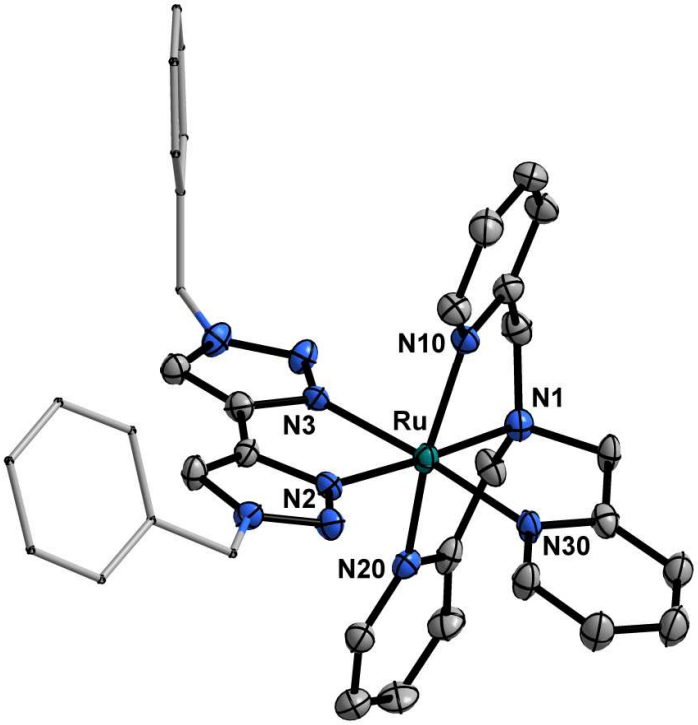

Figure S31. Perspective view of $\mathbf{7}^{2+}$. The thermal ellipsoids are drawn at the 50% probability level, and the benzyl moieties are drawn as stick models. H atoms, counterions, and crystal solvent molecules are omitted for clarity.

Table S1. Important bondlengths and angles of $\mathbf{1}^{2+}$–$\mathbf{4}^{2+}$ and $\mathbf{7}^{2+}$. Lengths of bonds featuring triazoles are highlighted in grey. [a] Atom numbering is different in $\mathbf{1}^{2+}$.[3]

[Å] [a]	$\mathbf{1}^{2+}$ [3]	$\mathbf{2}^{2+}$	$\mathbf{3}^{2+}$	$\mathbf{4}^{2+}$	$\mathbf{7}^{2+}$
Ru–N1	2.085(3)	2.118(4)	2.144(4)	2.162(2) / 2.166(2)	2.079(5)
Ru–N2	2.065(3)	2.064(4)	2.058(4)	2.068(2) / 2.064(2)	2.072(5)
Ru–N3	2.101(3)	2.090(4)	2.100(4)	2.110(2) / 2.103(2)	2.072(5)
Ru–N10	2.078(3)	2.071(4)	2.070(4)	2.063(2) / 2.046(3)	2.069(5)
Ru–N20	2.048(3)	2.059(4)	2.059(4)	2.074(2) / 2.051(2)	2.053(5)
Ru–N30	2.102(3)	2.041(4)	2.049(4)	2.052(2) / 2.054(2)	2.055(5)
C–H···N		2.287(4)	2.255(4)	2.284(2) / 2.294(2)	2.395(6)
[°]					
N1–Ru–N2	175.9(1)	177.18(16)	172.77(16)	178.40(9) / 178.37(9)	176.8(2)
N10–Ru–N20	163.0(1)	163.07(15)	161.30(16)	159.41(9) / 160.35(9)	164.0(2)
N3–Ru–N30	167.9(1)	174.25(15)	176.19(16)	177.90(9) / 177.49(9)	175.7(2)
N1–Ru–N30	79.1(1)	79.17(15)	79.53(16)	79.22(9) / 79.22(9)	82.5(2)
N1–Ru–N10	80.6(1)	80.74(16)	80.44(16)	79.87(9) / 80.75(10)	81.4(2)
N1–Ru–N20	83.5(1)	82.33(15)	81.05(16)	79.56(9) / 79.22(9)	82.9(2)
N10–Ru–N30	101.9(1)	91.34(16)	87.77(16)	85.83(9) / 85.11(9)	93.8(2)
N20–Ru–N30	80.7(1)	85.67(15)	91.45(16)	89.33(9) / 94.75(9)	87.3(2)
N2–Ru–N30	100.6(1)	99.65(15)	99.06(16)	100.13(9) / 99.53(9)	100.6(2)
N2–Ru–N3	77.3(1)	77.94(15)	77.70(16)	77.84(9) / 78.30(9)	77.0(2)
Torsion angle	42.9	15.5	0.4	0.4 / 0.9	12.1

Table S2. Crystallographic parameters of $\mathbf{2}^{2+}$–$\mathbf{4}^{2+}$ and $\mathbf{7}^{2+}$.

	$\mathbf{2}(PF_6)_2\cdot 0.25H_2O$	$\mathbf{3}(PF_6)_2\cdot MeOH$	$\mathbf{4}(PF_6)_2\cdot 0.25MeOH$	$\mathbf{7}(PF_6)_2\cdot MeOH$
Formula	$C_{32}H_{30}F_{12}N_8O_{0.25}P_2Ru$	$C_{37}H_{38}F_{12}N_{10}OP_2Ru$	$C_{40.25}H_{38}F_{12}N_{12}O_{0.25}P_2Ru$	$C_{37}H_{38}F_{12}N_{10}OP_2Ru$
M_r	921.65	1029.78	1087.84	1029.78
T [K]	100(2)	100(2)	100(2)	140(2)
λ [Å]	0.71073	0.71073	0.71073	0.71073
Crystal system	orthorhombic	triclinic	triclinic	orthorhombic
Space group	Pcaa	$P\bar{1}$	$P\bar{1}$	Pbca
a [Å]	17.888(5)	11.138(3)	13.842(4)	13.782(4)
b [Å]	18.350(6)	12.996(4)	13.903(4)	17.532(5)
c [Å]	22.569(7)	14.487(4)	23.006(7)	33.900(9)
α [Å]	90.00	78.682(5)	88.429(6)	90.00
β [Å]	90.00	87.424(6)	85.538(7)	90.00
γ [Å]	90.00	84.084(6)	79.015(6)	90.00
Cell volume [Å^3]	7408(4)	2044.6(10)	4333(2)	8191(4)
Z	8	2	1	8
$D_{calcd.}$ [g cm^{-3}]	1.653	1.673	1.668	1.670
μ [mm^{-1}]	0.608	0.563	0.536	0.562
F(000)	3696	1040	2196	4160
Radiation type	Mo-Kα	Mo-Kα	Mo-Kα	Mo-Kα
Crystal size [mm]	0.35 × 0.21 × 0.05	0.25 × 0.20 × 0.02	0.45 × 0.15 × 0.15	0.70 × 0.10 × 0.09
θ limits [°]	1.80–25.08	1.43–27.54	0.89–25.41	1.20–26.43
Refl. collected	75311	26528	47658	24101
Independent refl.	6551	9300	15799	8311
Obsvd. [$I > 2\sigma(I)$] refl.	4915	6312	11075	4835
Data/restraints/param.	6551/0/558	9300/0/570	15799/1/1222	8311/0/570
GoF in F^2	1.059	1.056	1.049	1.027
R_{int}	0.0607	0.0616	0.0522	0.0720
R_1 [$F^2 > 2\sigma(F^2)$]	0.0667	0.0596	0.0513	0.0515
$wR_2(F^2)$	0.2081	0.1551	0.1441	0.1631
$\Delta\rho_{max}$, $\Delta\rho_{min}$ [e Å^{-3}]	2.067, –0.982	1.342, –1.282	1.860, –1.004	0.782, –0.888
CCDC	918972	918973	918974	1015560

Electrochemistry

In DCM, all complexes show one reversible oxidation process, which is a metal-centered Ru^{II}-to-Ru^{III} process. The oxidation potential remains unaffected by the substitution of pyridine rings by triazoles (Table S3). On the reduction side of the cyclic voltammograms, only irreversible processes were observed in DCM. When measured in acetonitrile, the bipyridine-containing complexes ($\mathbf{1}^{2+}$–$\mathbf{4}^{2+}$) show reversible reduction processes, which become irreversible when pyridine rings of the bidentate ligand are substituted ($\mathbf{5}^{2+}$–$\mathbf{7}^{2+}$). Upon triazole-for-pyridine substitution in the bindentate ligand ($\mathbf{5}^{2+}$–$\mathbf{7}^{2+}$), the peak potential of the irreversible reduction process shifts drastically to more negative values (–2.59 V vs ferrocen for $\mathbf{6}^{2+}$). Hence, the reduction is a one-electron process centered on the bidentate ligand. This is corroborated by EPR spectra of the reduced species of $\mathbf{1}^{2+}$–$\mathbf{4}^{2+}$. Figure S56 shows the experimental and simulated EPR spectra of $\mathbf{2}^{+}$. When the CV of the Ru^{II}/Ru^{III} oxidation process of $\mathbf{1}^{2+}$ is measured in acetonitrile, two irreversible oxidation waves at 0.71 and 0.94 V (vs Fc/Fc^{+}) are observed. The CV of $[\mathbf{1}(CH_3CN)]^{2+}$ (formed by heating) only shows the second irreversible oxidation. Hence, the oxidation of $\mathbf{1}^{2+}$ in the first process leads to the formation of $[\mathbf{1}(CH_3CN)]^{2+}$. This reaction can be rationalized by the pathway shown in Scheme S6.

Table S3. Redox potentials of the complexes $\mathbf{1}^{2+}$–$\mathbf{7}^{2+}$ measured at 100 mV/s with 0.1 M Bu_4NPF_6 and referenced vs the ferrocene/ferrocenium couple. [a] peak potentials of the forward processes are given.

Complex	$\mathbf{1}^{2+}$	$\mathbf{2}^{2+}$	$\mathbf{3}^{2+}$	$\mathbf{4}^{2+}$	$\mathbf{5}^{2+}$	$\mathbf{6}^{2+}$	$\mathbf{7}^{2+}$
Oxidation in DCM [V] (peak separation [mV])	0.75 (81)	0.75 (76)	0.76 (85)	0.76 (85)	0.76 (92)	0.76 (118)	0.76 (103)
Oxidation in CH_3CN [V] (peak separation [mV])	0.71[a]; 0.94[a]	0.69 (69); 0.91[a]	0.70[a]; 0.87[a]	0.72[a]; 0.85[a]	0.77 (65)	0.76 (70)	0.72 (70)
Reduction in CH_3CN [V] (peak separation [mV])	–1.83 (75)	–1.86 (75)	–1.88 (68)	–1.89 (66)	–2.36[a]	–2.59[a]	–2.40[a]

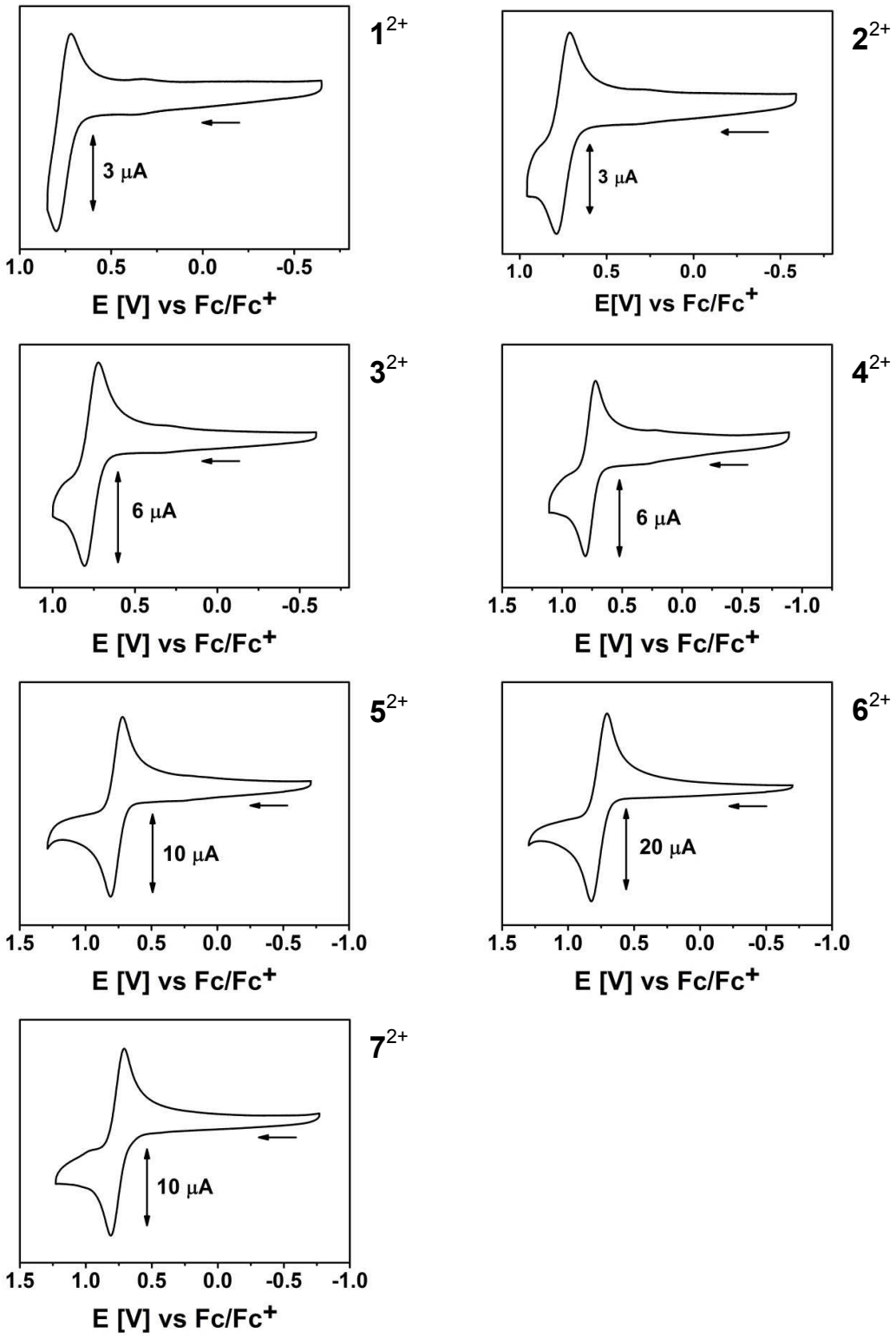

Figure S32. Cyclic voltammograms of the oxidation processes of $\mathbf{1}^{2+}$–$\mathbf{7}^{2+}$ measured in DCM at 100 mV/s with 0.1 M Bu_4NPF_6.

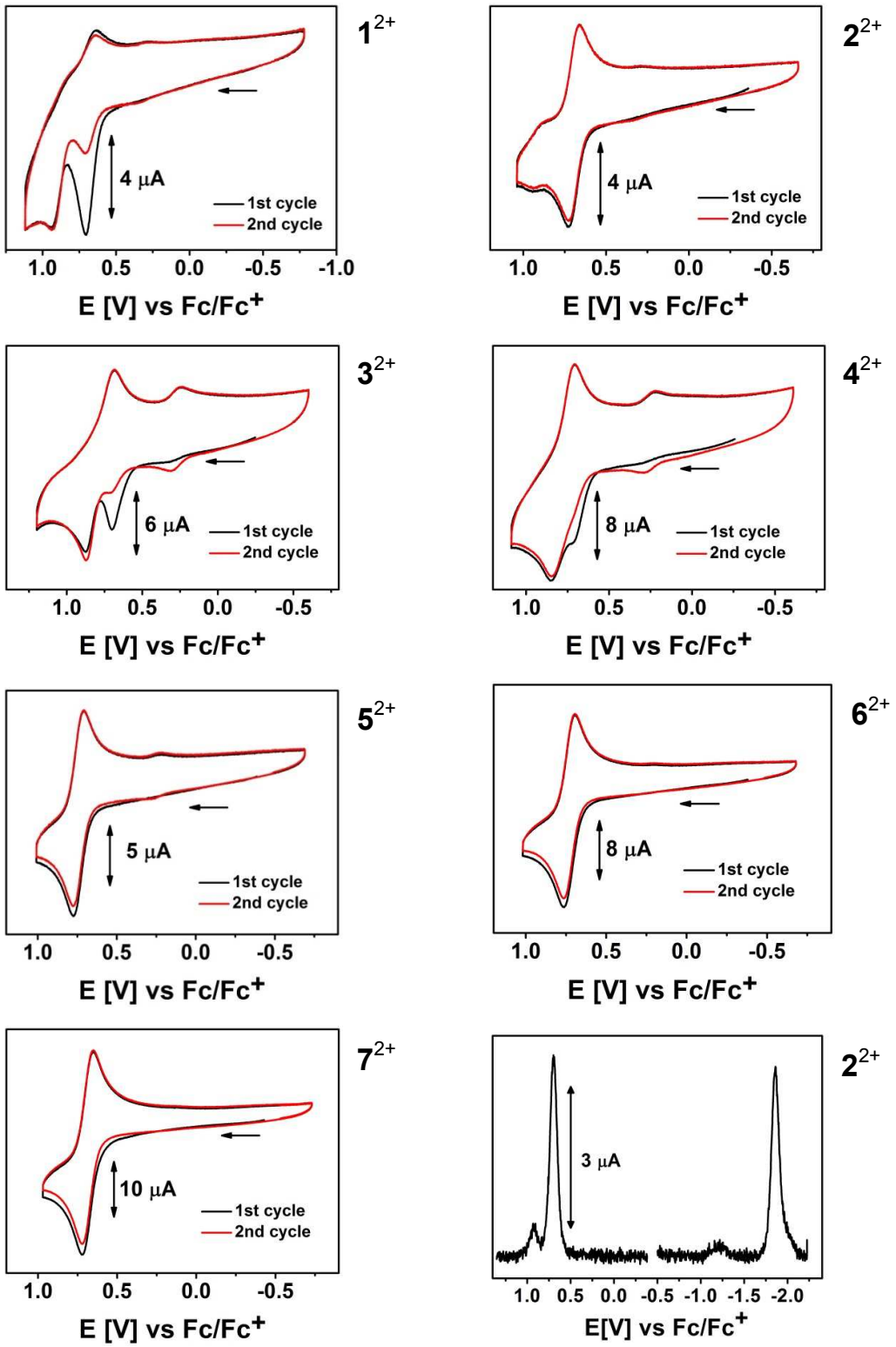

Figure S33. Cyclic voltammograms of the oxidation processes of $\mathbf{1}^{2+}$–$\mathbf{7}^{2+}$ measured in CH_3CN at 100 mV/s with 0.1 M Bu_4NPF_6. Bottom right: Differential pulse voltammogram of the oxidation and reduction process of $\mathbf{2}^{2+}$.

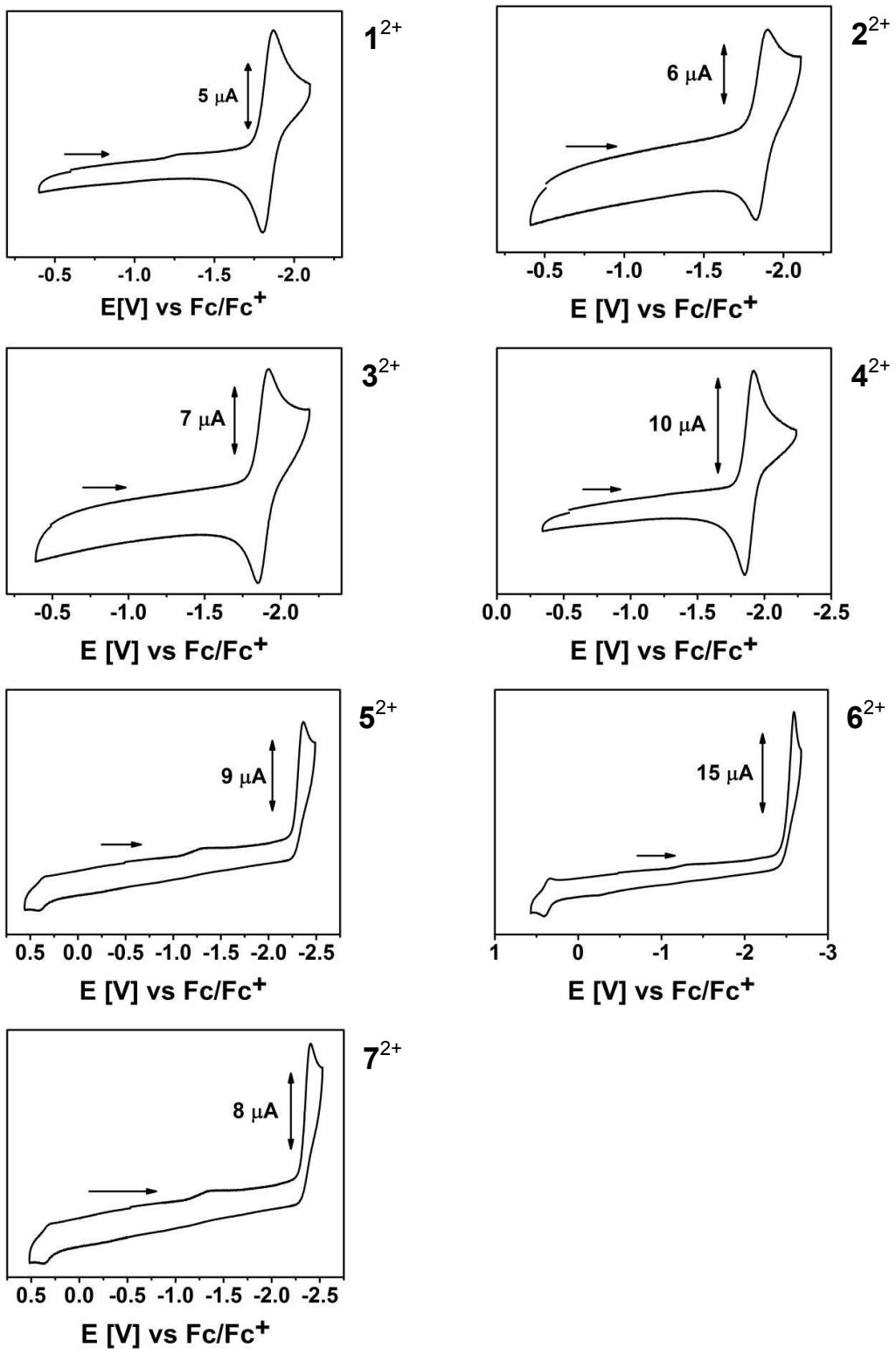

Figure S34. Cyclic voltammograms of the reduction processes of $\mathbf{1}^{2+}$–$\mathbf{7}^{2+}$ measured in CH_3CN at 100 mV/s with 0.1 M Bu_4NPF_6.

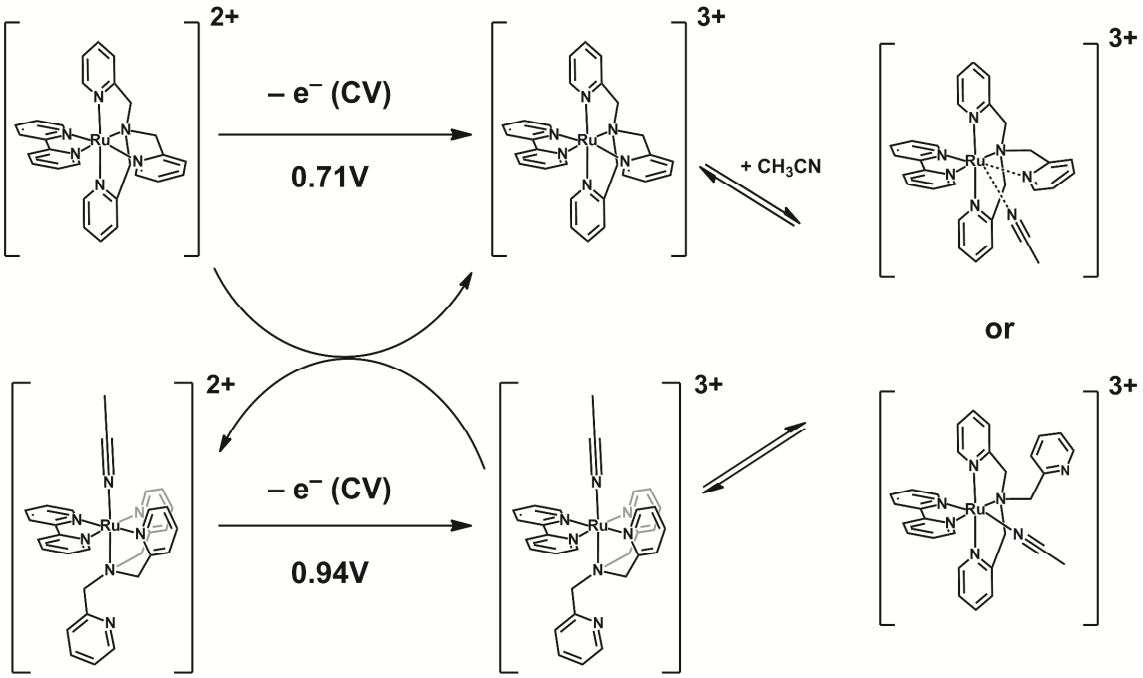

Scheme S6. Redox-triggered reactivity of $\mathbf{1}^{2+}$ in acetonitrile.

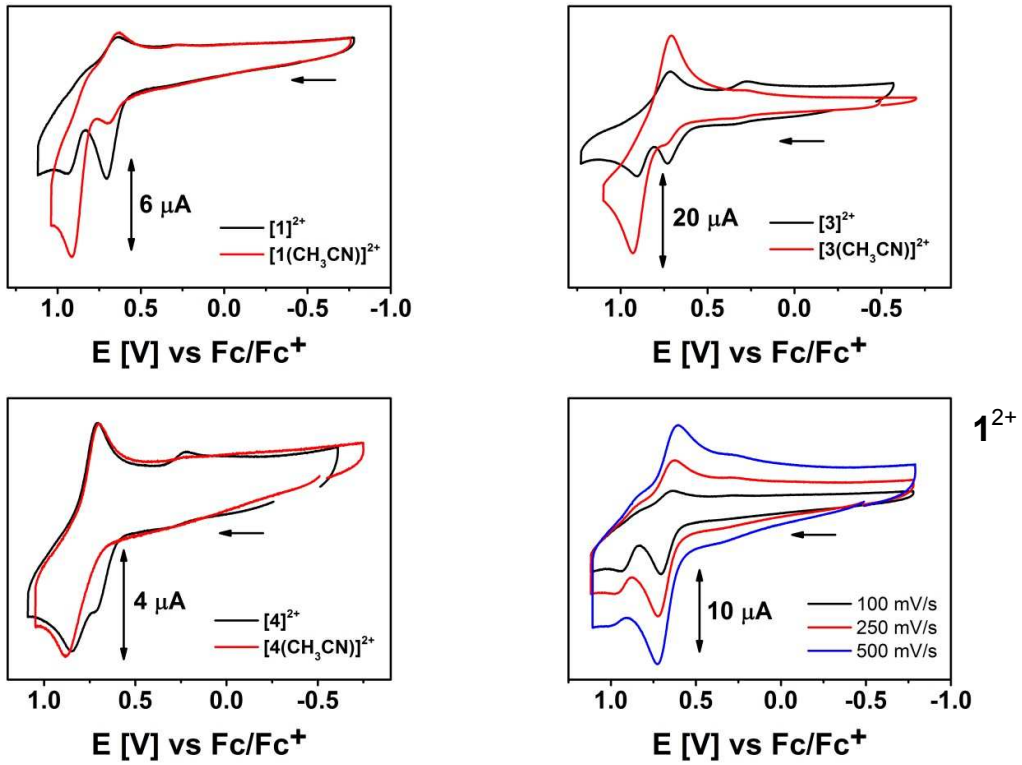

Figure S35. Cyclic voltammograms of the oxidation processes of $[\mathbf{1}(CH_3CN)]^{2+}$, $[\mathbf{3}(CH_3CN)]^{2+}$, and $[\mathbf{4}(CH_3CN)]^{2+}$ measured in CH_3CN at 100 mV/s with 0.1 M Bu_4NPF_6. Bottom right: Cyclic voltammograms of the oxidation process of $\mathbf{1}^{2+}$ measured in CH_3CN at different scan rates.

CV Simulation

On the basis of the proposed redox reaction mechanism, we were able to simulate the CVs of $\mathbf{1}^{2+}$–$\mathbf{4}^{2+}$, $[\mathbf{1}(CH_3CN)]^{2+}$, $[\mathbf{3}(CH_3CN)]^{2+}$, and $[\mathbf{4}(CH_3CN)]^{2+}$ in acetonitrile at different scan rates. The simulated voltammograms match the experimental ones well, and the parameters used for the simulations are summarized in Table S4. Figures S37–S40 Show a comparison of the simulated and experimental voltammograms. The following reactions were included in the simulation.

$$\mathbf{X}^{3+} + CH_3CN \rightarrow [\mathbf{X}^*(CH_3CN)]^{3+} \quad (1)$$

$$[\mathbf{X}^*(CH_3CN)]^{3+} \rightarrow [\mathbf{X}(CH_3CN)]^{3+} \quad (2)$$

$$\mathbf{X}^{2+} + [\mathbf{X}(CH_3CN)]^{3+} \rightarrow \mathbf{X}^{3+} + [\mathbf{X}(CH_3CN)]^{2+} \quad (3)$$

Here, $\mathbf{X}^{n+}$ is the starting complex with all tripod arms attached, $[\mathbf{X}^*(CH_3CN)]^{n+}$ is an intermediate, and $[\mathbf{X}(CH_3CN)]^{n+}$ is the acetonitrile adduct with a de-coordinated tripod arm.

Table S4. Parameters used for the simulation of cyclic voltammograms.

Reaction		$\mathbf{1}^{2+}$	$\mathbf{2}^{2+}$	$\mathbf{3}^{2+}$	$\mathbf{4}^{2+}$
$\mathbf{X}^{3+} + CH_3CN \rightarrow [\mathbf{X}^*(CH_3CN)]^{3+}$	K_1	1	0.005	0.2	0.3
	k_{f1} [s^{-1}]	6	6	12	12
	k_{b1} [s^{-1}]	6	1200	60	40
$[\mathbf{X}^*(CH_3CN)]^{3+} \rightarrow [\mathbf{X}(CH_3CN)]^{3+}$	K_2	0.04	0.2	0.4	0.8
	k_{f2} [s^{-1}]	2.5	2.5	12	20
	k_{b2} [s^{-1}]	62.5	12.5	30	25
$\mathbf{X}^{2+} + [\mathbf{X}(CH_3CN)]^{3+} \rightarrow \mathbf{X}^{3+} + [\mathbf{X}(CH_3CN)]^{2+}$	K_3	11379	11379	1102	158
	k_{f3} [$L \cdot mol^{-1} \cdot s^{-1}$]	10^7	10^7	10^7	10^7
	k_{b3} [$L \cdot mol^{-1} \cdot s^{-1}$]	879	879	9077	63526
$[\mathbf{X}^*(CH_3CN)]^{2+}$ / $[\mathbf{X}^*(CH_3CN)]^{3+}$		0.36 V	0.35 V	0.36 V	0.33 V
$\mathbf{X}^{2+}$ / $\mathbf{X}^{3+}$		0.71 V	0.72 V	0.70 V	0.72 V
$[\mathbf{X}(CH_3CN)]^{2+}$ / $[\mathbf{X}(CH_3CN)]^{3+}$		0.97 V	0.96 V	0.88 V	0.85 V

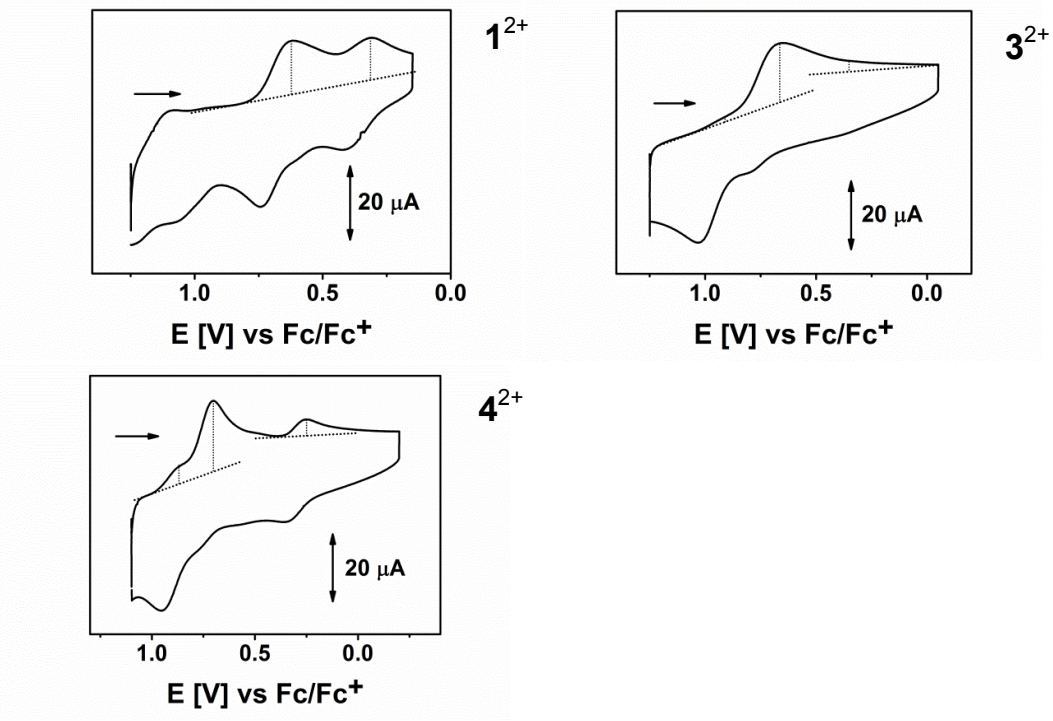

Figure S36. Fast cathodic scans (500 mV/s) after electrolysis at high positive potential.

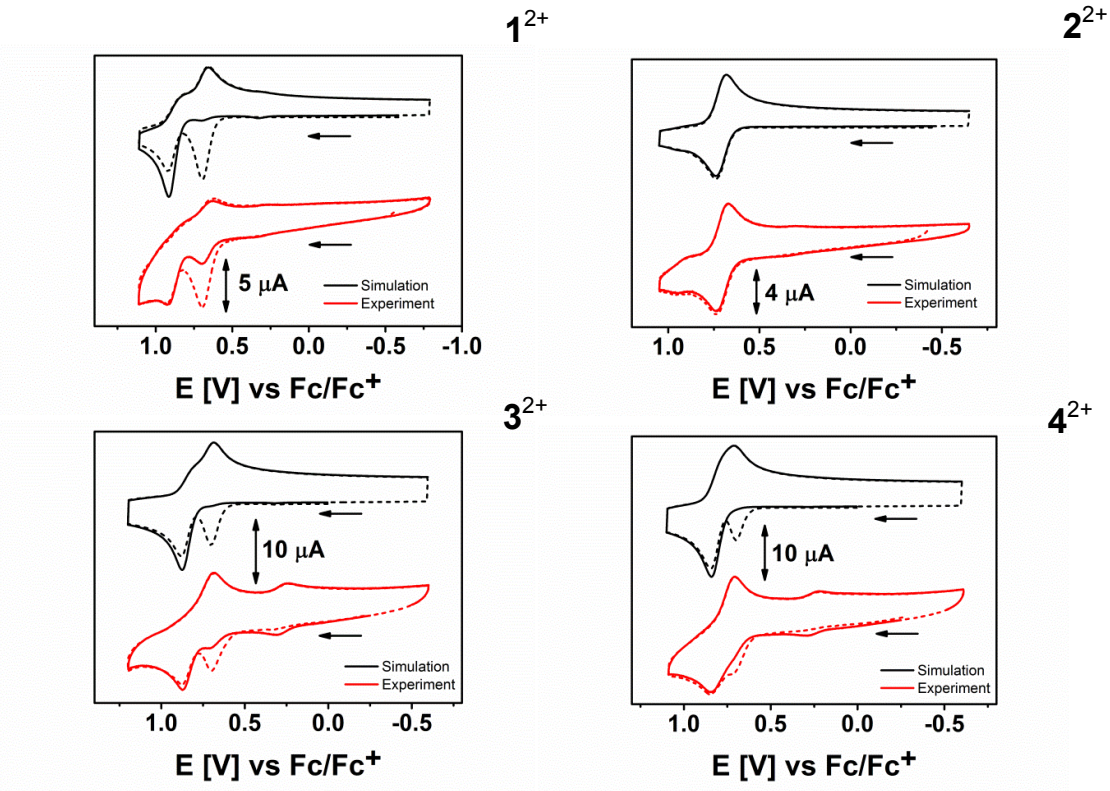

Figure S37. Comparison of simulated and experimental CVs measured at 100 mV/s in CH_3CN with 0.1 M Bu_4NPF_6. Dotted lines indicate the first cycles, straight lines indicate the second cycles.

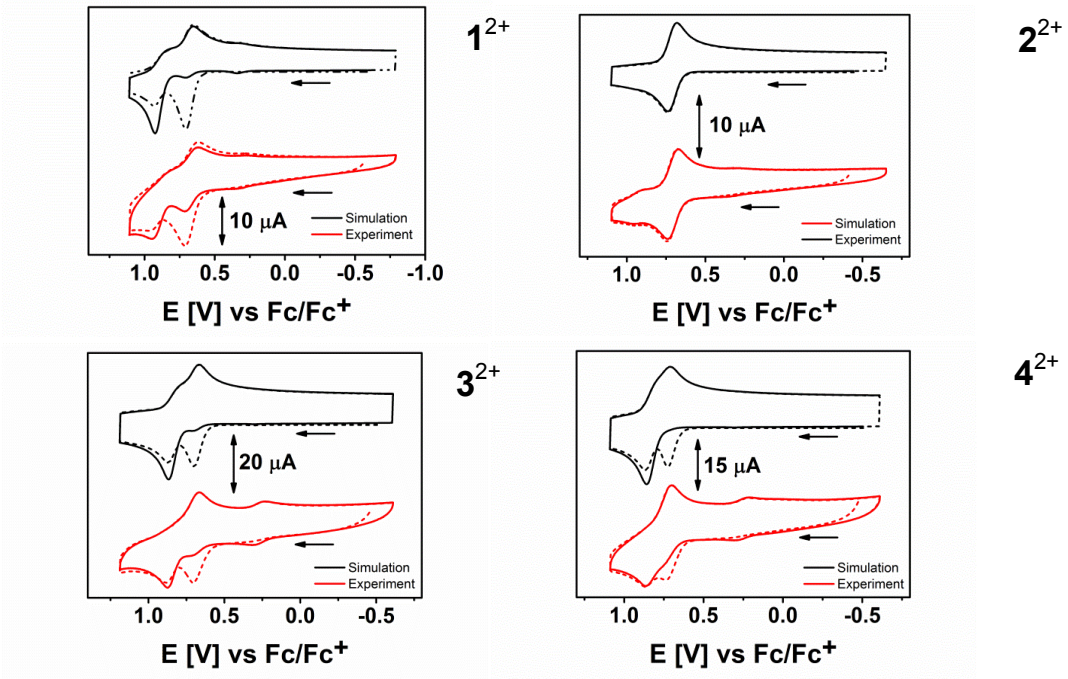

Figure S38. Comparison of simulated and experimental CVs measured at 250 mV/s in CH_3CN with 0.1 M Bu_4NPF_6. Dotted lines indicate the first cycles, straight lines indicate the second cycles.

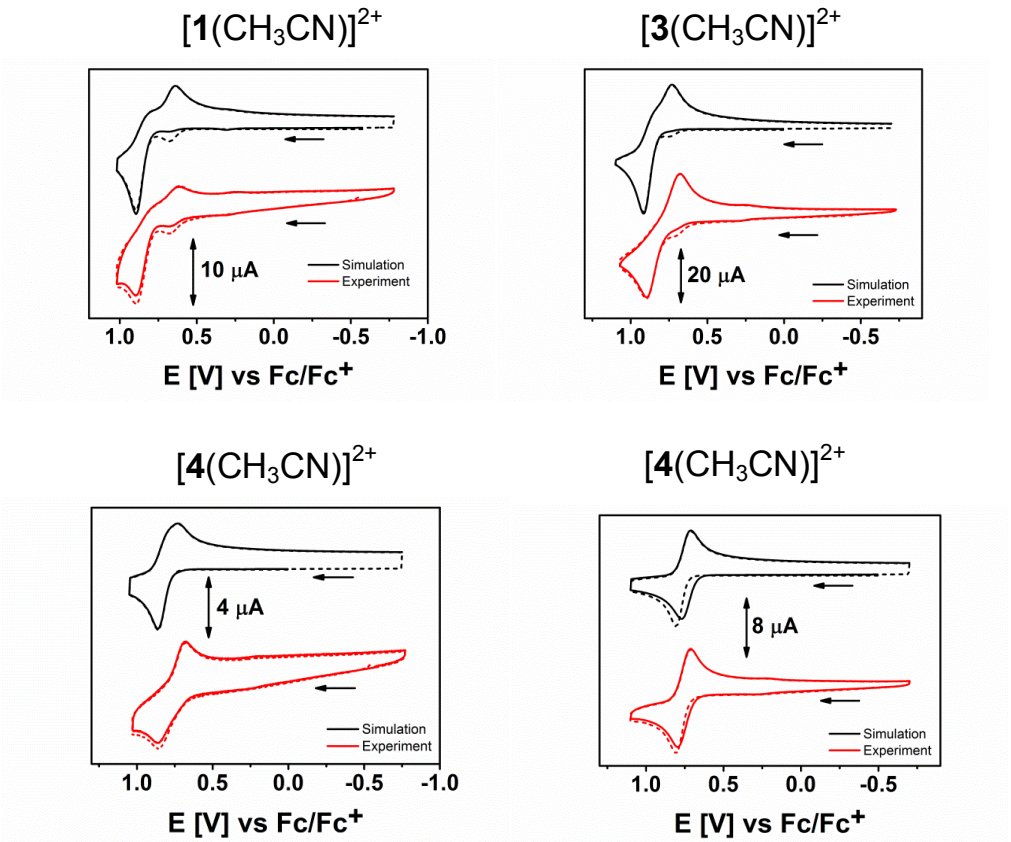

Figure S39. Comparison of simulated and experimental CVs measured at 100 mV/s in CH_3CN with 0.1 M Bu_4NPF_6. Dotted lines indicate the first cycles, straight lines indicate the second cycles. The CV shown at the bottom right side was measured in DCM.

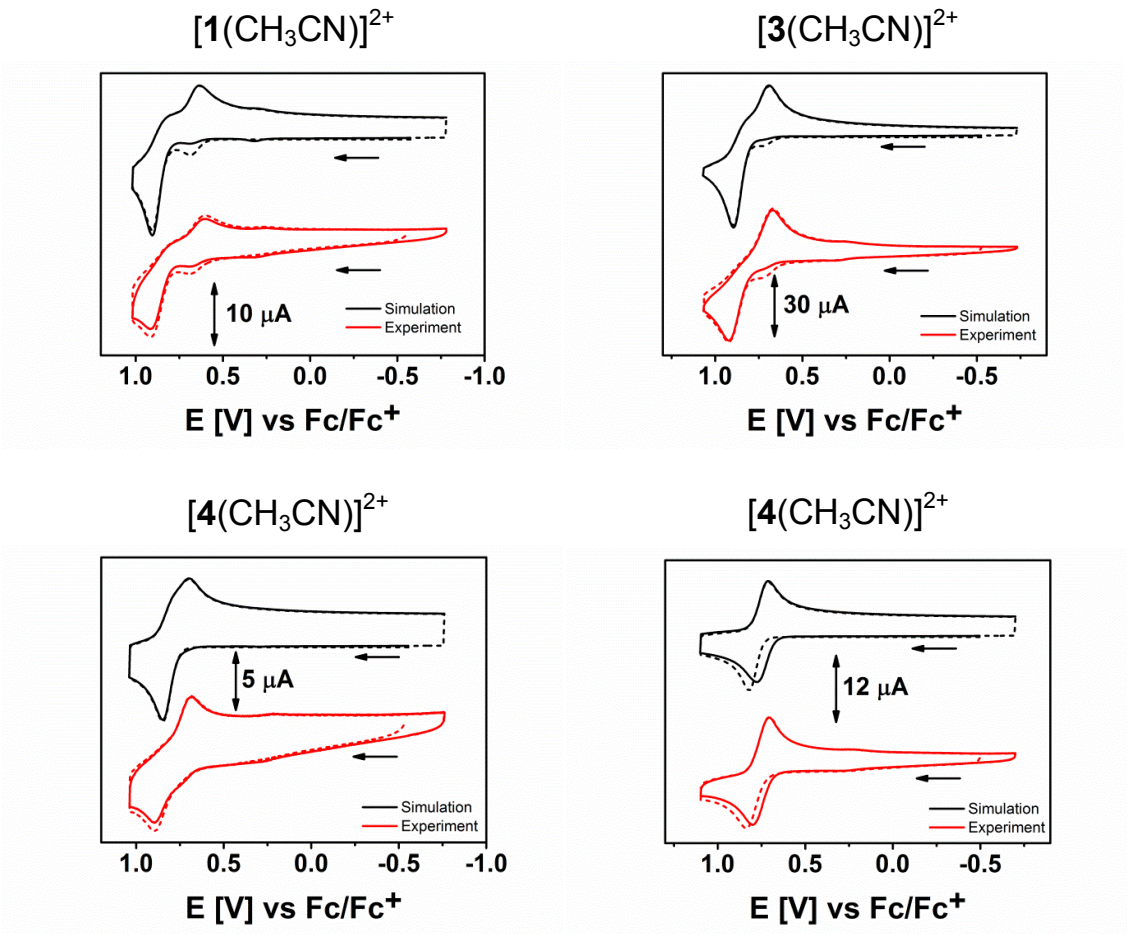

Figure S40. Comparison of simulated and experimental CVs measured at 250 mV/s in CH_3CN with 0.1 M Bu_4NPF_6. Dotted lines indicate the first cycles, straight lines indicate the second cycles. The CV shown at the bottom right side was measured in DCM.

Bulk Electrolysis

We placed $\mathbf{1}^{2+}$ (3.2 mg, 0.004 mmol) in acetonitrile (12 mL) in the working-electrode compartment of a bulk-electrolysis cell and applied a voltage of 0.9 V (vs Fc/Fc^{+}) at the working electrode while stirring. Prior to addition of $\mathbf{1}^{2+}$, the solution containing only electrolyte had been electrolyzed at the same potential until the background current was close to 0 A. Upon oxidation, we started monitoring the electrolysis solution by UV/vis spectroscopy by taking small samples of 0.1 mL and diluting them in a cuvette, and we observed a complete transformation from the spectrum of $\mathbf{1}^{2+}$ to a spectrum matching that of pure $[\mathbf{1}(CH_3CN)]^{2+}$ (obtained by heating of $\mathbf{1}^{2+}$). The solution was electrolyzed two times for 60 s to achieve a complete transformation of $\mathbf{1}^{2+}$. The total charge transferred at the working electrode during the experiment was 14.9 mC, which corresponds to 0.00008 mmol of electrons or 2% of the complex molecules.

Furthermore, we placed $\mathbf{1}^{2+}$ (5.1 mg, 0.006 mmol) in DCM/CH_3CN (99:1, 12 mL) in a bulk electrolysis cell and applied a voltage of 0.9 V in several intervals for a total time of 35 min. After this time, the starting UV/vis spectrum of $\mathbf{1}^{2+}$ had turned into that of $[\mathbf{1}(CH_3CN)]^{2+}$. The total amount charge transferred at the working electrode during the experiment was 263 mC, which corresponds to 0.0027 mmol of electrons or 45% of the complex molecules. However, when one compares the spectrum obtained at the end of the experiment with that of $[\mathbf{1}(CH_3CN)]^{2+}$ obtained through heating and with that of $\mathbf{1}^{3+}$ obtained in the OTTLE cell, it is evident that the amount of oxidized complex $\mathbf{1}^{3+}$ must be much less than 45%. Hence, there are additional oxidation processes at the working electrode, which do not involve the complex, and this could be due to relatively high potential applied. Therefore, the amount of complex oxidized in the second electrolysis experiment could not be determined with certainty. However, because the final spectrum matches that of pure $[\mathbf{1}(CH_3CN)]^{2+}$ very well, we estimate that the amount of $\mathbf{1}^{3+}$ is <10%.

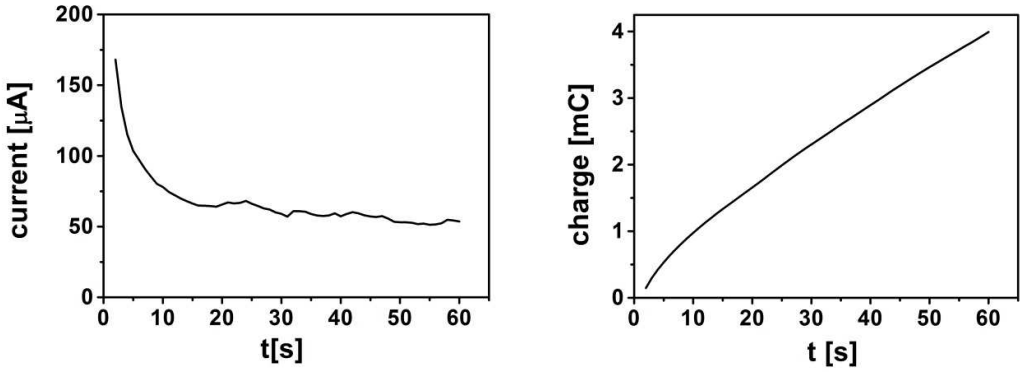

Figure S41. Typical current (left) and charge (right) curves, measured during the electrolysis of $\mathbf{1}^{2+}$ in CH_3CN.

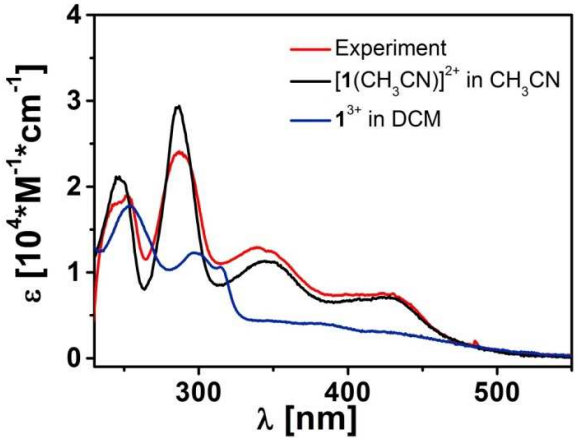

Figure S42. UV/Vis-spectrum (red) obtained after electrolyzing $\mathbf{1}^{2+}$ in CH_3CN for 2 minutes compared to spectra of $[\mathbf{1}(CH_3CN)]^{2+}$ and $\mathbf{1}^{3+}$.

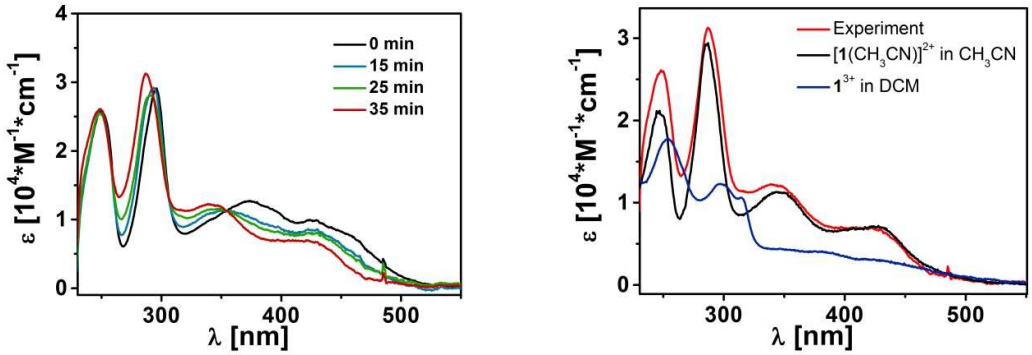

Figure S43. UV/Vis-spectra (left) recorded during the electrolysis of $\mathbf{1}^{2+}$ in DCM/CH_3CN (99:1). UV/Vis-spectrum (left, red) obtained after electrolyzing $\mathbf{1}^{2+}$ DCM/CH_3CN (99:1) for 35 minutes compared to spectra of $[\mathbf{1}(CH_3CN)]^{2+}$ and $\mathbf{1}^{3+}$.

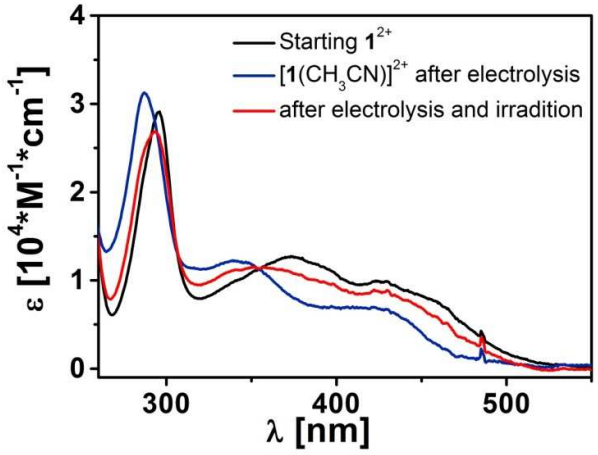

Figure S44. UV/Vis-spectra recorded before (black) and after (blue) the electrolysis of $\mathbf{1}^{2+}$ in DCM/CH_3CN (99:1). When after electrolysis the solution was irradiated at 369 nm, the red spectrum was obtained.

UV/Vis Spectroelectrochemistry

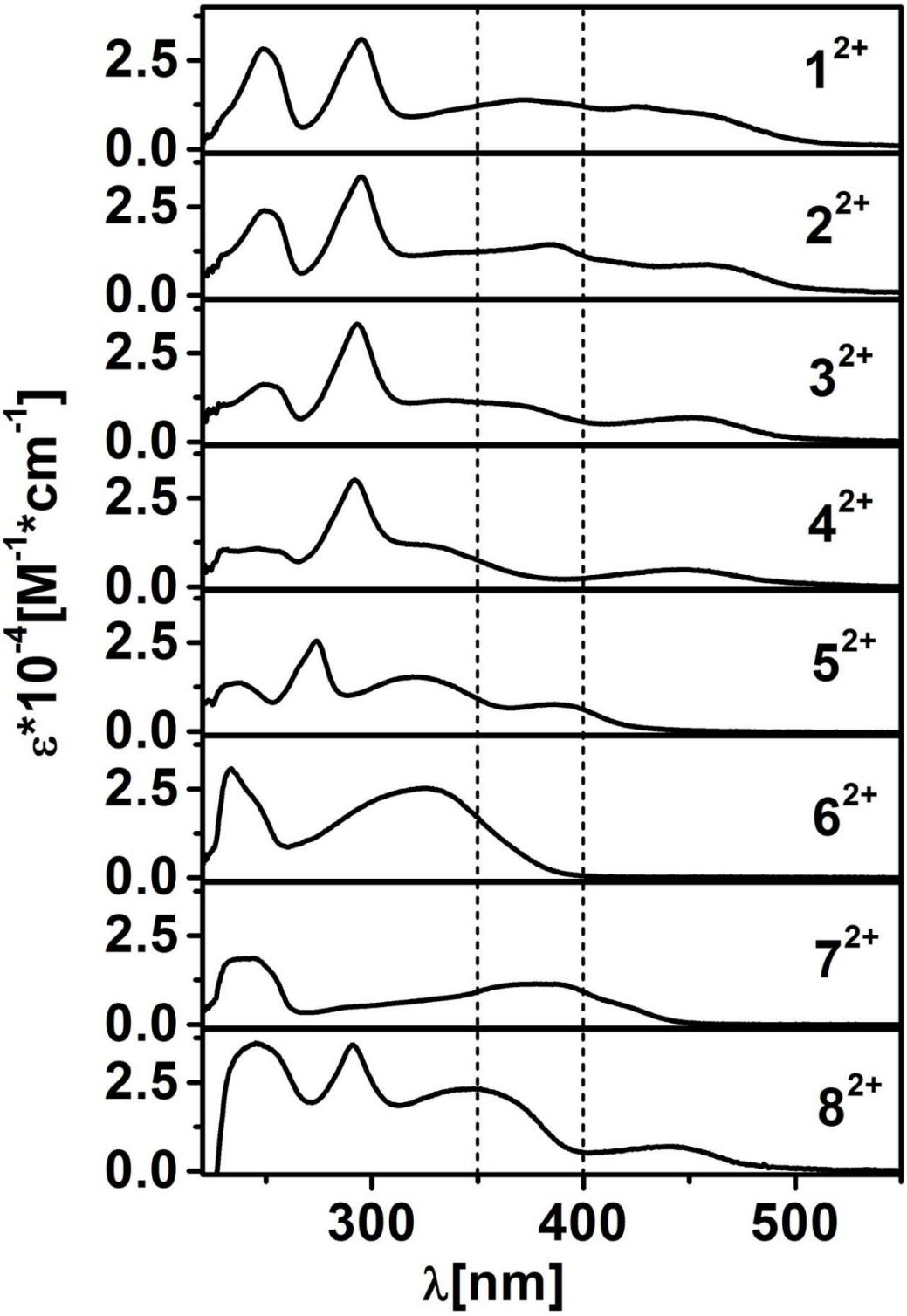

Figure S45. UV/Vis spectra of the complexes $\mathbf{1}^{2+}$–$\mathbf{8}^{2+}$ recorded in DCM. The dotted lines indicate the width of the emission band of the light source used in the photoreactivity experiments.

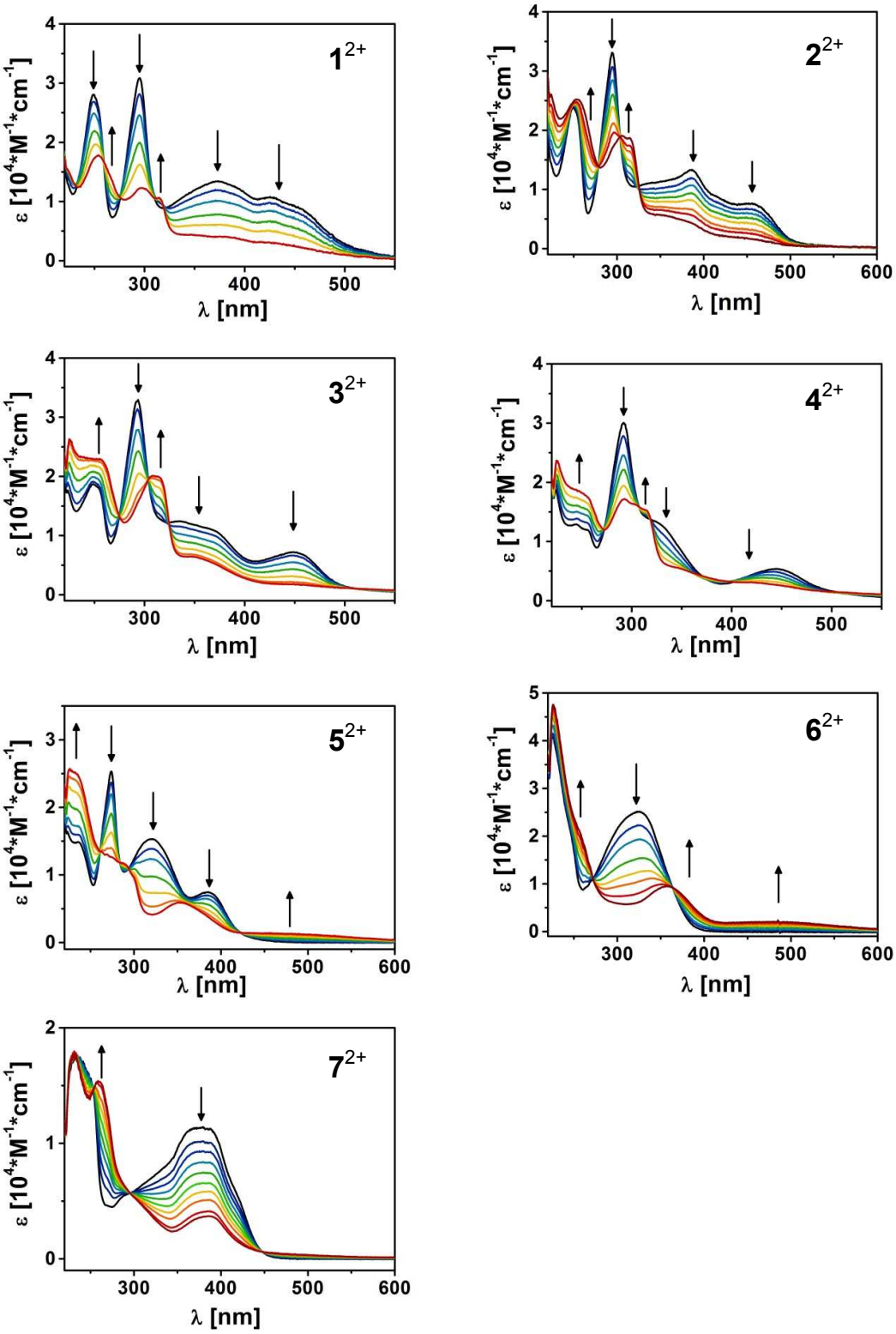

Figure S46. UV/Vis spectra recorded during the oxidation of complexes $\mathbf{1}^{2+}$–$\mathbf{7}^{2+}$ in DCM.

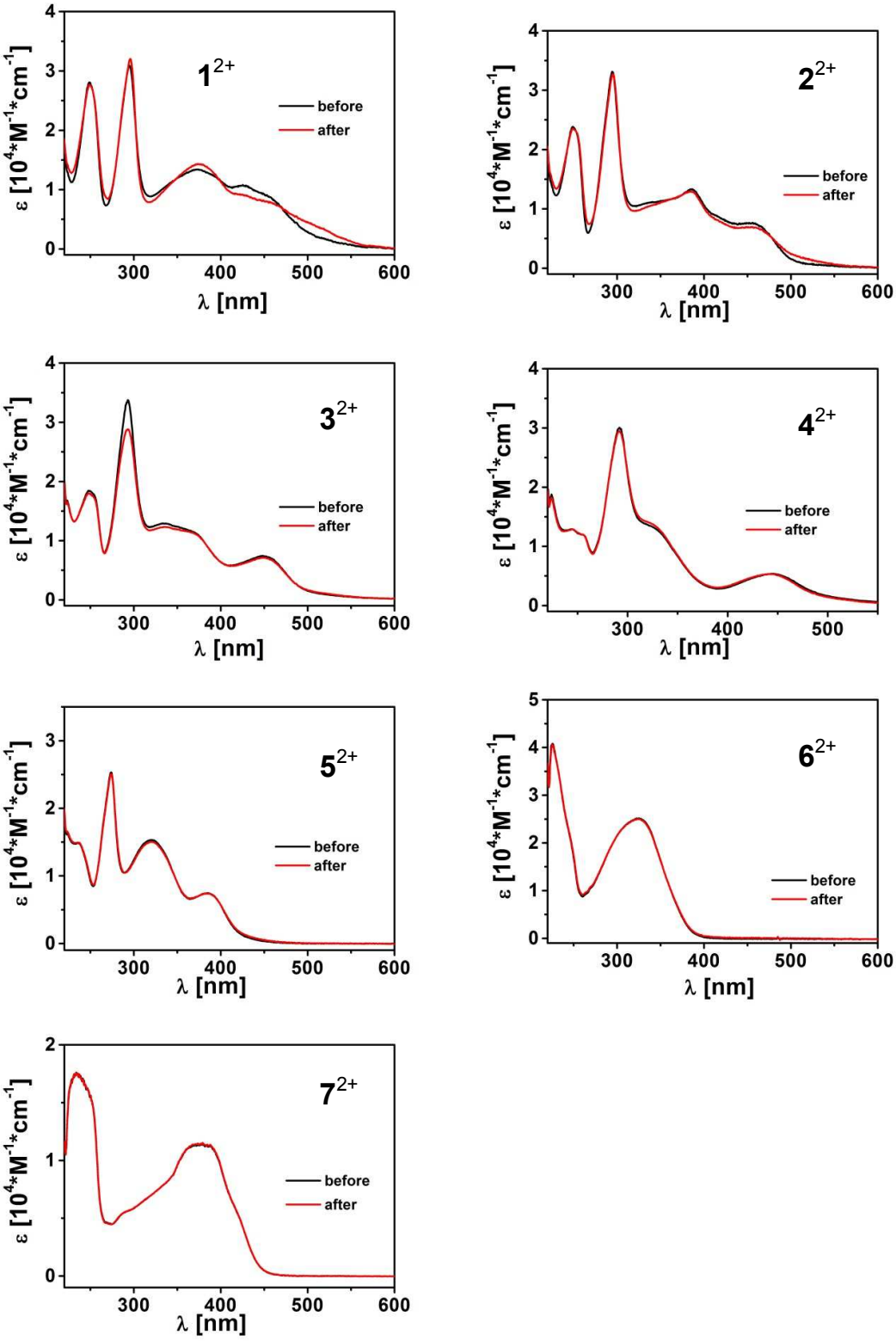

Figure S47. UV/Vis spectra recorded before and after the SEC of the oxidation process of complexes $\mathbf{1}^{2+}$–$\mathbf{7}^{2+}$ in DCM.

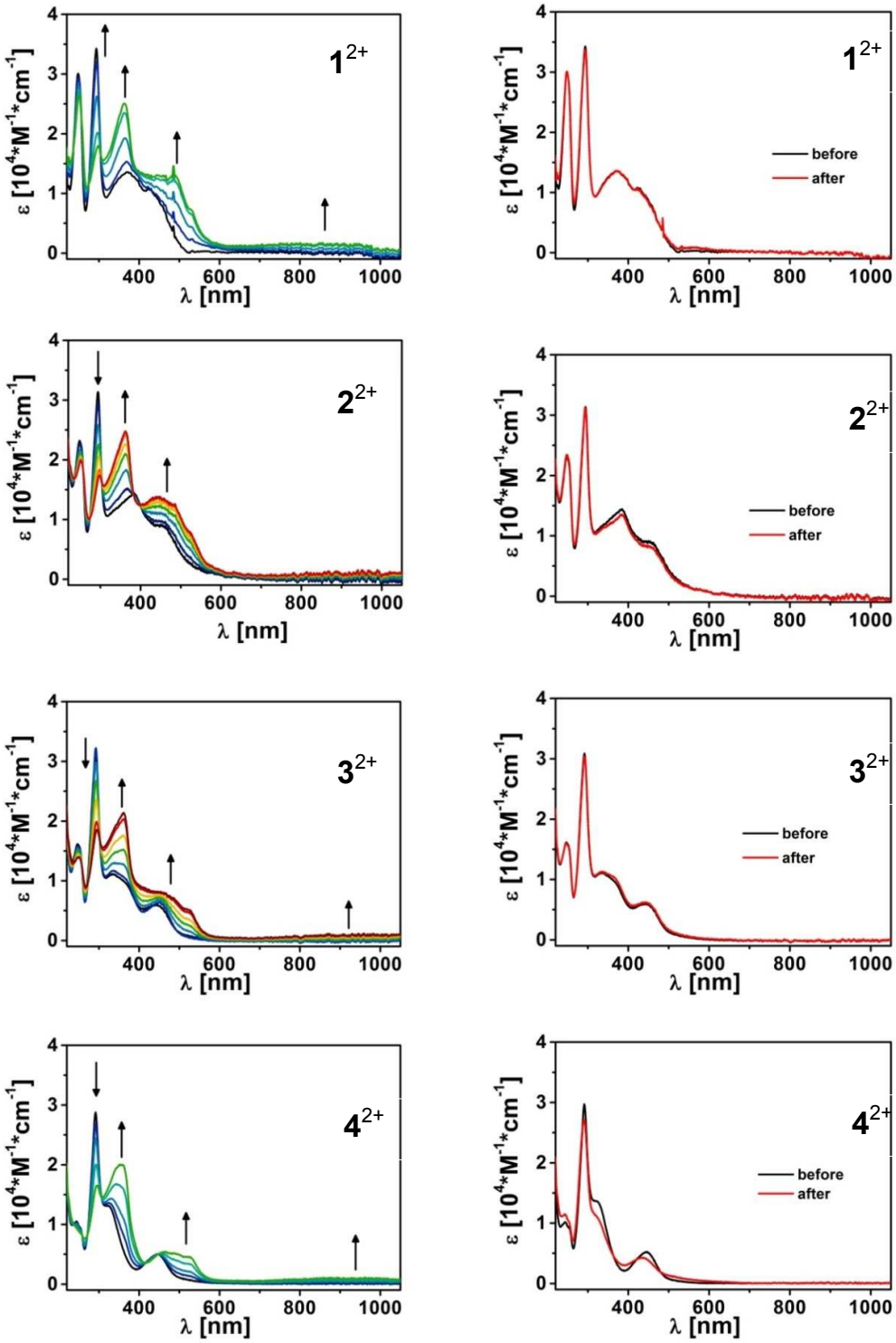

Figure S48. UV/Vis spectra (left) recorded during the reduction process of complexes $\mathbf{1}^{2+}$–$\mathbf{4}^{2+}$ in CH_3CN. On the right: comparison of the spectra taken before and after each SEC cycle.

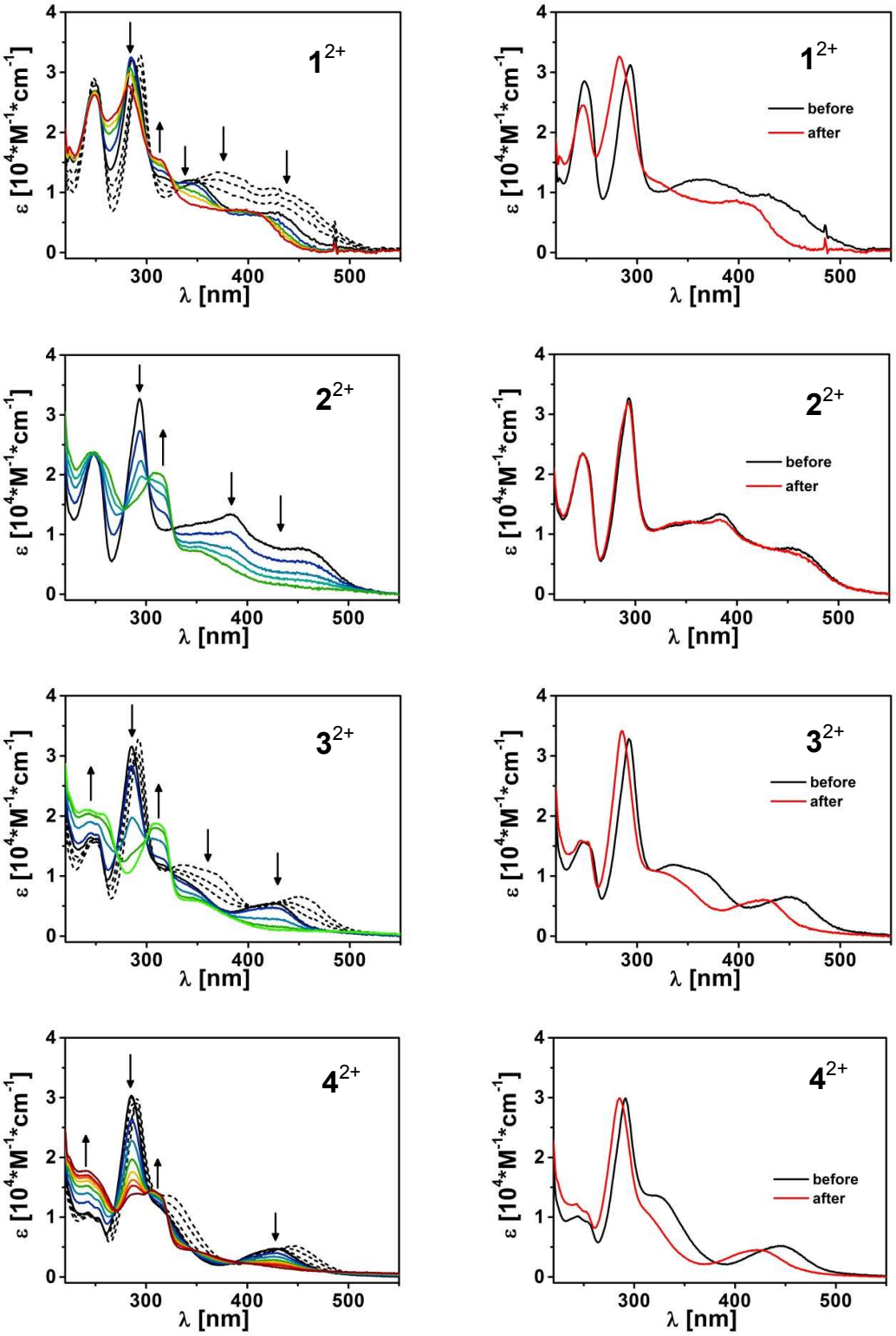

Figure 49. UV/Vis spectra recorded during the oxidation of complexes $\mathbf{1}^{2+}$–$\mathbf{4}^{2+}$ in CH_3CN. The spectral changes indicated by dotted lines are due to the redox reactivity described above (Scheme S6, Figure S33).

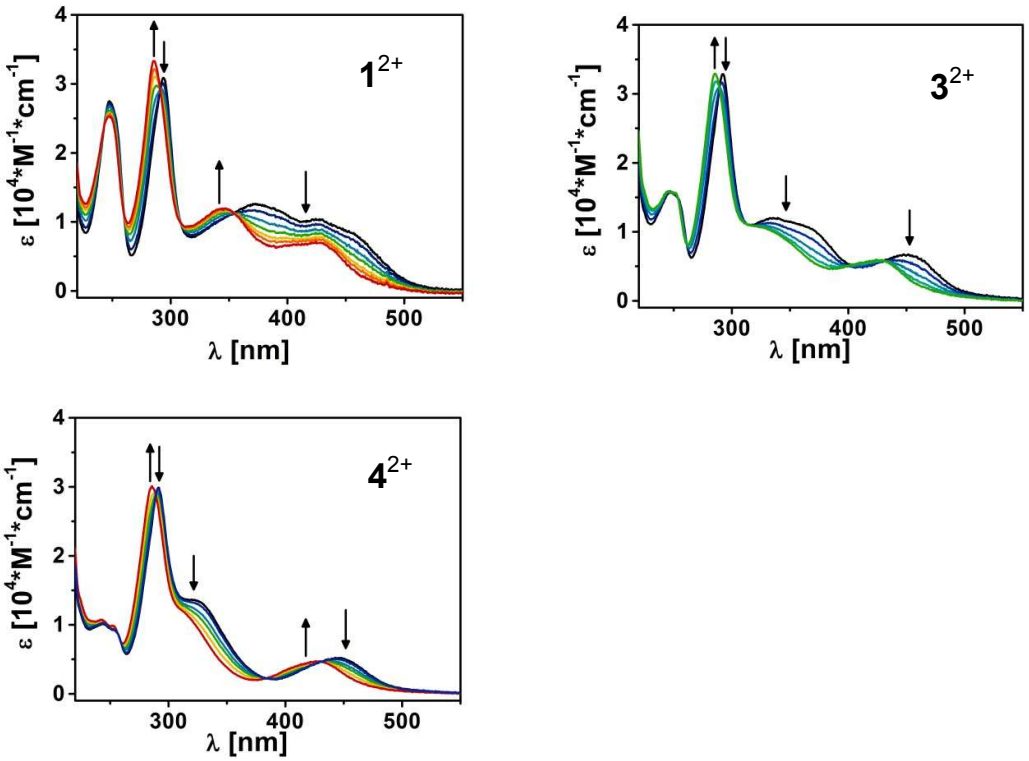

Figure S50. Changes in the UV/Vis spectra of $\mathbf{1}^{2+}$, $\mathbf{3}^{2+}$, and $\mathbf{4}^{2+}$, caused by the redox-triggered transformation of $\mathbf{X}^{2+}$ to $[\mathbf{X}(CH_3CN)]^{2+}$.

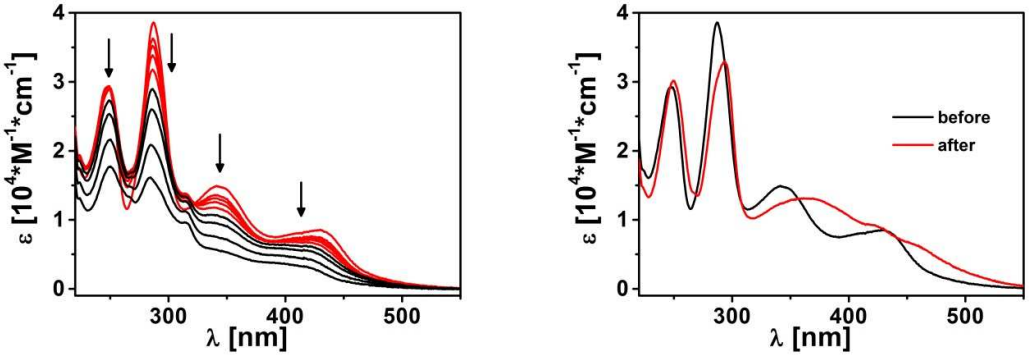

Figure S51. Left: changes in the UV/Vis spectrum (left) of $[\mathbf{1}(CH_3CN)]^{2+}$ upon oxidation in DCM; Initial spectral changes (red) have an isosbestic point. Right: comparison of the UV/Vis spectra measured before and after the SEC cycle shown on the left.

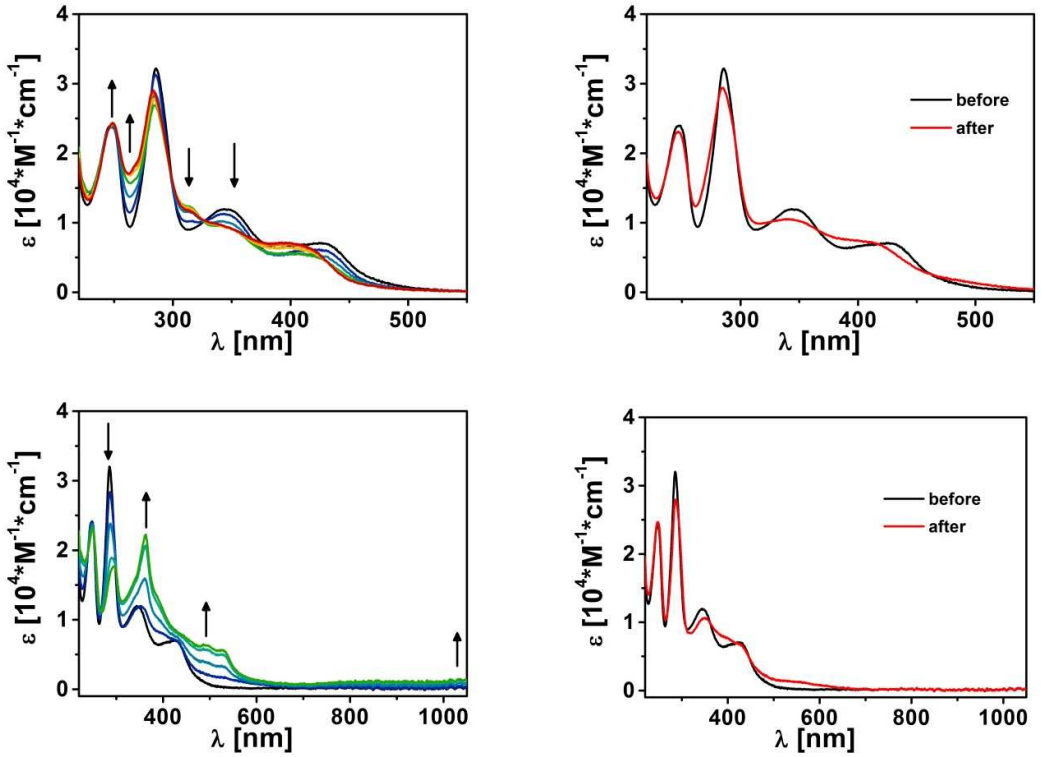

Figure S52. Left: changes in the UV/Vis spectrum of [**1**(CH_3CN)]$^{2+}$ upon oxidation (top left) and reduction (bottom left) in CH_3CN. Right: comparison of the UV/Vis spectra measured before and after the SEC cycles shown on the left.

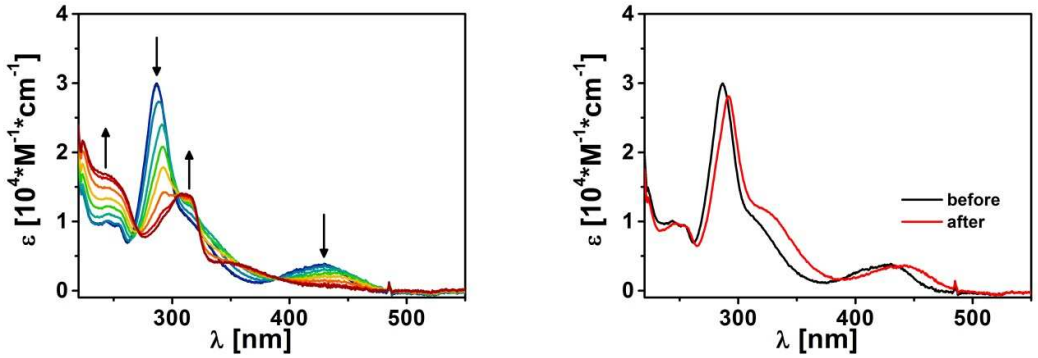

Figure S53. Left: changes in the UV/Vis spectrum (left) of [**4**(CH_3CN)]$^{2+}$ upon oxidation in DCM. Right: comparison of the UV/Vis spectra measured before and after the SEC cycle shown on the left.

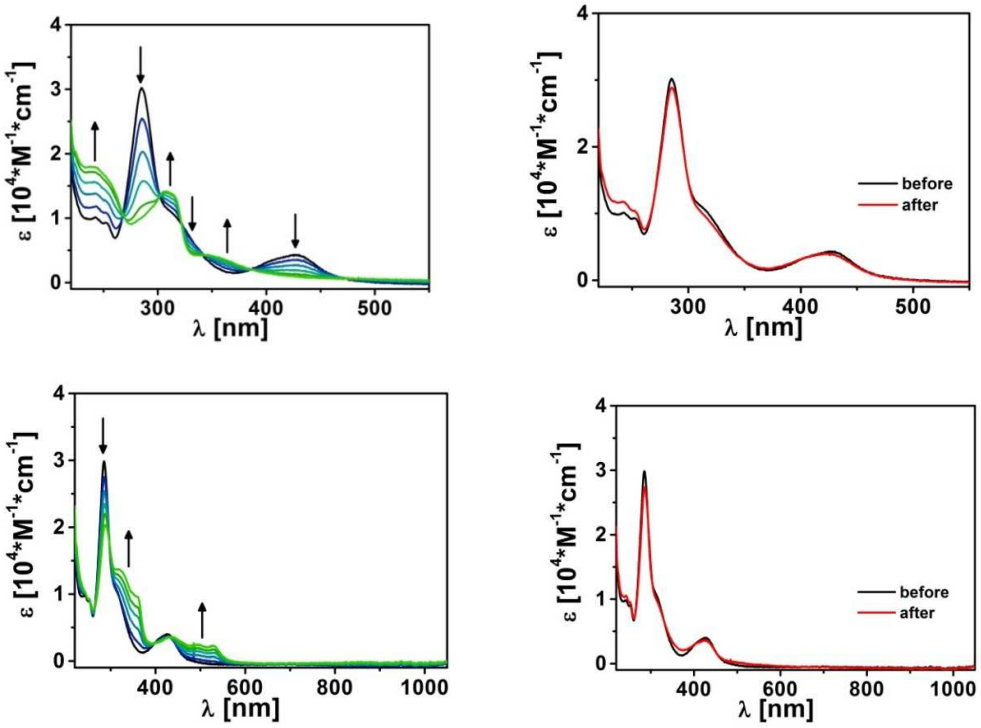

Figure S54. Left: changes in the UV/Vis spectrum of [**4**(CH_3CN)]$^{2+}$ upon oxidation (top left) and reduction (bottom left) in CH_3CN. Right: comparison of the UV/Vis spectra measured before and after the SEC cycles shown on the left.

Table S5. UV/Vis spectral data of the complexes **1**$^{2+}$–**8**$^{2+}$, their acetonitrile adducts, and their reduced and oxidized forms. sh = shoulder, br = broad.

Complex	Bands: λ [nm] (ε [M^{-1} cm^{-1}])
1^{2+} in DCM	249 (28210), 295 (31010), 370 (13880), 425 (11930), 452 (10090) sh
2^{2+} in DCM	249 (23760), 295 (33400), 337 (12050) sh, 384 (14370), 457 (8760)
3^{2+} in DCM	250 (16140), 293 (33030), 334 (11690), 367 (10530) sh, 450 (6810)
4^{2+} in DCM	245 (10830), 255 (10040) sh, 292 (29980), 326 (11800) sh, 446 (4920)
5^{2+} in DCM	236 (13570), 274 (25460), 320 (15410), 386 (7630)
6^{2+} in DCM	233 (30630), 325 (25180)
7^{2+} in DCM	240 (18480), 286 (4670) sh, 378 (11400), 417 (5630) sh
8^{2+} in DCM	245 (36164), 291 (35556), 347 (23196), 441 (7010)
[**1**(CH_3CN)]$^{2+}$ in MeCN	247 (25259), 286 (33304), 347 (11938), 427 (6951)
[**3**(CH_3CN)]$^{2+}$ in MeCN	246 (15859), 252 (15588), 286 (32932), 326 (10633) sh, 424 (5960)
[**4**(CH_3CN)]$^{2+}$ in MeCN	243 (10702), 252 (9868), 286 (30088), 316 (11513), 427 (4653)
1^{3+} in DCM	254 (17827), 297 (12259), 314 (10617), 378 (4021) sh, 427 (2934) sh
2^{3+} in DCM	253 (25204), 305 (19092), 314 (18700), 354 (5641) sh, 386 (4355) sh, 441 (1902) sh
3^{3+} in DCM	255 (22969) sh, 308 (20088), 316 (19768) sh, 350 (6407) sh
4^{3+} in DCM	247 (18554) sh, 292 (17145), 303 (16309) sh, 314 (15277) sh, 348 (5435) sh, 424 (3055) sh
5^{3+} in DCM	233 (24989) sh, 290 (11574) sh, 352 (5876), 480 (1291) br
6^{3+} in DCM	258 (20203) sh, 357 (9471), 486 (2159) br
7^{3+} in DCM	259 (15306), 308 (4687) sh, 371 (3441) sh, 386 (3659), 477 (424) sh
1^{+} in MeCN	250 (26523), 298 (17968), 363 (25066), 488 (12906) sh, 854 (1644) br
2^{+} in MeCN	251 (19929), 298 (17353), 363 (24743), 443 (13790), 489 (12002) sh, 527 (7447) sh, 990 (1492) br
3^{+} in MeCN	249 (13883), 295 (18555), 361 (21374), 459 (7953) sh, 524 (5111) sh, 992 (1040) br
4^{+} in MeCN	295 (16536), 354 (19902), 464 (5366), 493 (5027) sh, 525 (4502) sh, 924 (1136) br
[**1**(CH_3CN)]$^{+}$ in MeCN	248 (23106), 295 (17690), 362 (22173), 395 (12261) sh, 439 (7941) sh, 492 (6329), 529 (5635) sh, 984 (1448) br
[**4**(CH_3CN)]$^{+}$ in MeCN	288 (20353), 321 (13569) sh, 358 (9639) sh, 435 (3591) sh, 495 (2341), 529 (2199), 964 (1040) br

EPR Spectroelectrochemistry

The bpy-containing complexes $\mathbf{1}^{2+}$–$\mathbf{4}^{2+}$ could be reduced reversibly. The EPR spectra of $\mathbf{1}^{+}$, $\mathbf{2}^{+}$, $\mathbf{3}^{+}$, and $\mathbf{4}^{+}$ were measured in DCM at room temperature, and they show isotropic signals with *g* values of 1.992, 1.993, 1.993, and 1.992, respectively. All signals show Ru satellites and are split into 5 lines, because the bpy-centered radicals couple with the spins of the two ^{14}N nuclei (S = 1) of the bidentate ligand. For $\mathbf{2}^{+}$, the EPR spectrum could be simulated with g = 1.9925, $a(^{14}\text{N})$ = 4.4 G, $a(^{14}\text{N})$ = 3.4 G, and $a(^{99,101}\text{Ru})$ = 3.8 G (Figure S55).

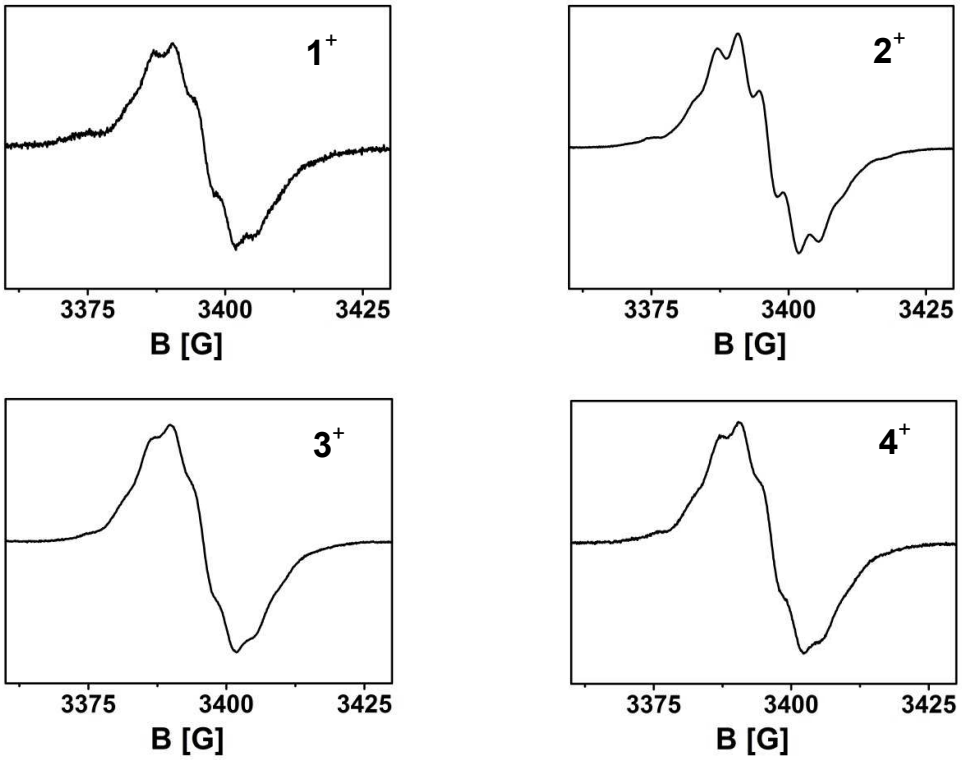

Figure S55. EPR spectra of $\mathbf{1}^{+}$–$\mathbf{4}^{+}$, measured in DCM at room temperature.

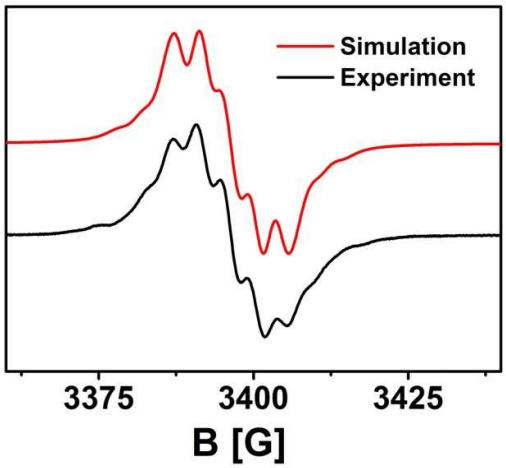

Figure S56. Comparison of the simulated and experimental EPR spectrum of $\mathbf{2}^{+}$ in DCM at room temperature.

Thermo- and Photoreactivity

For assignment of the ^{1}H NMR signals to the photoproducts see the ^{1}H NMR section above.

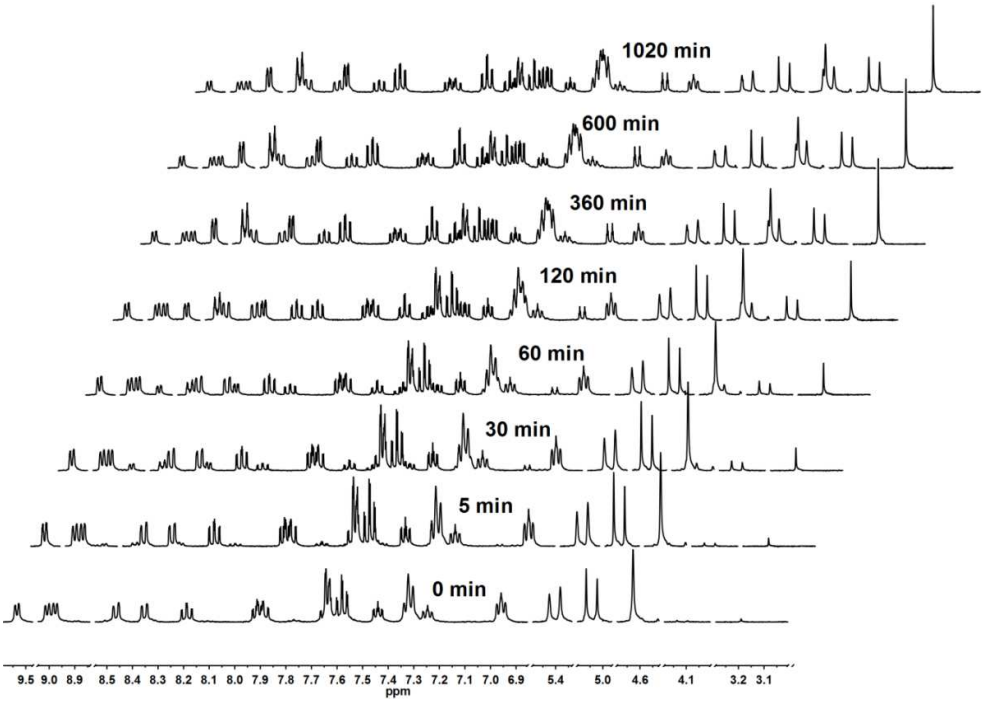

Figure S57. Changes in the ^{1}H NMR spectrum of $\mathbf{1}^{2+}$ in CD_3CN upon irradiation (369 nm).

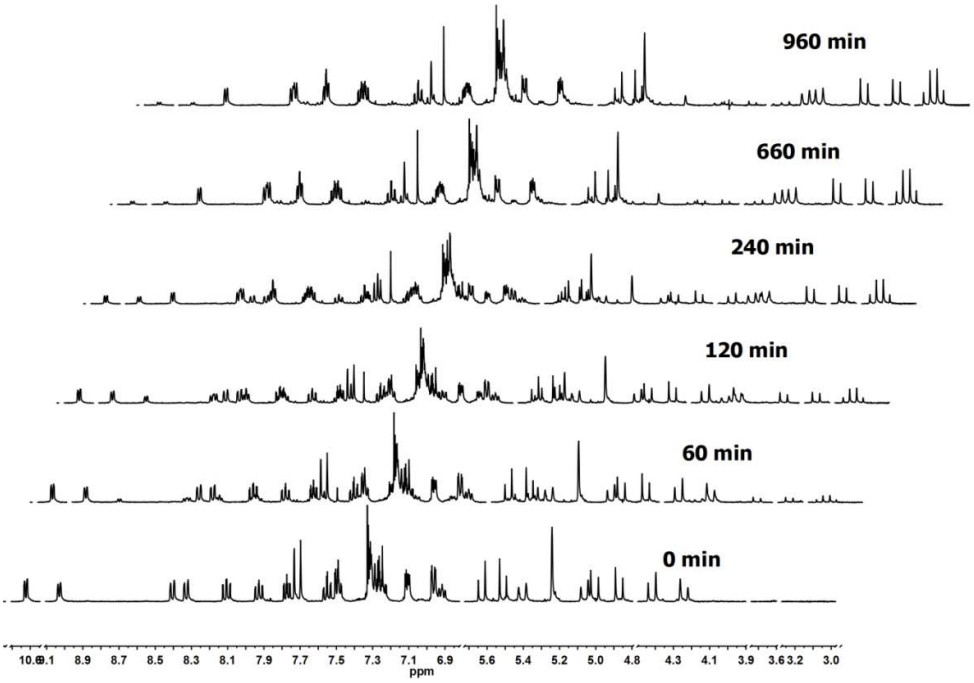

Figure S58. Changes in the ^{1}H NMR spectrum of $\mathbf{3}^{2+}$ in CD_3CN upon irradiation (369 nm).

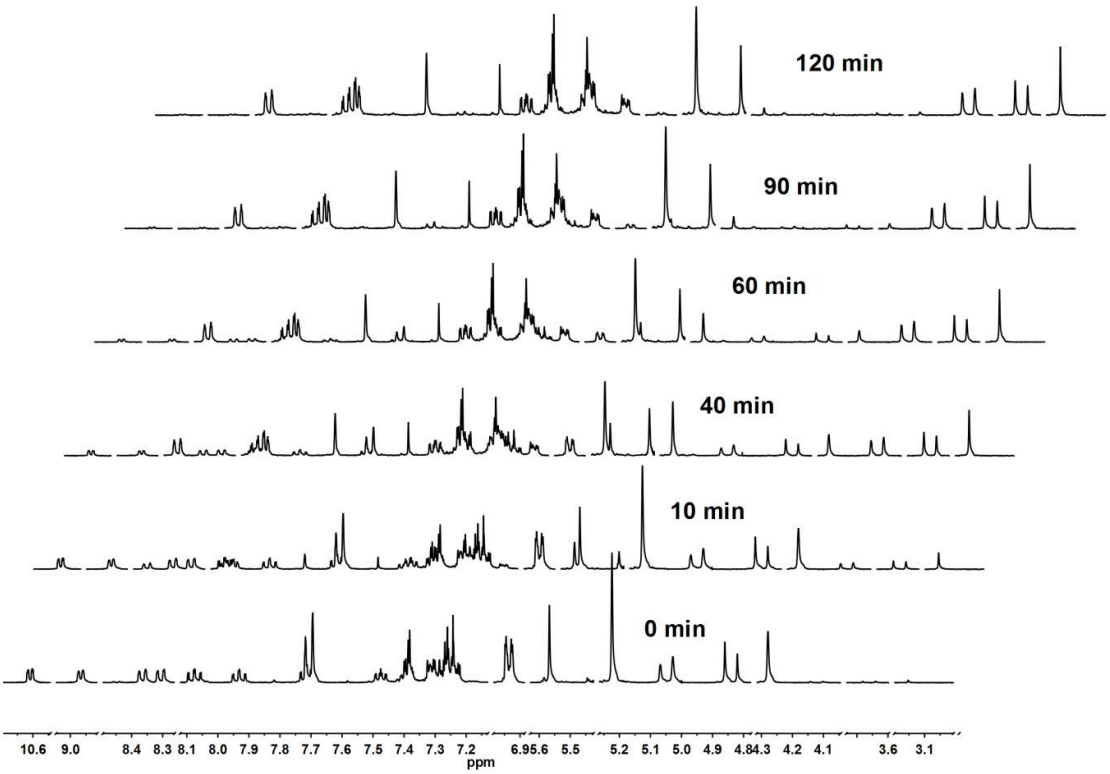

Figure S59. Changes in the ^{1}H NMR spectrum of $\mathbf{4}^{2+}$ in CD_3CN upon irradiation (369 nm).

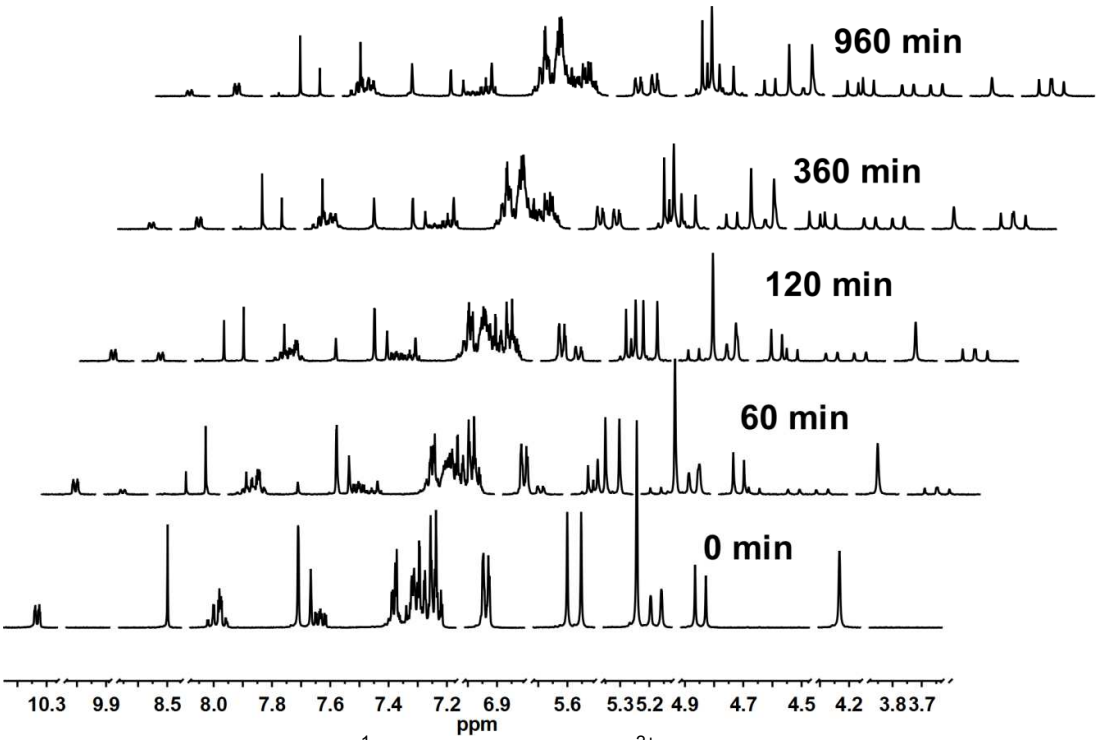

Figure S60. Changes in the ^{1}H NMR spectrum of $\mathbf{5}^{2+}$ in CD_3CN upon irradiation (369 nm).

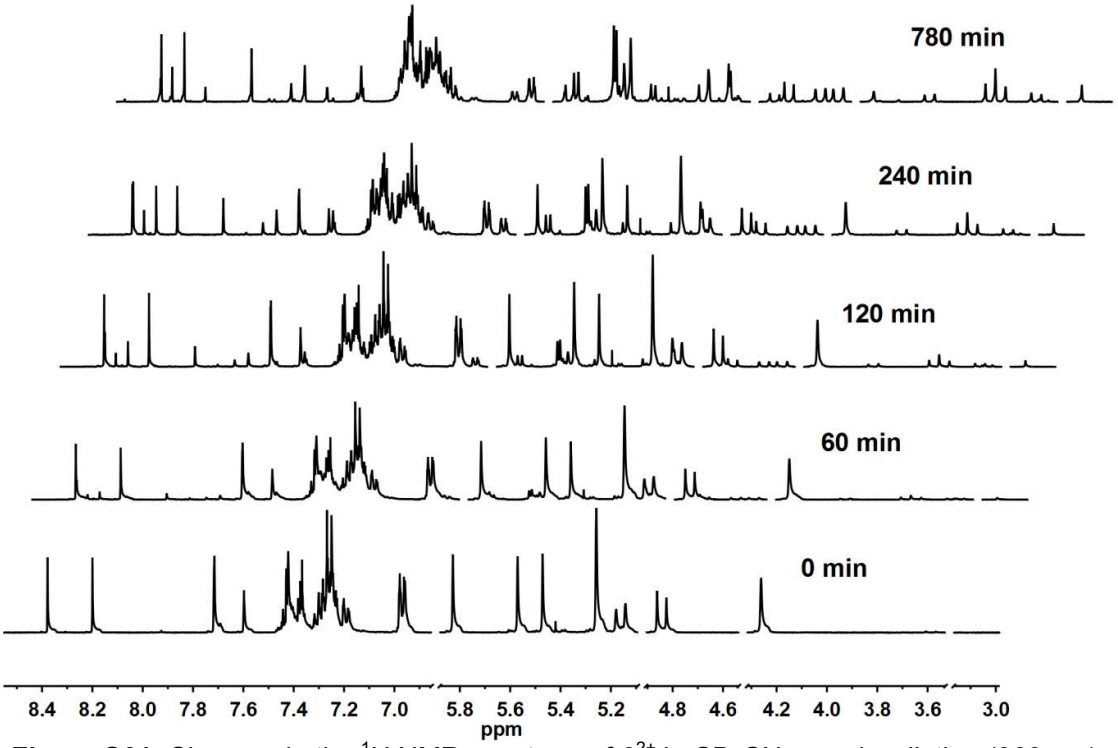

Figure S61. Changes in the ^{1}H NMR spectrum of $\mathbf{6}^{2+}$ in CD_3CN upon irradiation (369 nm).

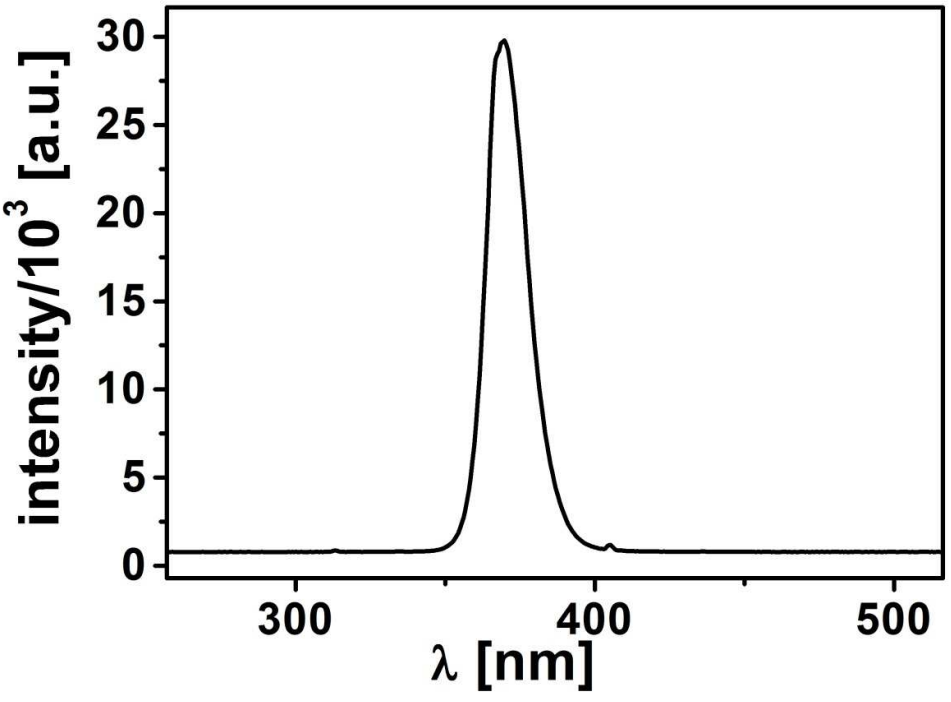

Figure S62. Emission profile of the light source used for the photoexperiments.

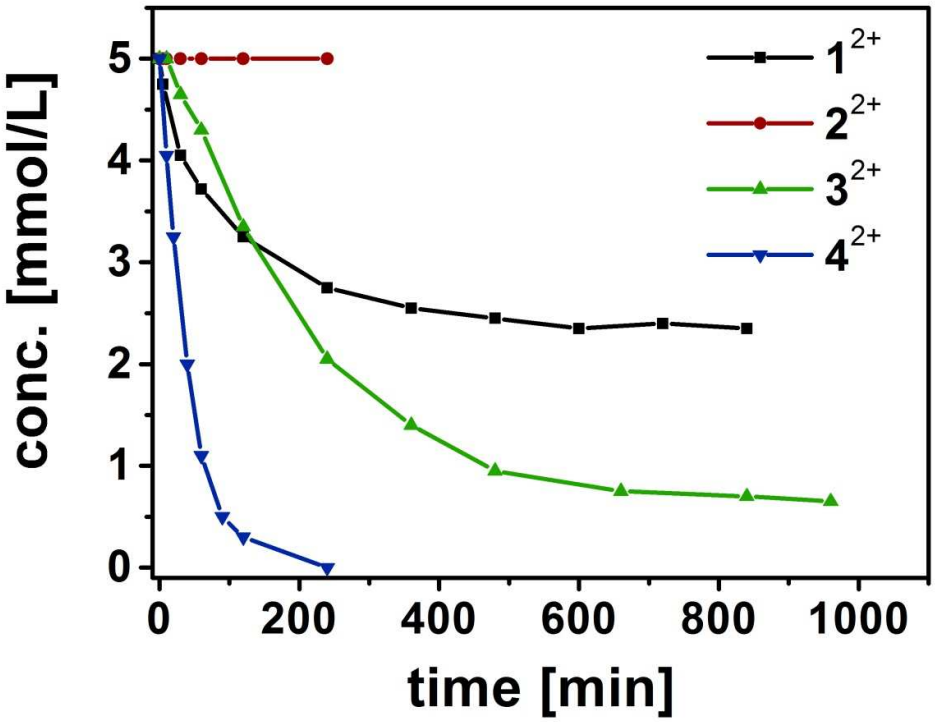

Figure S63. Change in concentration of $\mathbf{X}^{2+}$ (complexes $\mathbf{1}^{2+}$–$\mathbf{4}^{2+}$) over time upon irradiation (369 nm) in CD_3CN.

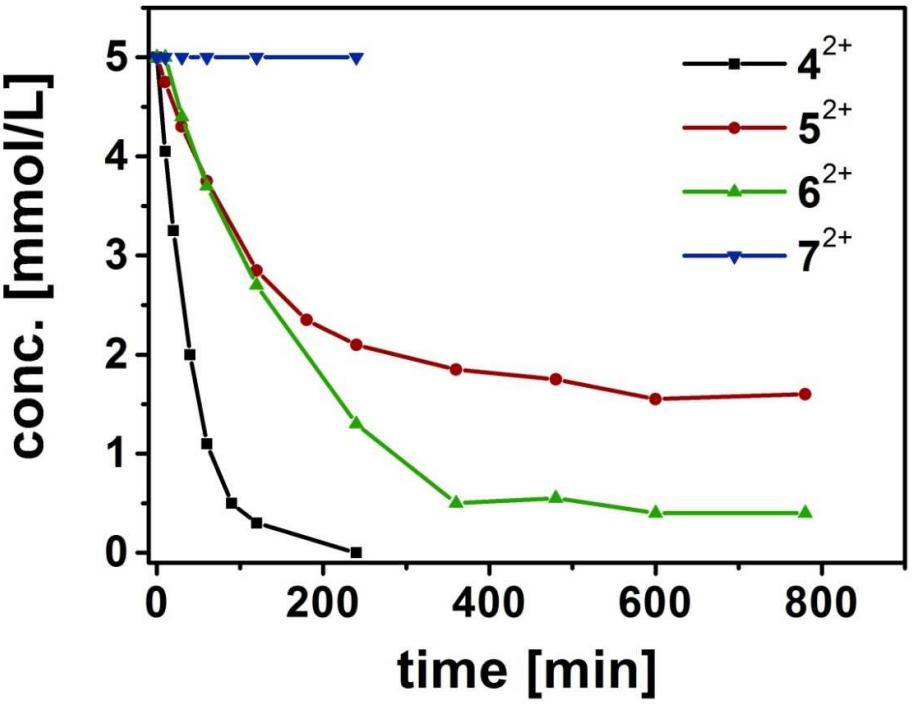

Figure S64. Change in concentration of $\mathbf{X}^{2+}$ (complexes $\mathbf{4}^{2+}$–$\mathbf{7}^{2+}$) over time upon irradiation (369 nm) in CD_3CN.

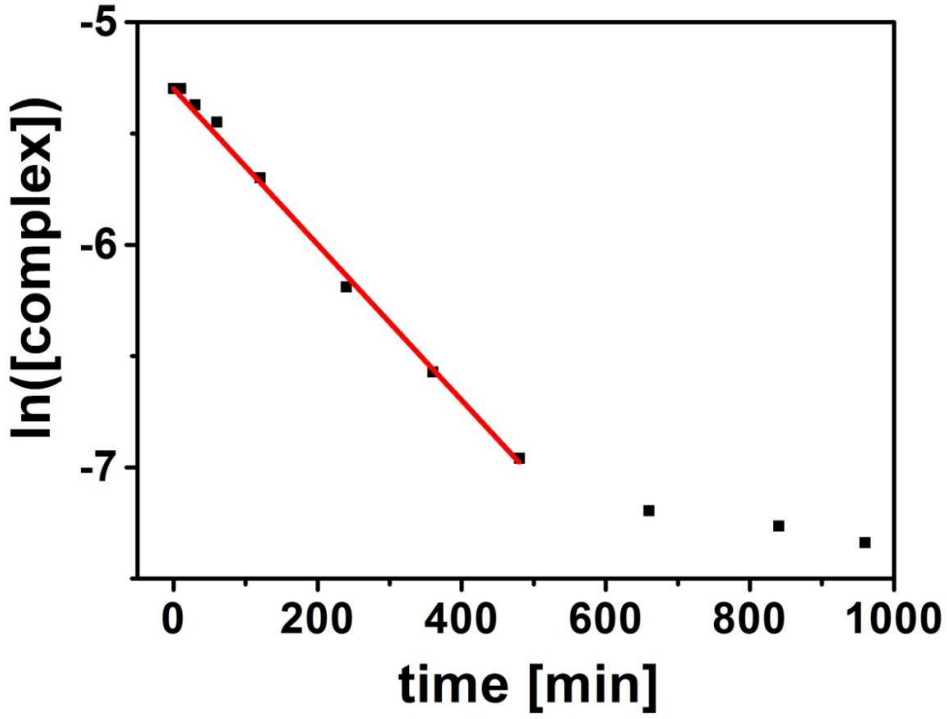

Figure S65. Logarithmic plot of the concentration of $\mathbf{3}^{2+}$ over time upon irradiation (369 nm) in CD_3CN. Initially, the transformation of $\mathbf{3}^{2+}$ follows first-order kinetics (linear fit, red).

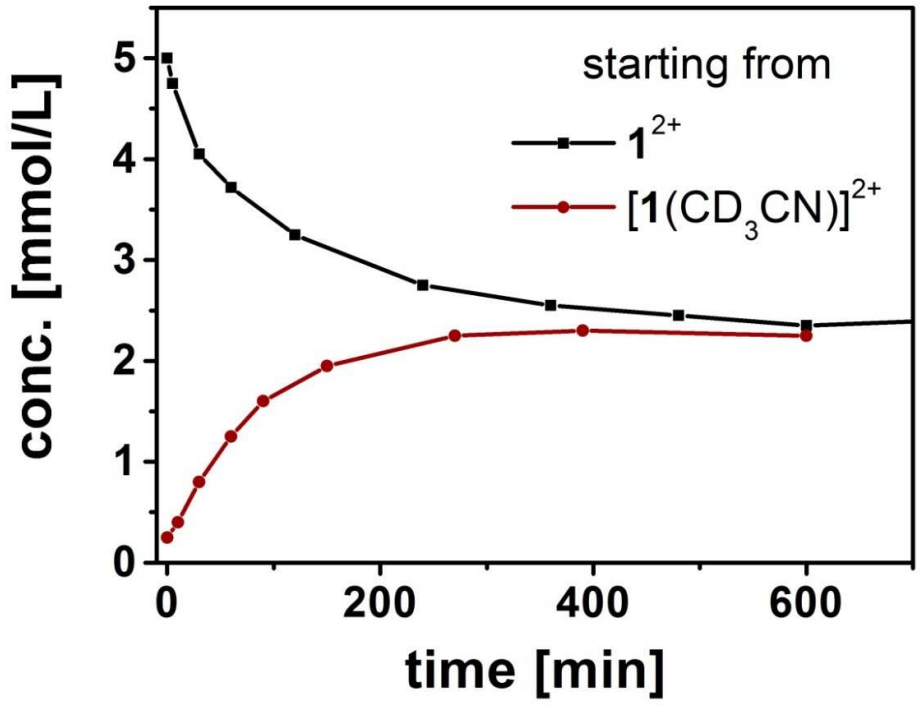

Figure S66. Comparison of the light-driven dissociation of $\mathbf{1}^{2+}$ and $[\mathbf{1}(CD_3CN)]^{2+}$ upon irradiation (369 nm) in CD_3CN.

{**3**(CD_3CN)]·(PF_6)}$^+$ {**4**(CD_3CN)]·(PF_6)}$^+$

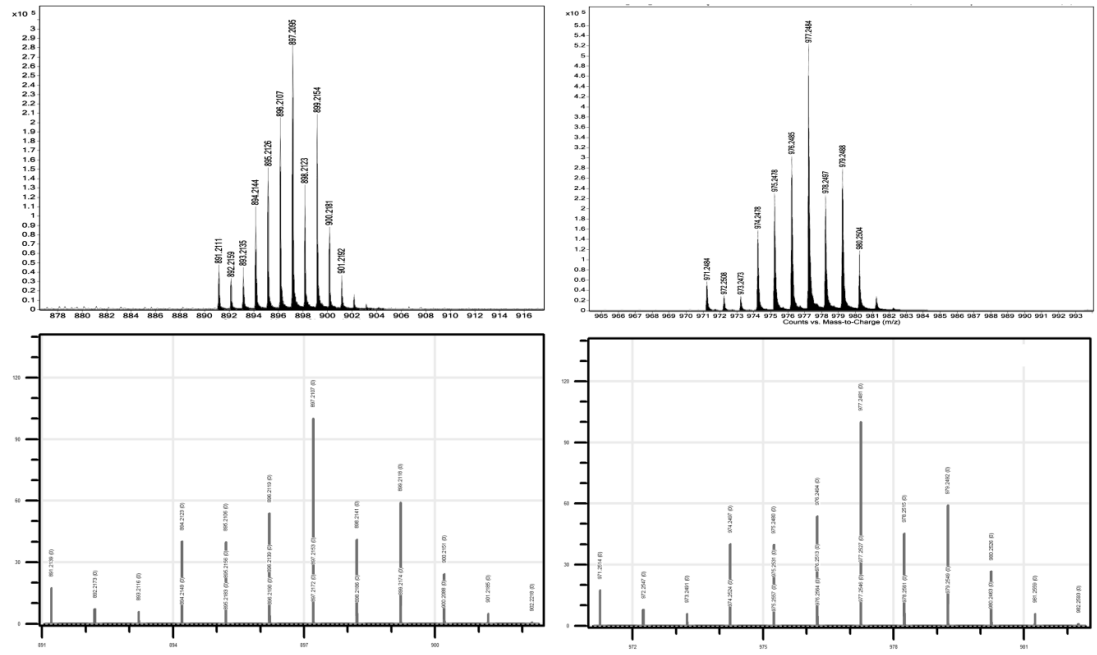

{**5**(CD_3CN)]·(PF_6)}$^+$ {**6**(CD_3CN)]·(PF_6)}$^+$

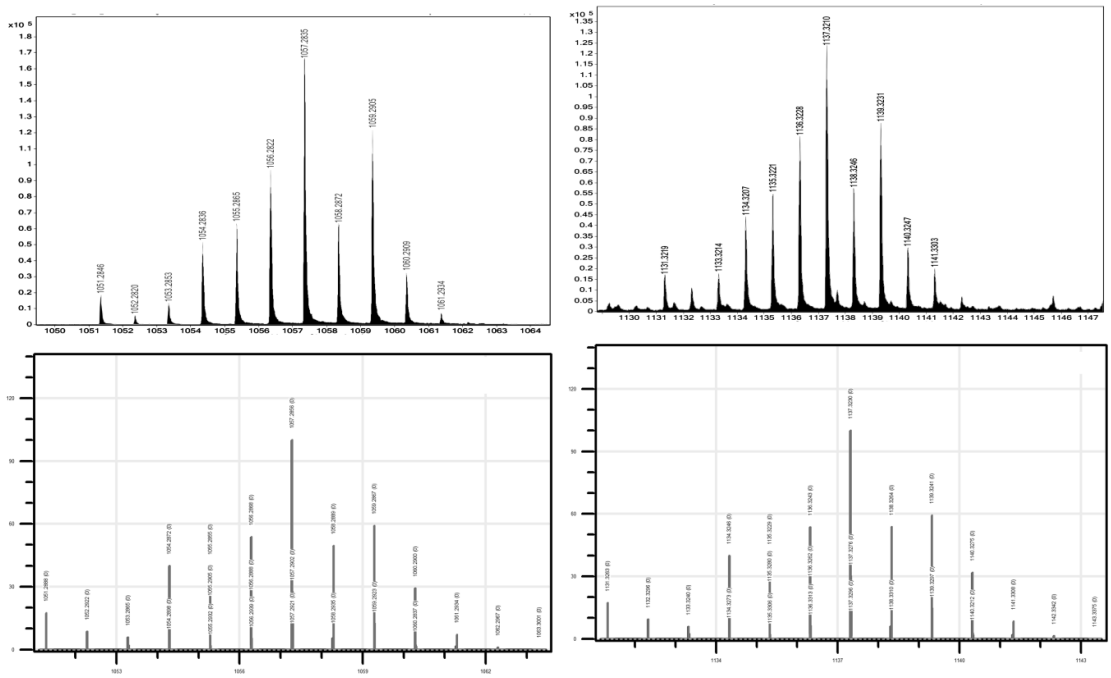

Figure S67. Experimental (top) and simulated (bottom) ESI mass spectra of {**3**(CD_3CN)]·(PF_6)}$^+$, {[**4**(CD_3CN)]·(PF_6)}$^+$, {[**5**(CD_3CN)]·(PF_6)}$^+$, and {[**6**(CD_3CN)]·(PF_6)}$^+$.

Table S6. Rate constants and quantum yields of the photoreactions of $\mathbf{1}^{2+}$–$\mathbf{7}^{2+}$.

Complex	Initial reaction rate[a] k_{init} [10^{-3}·s^{-1}]	Conversion efficiency[a] [%] (time [min])	Quantum yield[b] (350–400 nm) $\phi_{350–400nm}$	Quantum yield (monochromatic irradiation) ϕ_{λ}
$\mathbf{1}^{2+}$	3.2	53 (600)	0.0054	0.0021 (λ = 423 nm)[4]
$\mathbf{2}^{2+}$	–	–	–	–
$\mathbf{3}^{2+}$	3.6	87 (960)	0.0081	–
$\mathbf{4}^{2+}$	24.2	99 (240)	0.0360	0.0604 (λ = 436 nm)[c]
$\mathbf{5}^{2+}$	4.4	70 (600)	–	
$\mathbf{6}^{2+}$	5.5	92 (600)	–	
$\mathbf{7}^{2+}$	–	–	–	

(a) Measured with 5 mmol/L samples (100 % absorbance) in NMR tubes with broad-band irradiation (350–400 nm, Figure S62). (b) Determined by using a ferrioxalat actinometer. Samples of $\mathbf{1}^{2+}$ ($3.2 \cdot 10^{-5}$mol/L), $\mathbf{3}^{2+}$ ($6.7 \cdot 10^{-5}$mol/L), and $\mathbf{4}^{2+}$ ($7.4 \cdot 10^{-5}$mol/L) absorbed 66, 78, and 48 %, respectively, of the light between 350 and 400 nm. (c) Determined by using a ferrioxalat actinometer and monochromated light (spectrofluorimeter source) at 436 nm, where the sample of $\mathbf{4}^{2+}$ ($6.3 \cdot 10^{-5}$mol/L) absorbed 46 % of the light.

Mechanism of the Photoreaction

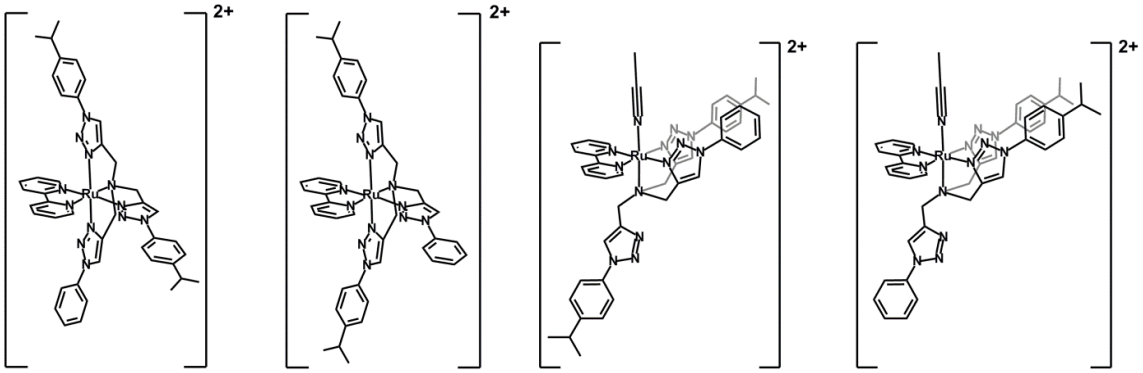

8a^{2+} **8b**$^{2+}$ [**8a**$(CD_3CN)]^{2+}$ [**8b**$(CD_3CN)]^{2+}$

Scheme S7. Isomers of complex **8**$^{2+}$ and of its acetonitrile adduct [**8**$(CD_3CN)]^{2+}$.

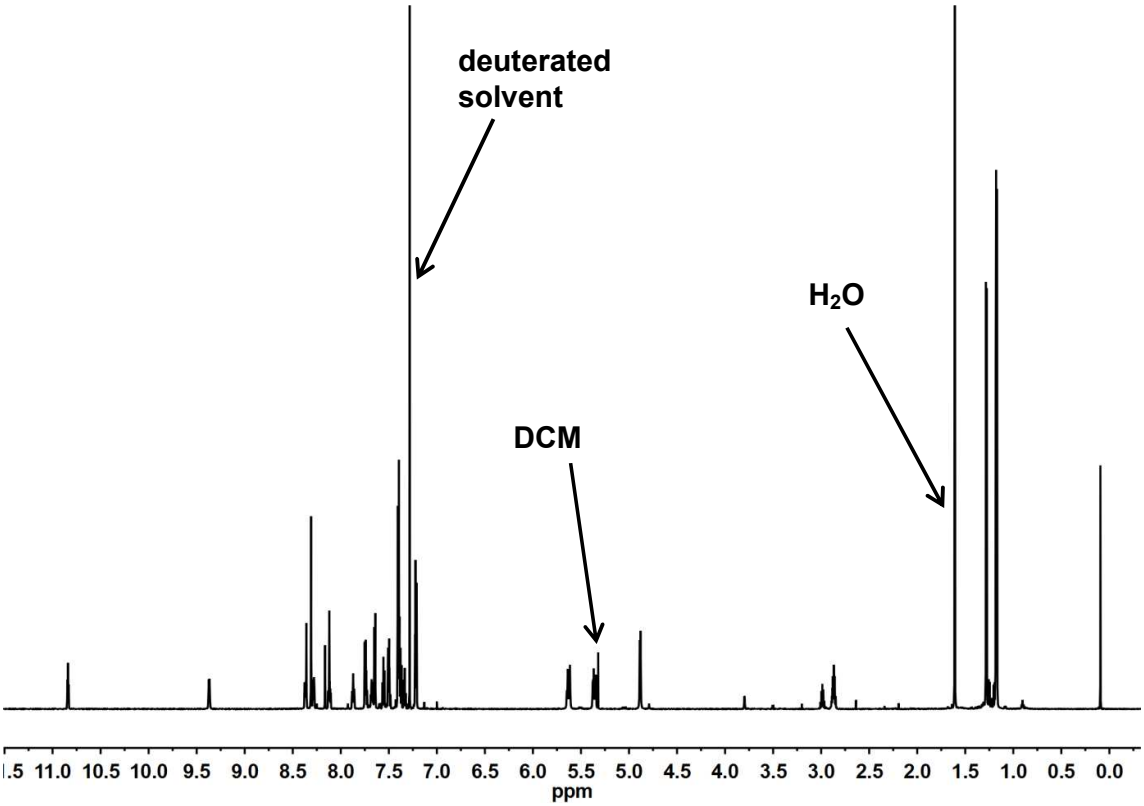

Figure S68. Full ^{1}H NMR spectrum (700 MHz, CD_3Cl) of **8**$^{2+}$. Solvent impurities are indicated.

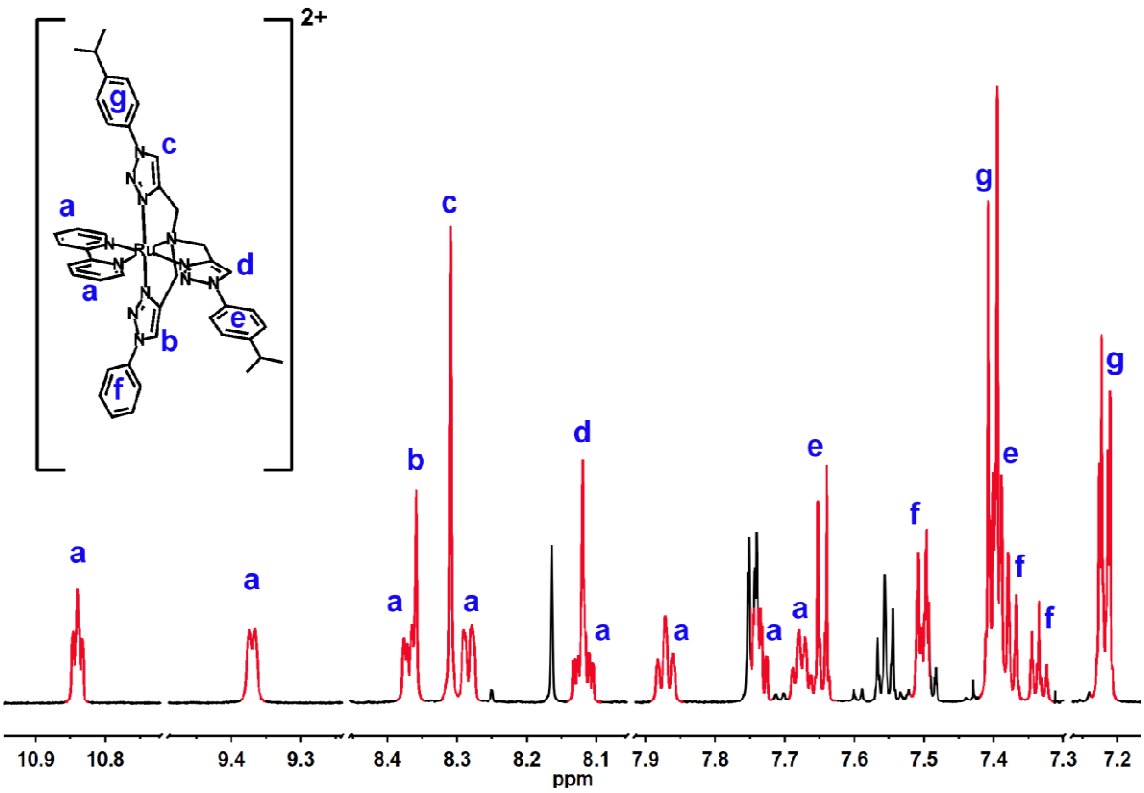

Figure S69. ^{1}H NMR resonances (700 MHz, $CDCl_3$) of **8a**$^{2+}$ (aromatic region).

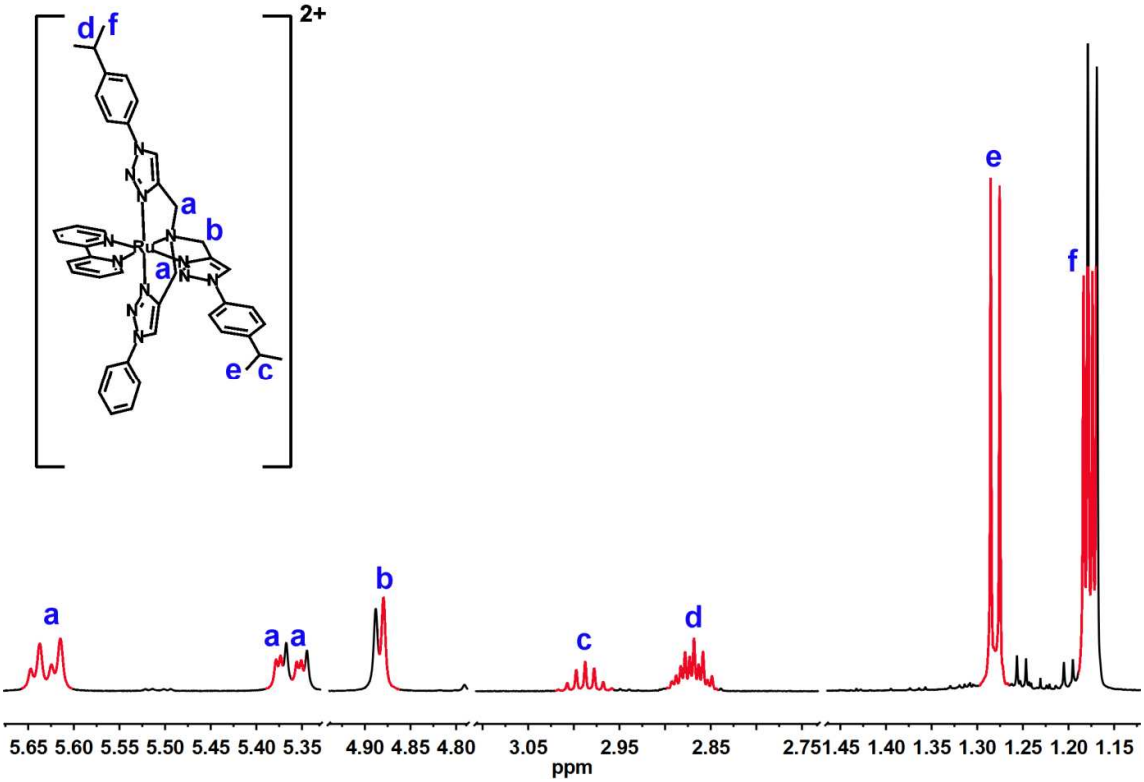

Figure S70. ^{1}H NMR resonances (700 MHz, $CDCl_3$) of **8a**$^{2+}$ (aliphatic region).

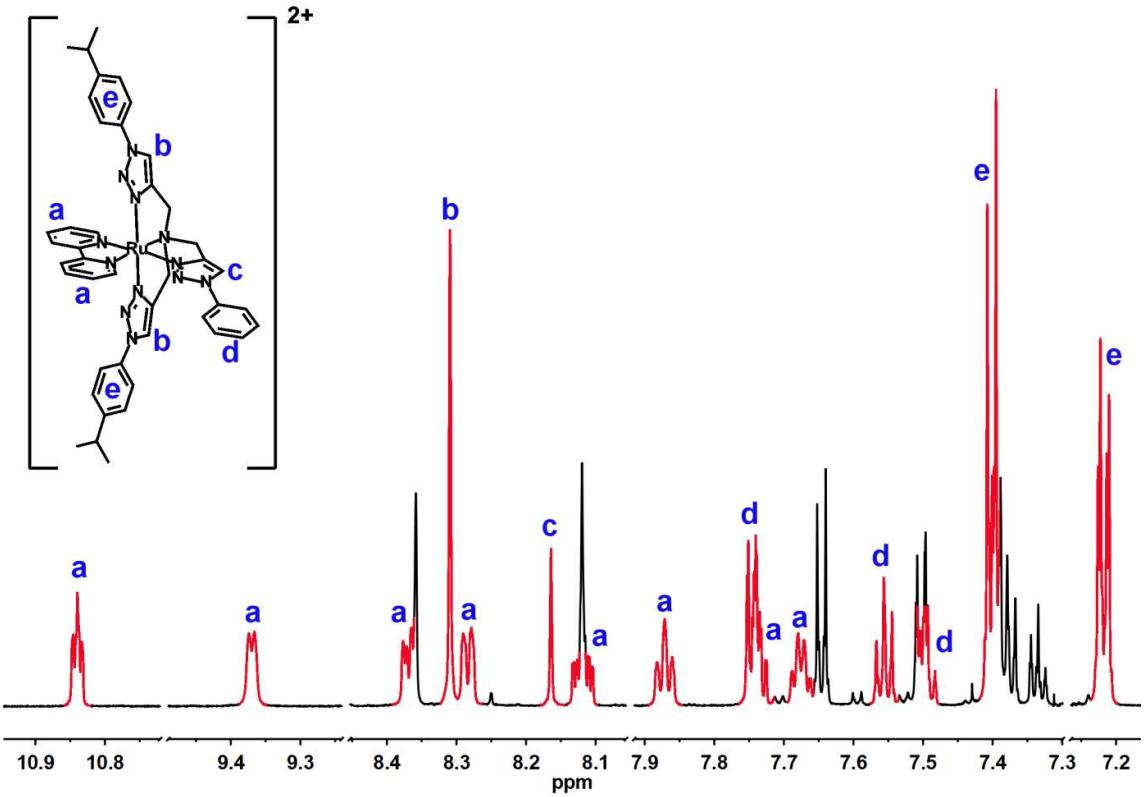

Figure S71. ^{1}H NMR resonances (700 MHz, $CDCl_3$) of **8b**$^{2+}$ (aromatic region).

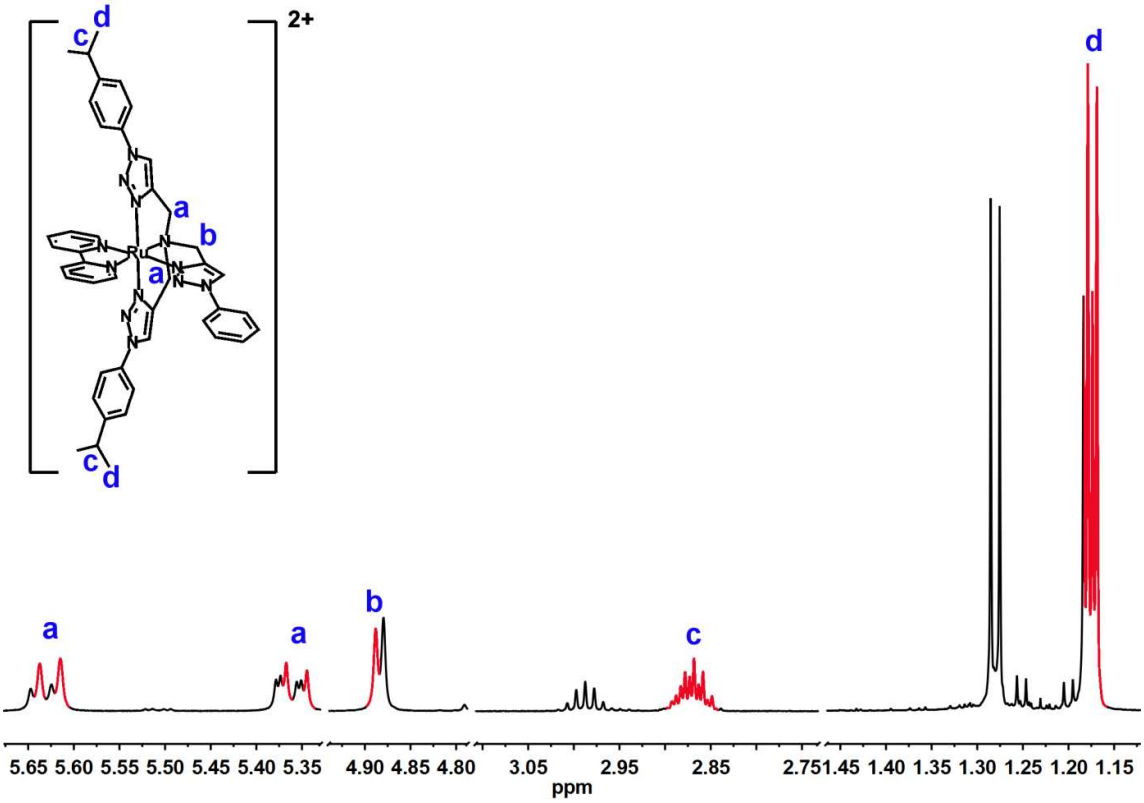

Figure S72. ^{1}H NMR resonances (700 MHz, $CDCl_3$) of **8b**$^{2+}$ (aliphatic region).

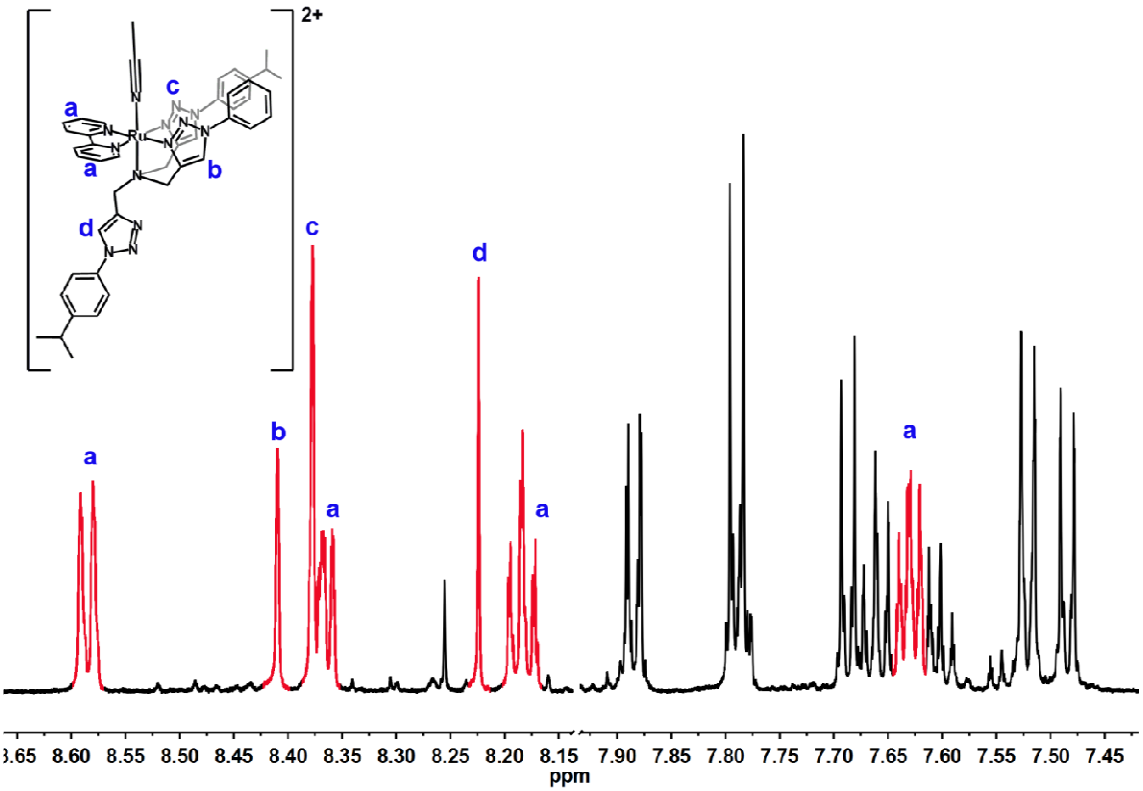

Figure S73. ^{1}H NMR resonances (700 MHz, CD_3CN) of [**8a**(CD_3CN)]$^{2+}$ (aromatic region).

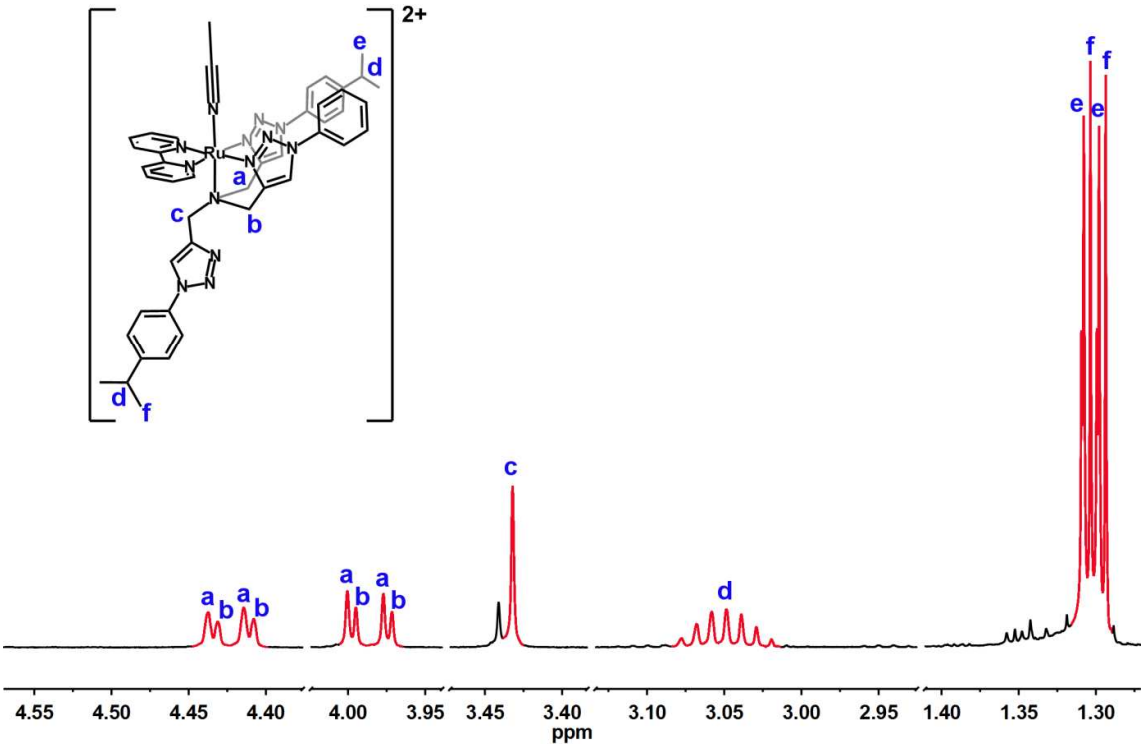

Figure S74. ^{1}H NMR resonances (700 MHz, CD_3CN) of [**8a**(CD_3CN)]$^{2+}$ (aliphatic region).

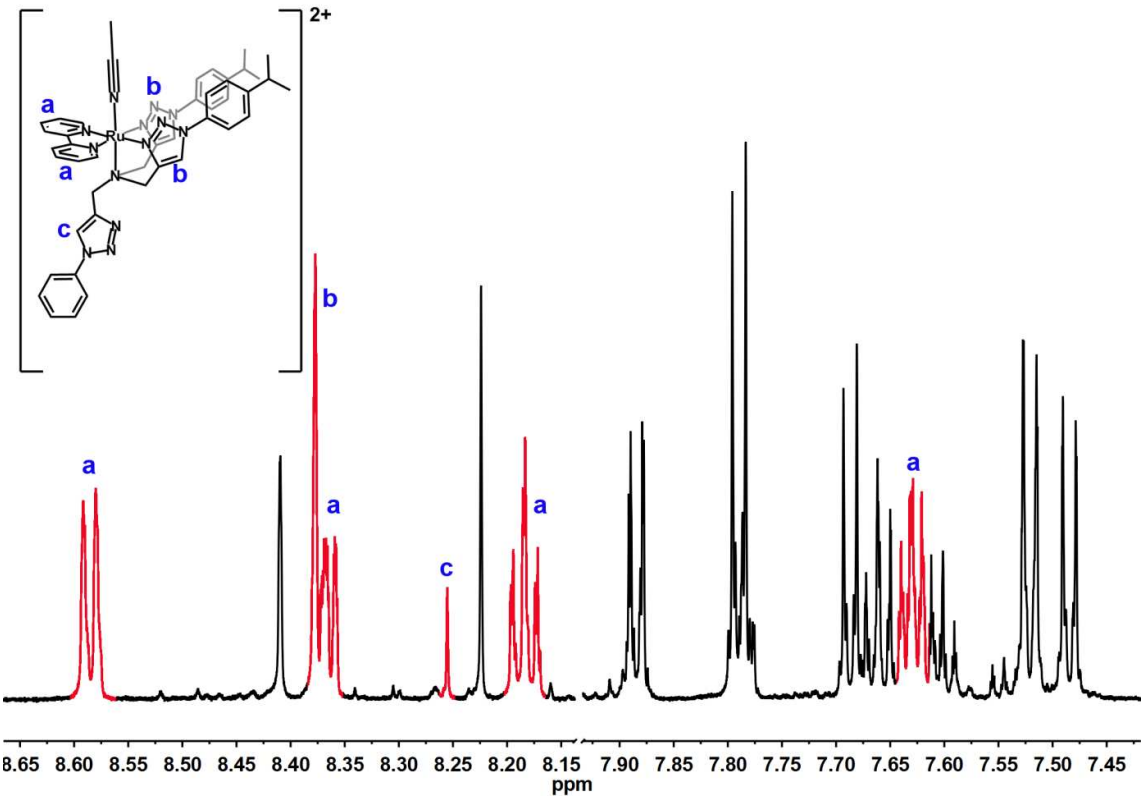

Figure S75. ^{1}H NMR resonances (700 MHz, CD_3CN) of [**8b**(CD_3CN)]$^{2+}$ (aromatic region).

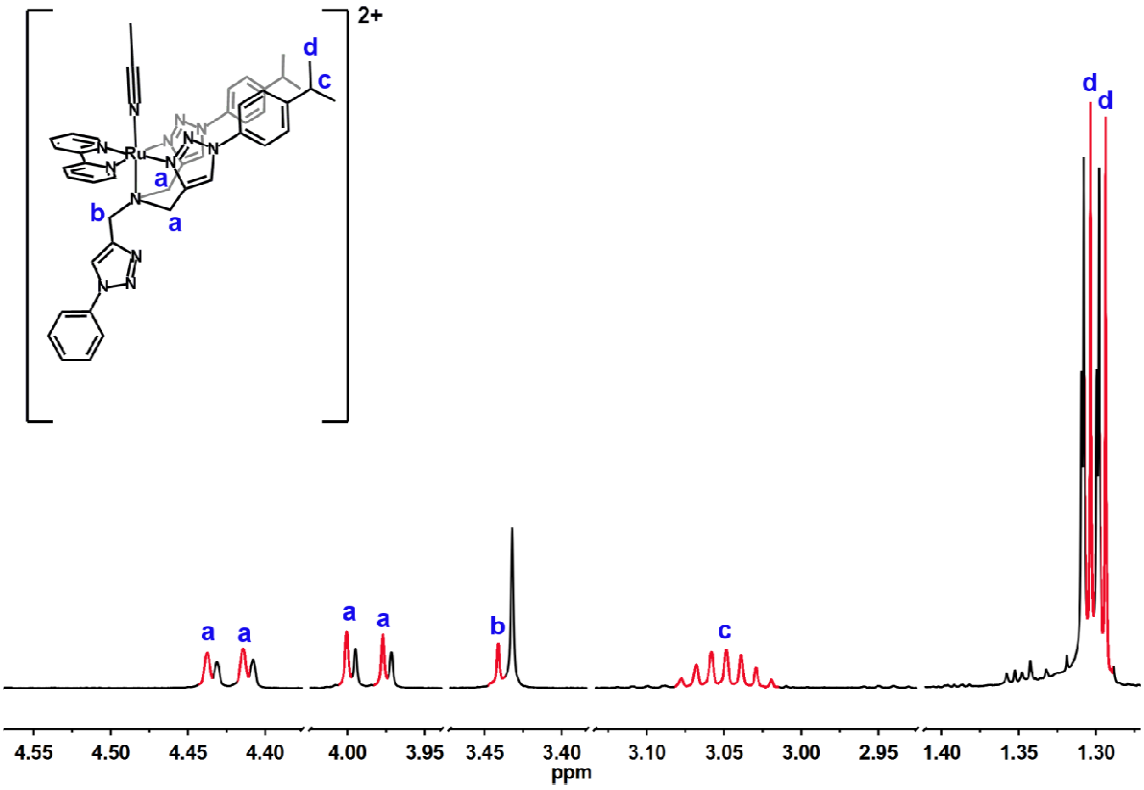

Figure S76. ^{1}H NMR resonances (700 MHz, CD_3CN) of [**8b**(CD_3CN)]$^{2+}$ (aliphatic region).

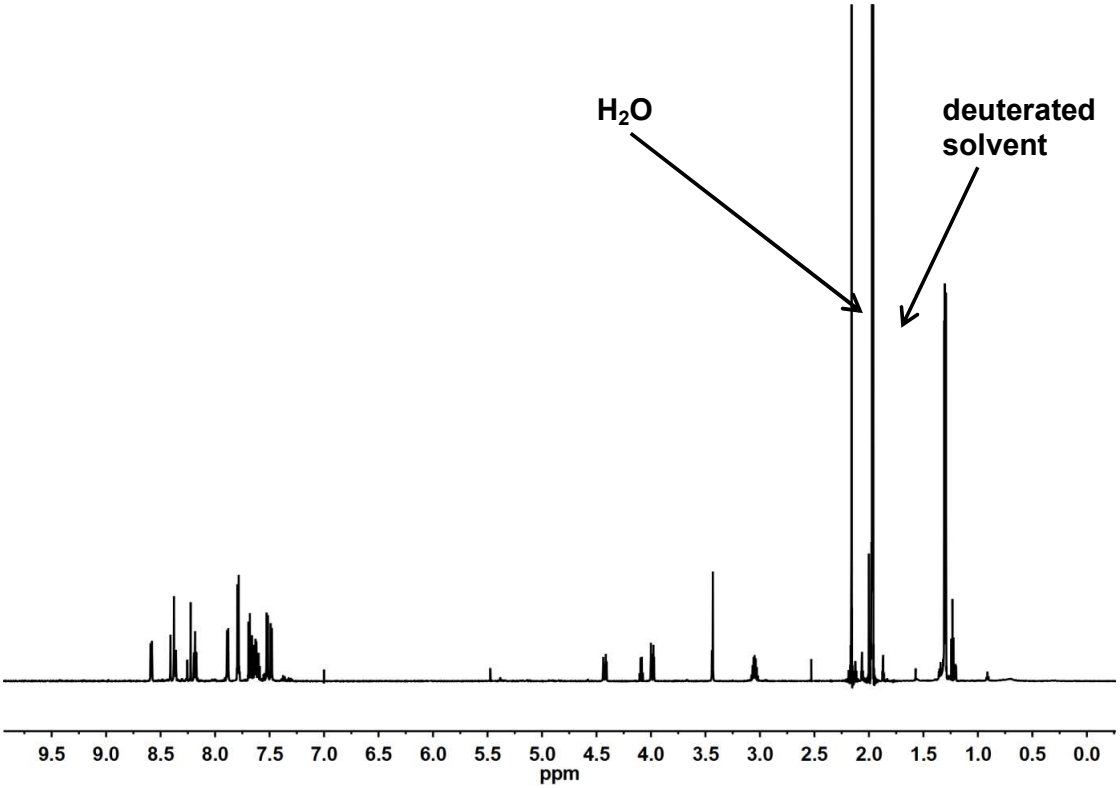

Figure S77. Full ^{1}H NMR spectrum (700 MHz, CD_3CN) of [**8**(CD_3CN)]$^{2+}$. Solvent impurities are indicated.

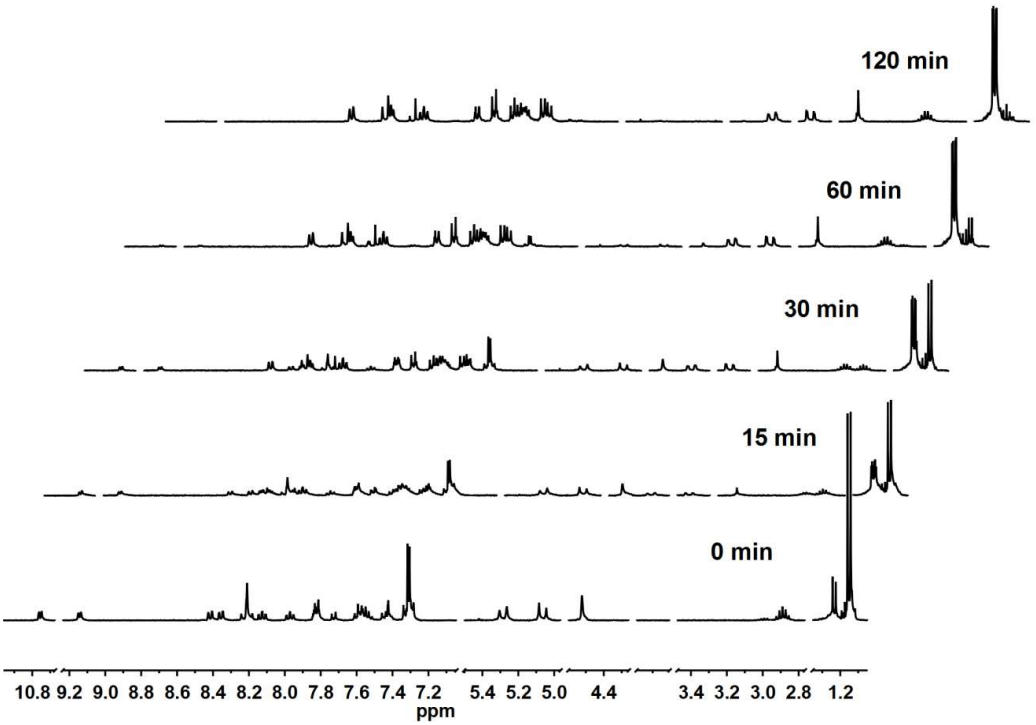

Figure S78. Changes in the ^{1}H NMR spectrum (400 MHz, CD_3CN) of **8**$^{2+}$ upon irradiation (369 nm).

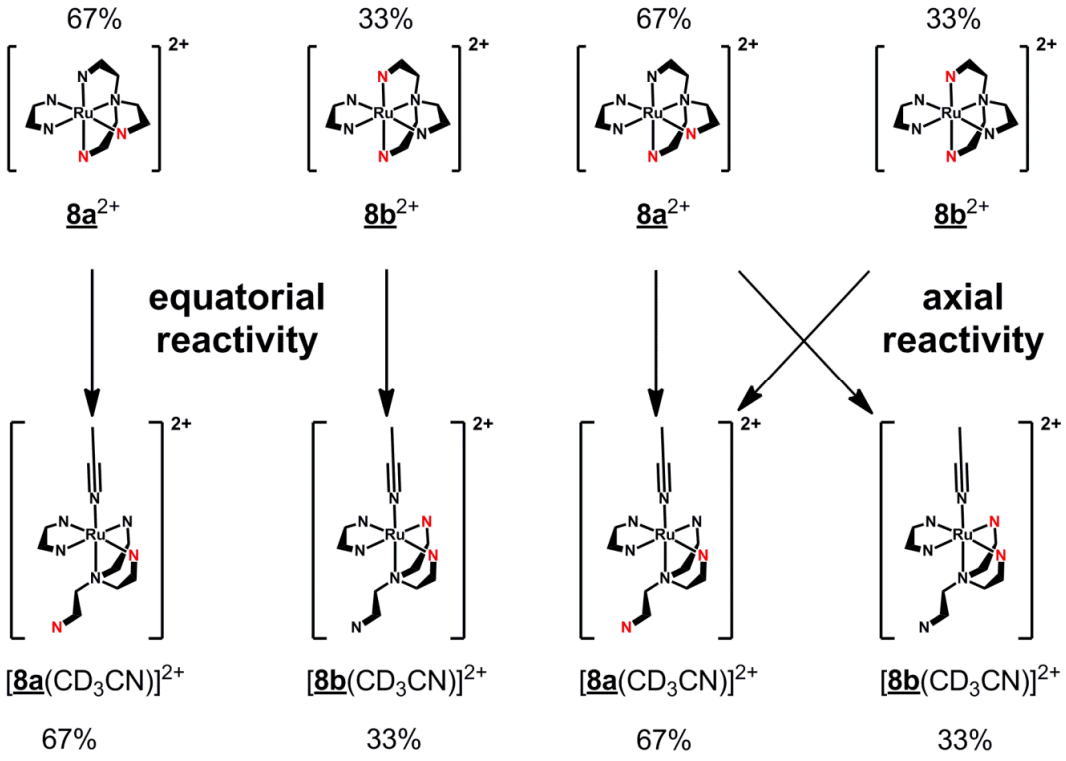

Scheme S8. Product ratios $[\mathbf{8a}(CD_3CN)]^{2+}/[\mathbf{8b}(CD_3CN)]^{2+}$ expected when starting from a 2:1 mixture of $\mathbf{8a}^{2+}/\mathbf{8b}^{2+}$. Isopropyl arms are indicated by a red N.

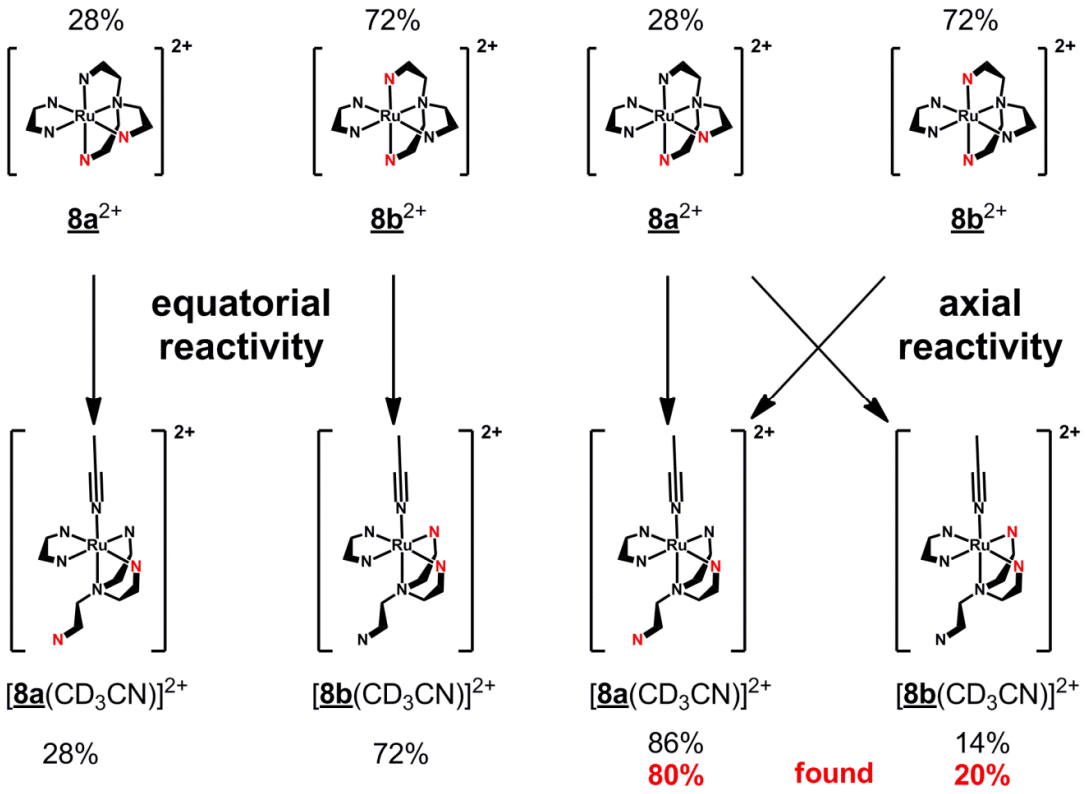

Scheme S9. Product ratios $[\mathbf{8a}(CD_3CN)]^{2+}/[\mathbf{8b}(CD_3CN)]^{2+}$ expected when starting from a 3:7 mixture of $\mathbf{8a}^{2+}/\mathbf{8b}^{2+}$. Isopropyl arms are indicated by a red N.

DFT Calculations

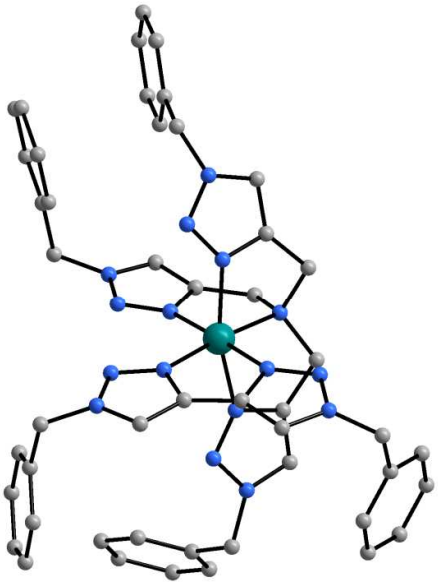

Figure S79. Optimized geometry of $\mathbf{6}^{2+}$ obtained by DFT calculations.

Table S7: Geometry coordinates of $\mathbf{6}^{2+}$

Ru	8.88549224533536	3.76304462001656	11.89049059493820
N	8.13282096930246	4.82521604840193	13.59471134455042
N	10.66813421601212	4.35435815578616	12.71135912144356
N	6.15847837199549	2.83500450302483	10.74483736303099
N	6.89006196903332	3.54607585832941	11.57735923553111
N	12.50271846525875	4.45504463304872	13.77649993575633
N	4.89191333507100	3.23425441502582	10.95328844541550
N	9.56687181105760	1.08344447259948	13.19970226146882
N	11.87881404420374	3.83528473766439	12.75519830608614
N	9.00359256922231	2.27400661466349	13.25759847599198
C	13.82687704904390	4.01170896343884	14.20556256559619
H	14.52169766810585	4.85947019753847	14.14632999102915
H	14.14116289519438	3.26114873701793	13.46763899208164
N	9.61943394370354	0.64991049115874	14.46904898749919
C	7.97795357156708	3.89513057017620	14.78586178045721

H	8.31799596274354	4.39973919534232	15.69943839003215
H	6.90578648957633	3.69055003484719	14.90769201606245
C	10.49853505226247	5.28492757165505	13.71518141625532
C	3.41823728678877	1.26073534948756	10.88298016846280
C	13.79865196824407	3.43270147020383	15.60384143997960
C	4.23732026738410	0.13311337395895	10.72913120988234
H	5.14330521089436	0.19686753714600	10.12377064221531
C	8.69814678327469	2.61365685284165	14.55031238022394
C	13.91997168415043	0.37454904991130	13.97147437352588
H	14.48211091396414	0.83299745833964	13.15652307377667
C	13.85719626322656	-0.61605637429811	16.17518065255004
H	14.36261877398661	-0.91790422379109	17.09293523442929
C	12.47758570608354	-0.80401574234763	16.04821480848271
H	11.91129346874821	-1.25585750542169	16.86509093350992
C	1.92254932579044	-0.03019965025803	12.29176140344929
H	1.01739592355456	-0.09128487604615	12.89739567890420
C	4.80793670048097	4.18512499887224	11.92418790062874
H	3.86834480407700	4.62551407073033	12.23094317985474
C	10.31906318154152	-0.60583708430926	14.75920404969607
H	10.07241212845366	-1.28969628723677	13.93680950734572
H	9.89546099947910	-1.01211549142065	15.68449456461716
C	9.14949031937905	5.90009743892054	13.86840605410412
H	9.01134693976688	6.34523449834370	14.86359702589649
H	8.99780762780096	6.68055670986136	13.11040317071761
C	11.81365485678173	-0.40124543602559	14.88561182390428
C	13.81968200950214	2.32388876907697	18.18019440884116
H	13.82629962355702	1.89200448044545	19.18166274138745
C	3.79972416320155	2.56929368904261	10.23166664669746
H	4.15039852795239	2.42167551867710	9.20303748013575
H	2.95595395037717	3.26872129184863	10.21469672999546
C	9.10900511046879	1.56200553991212	15.34341971440522
H	9.06345574680784	1.38781730182207	16.41162034949415

C	2.74290361872162	-1.15128072716933	12.13895550638402
H	2.48028652047735	-2.09147144772733	12.62580574982159
C	11.68711789321520	5.34609033728113	14.40426805132718
H	12.00228477680478	5.91711576051513	15.26895614644620
C	6.79356869878144	5.38899832135292	13.21297787765164
H	6.97846948133583	6.31045347732020	12.64435395938579
H	6.19622186856557	5.64041294354498	14.09993053948178
C	12.66293961234038	2.26506462654904	17.39862007549405
H	11.76629418978162	1.78095314245388	17.78679801187518
C	12.65373110689667	2.81184624248338	16.11588036963240
H	11.74876740152379	2.74611733358185	15.51080825727740
C	6.10878180788213	4.40204142422312	12.32133544226007
C	3.89997643430163	-1.06699341055029	11.35629540564222
H	4.53839775640549	-1.94248310831410	11.23305186227099
C	2.26123029877473	1.17324449125788	11.66580826285354
H	1.61931373546668	2.04882977995692	11.78334864484029
C	14.57990988368377	-0.02396550664509	15.13882356886965
H	15.65354941848427	0.13598949349167	15.24174562400096
C	12.54357188134406	0.18939745309176	13.84349880641534
H	12.02753203281752	0.51902265238101	12.94031154261462
C	14.95566319830160	3.49221879765329	16.38914616810100
H	15.85090657745672	3.97917440901473	15.99717277210384
C	14.96838720213618	2.93419767061023	17.66983783067473
H	15.87596351570084	2.98569881546875	18.27292373955272
H	8.22610660781365	5.96430792209827	7.30167967146986
C	8.35306647074435	5.85192129462285	8.37117236527594
N	7.99564634075571	6.81981608507436	9.25724215565381
C	7.11889630435683	7.97791493864036	9.02225834034110
H	7.51426073817968	8.82238224953774	9.59781501845655
C	5.71391373658831	7.61472219764215	9.45265305642747
C	5.21409400143530	8.06104368609911	10.68176403707704
C	3.94911993460090	7.65664349945529	11.11693770587788

H	3.56656657390220	8.00979504907988	12.07537400305866
C	3.17860882183317	6.79860356402929	10.32680587535911
H	2.19026854076738	6.48420178518280	10.66546111255045
C	3.67555162283839	6.34643881101789	9.09999712193811
H	3.07621367265653	5.68110054083545	8.47719890833430
H	5.81932188682548	8.72534602946170	11.30125316604742
C	4.93832706679786	6.75347280618838	8.66507228664848
H	5.32275431819223	6.39686354464766	7.70721789673721
H	7.18317604902654	8.21302303703243	7.95381654135750
N	8.21494707700297	6.44321428354688	10.53007448274427
N	8.72241237283351	5.23098393796067	10.46760078238905
C	8.83399444173391	4.81833627807978	9.15208449616438
C	9.27348625034779	3.46060331633095	8.99927553904707
N	9.44954369529759	2.78311371365881	10.19641188504880
N	9.80164604948288	1.53717826292296	9.97238145799750
N	9.84558081191507	1.40375876230864	8.63185534560671
C	9.99991564832862	0.05749979053014	8.06262211453545
H	10.80871732223193	-0.43299193560380	8.61707158290728
H	10.31160520322756	0.18440172145724	7.01988658926854
C	8.70127191118209	-0.70948215004312	8.17112463301587
C	8.34928120813445	-1.32451851572388	9.38024175759752
H	9.03061588186329	-1.26969523548883	10.23046592270850
C	7.12685375181981	-1.98694605016912	9.50129154837767
H	6.86435755469257	-2.46884097003730	10.44415369133097
C	6.24359209003056	-2.03424337853489	8.41751136925856
C	6.58922673775394	-1.42006015399922	7.21053580629343
H	5.90488996369849	-1.45616381087701	6.36183846515854
H	5.28704088426118	-2.54989160097185	8.51277843330199
C	7.81569799608673	-0.76052540765405	7.08815904519322
H	8.08615693402622	-0.28246453980960	6.14428379759148
C	9.52097997520390	2.55496830366020	7.98759173323147
H	9.48769374592304	2.63418281796229	6.90802947330354

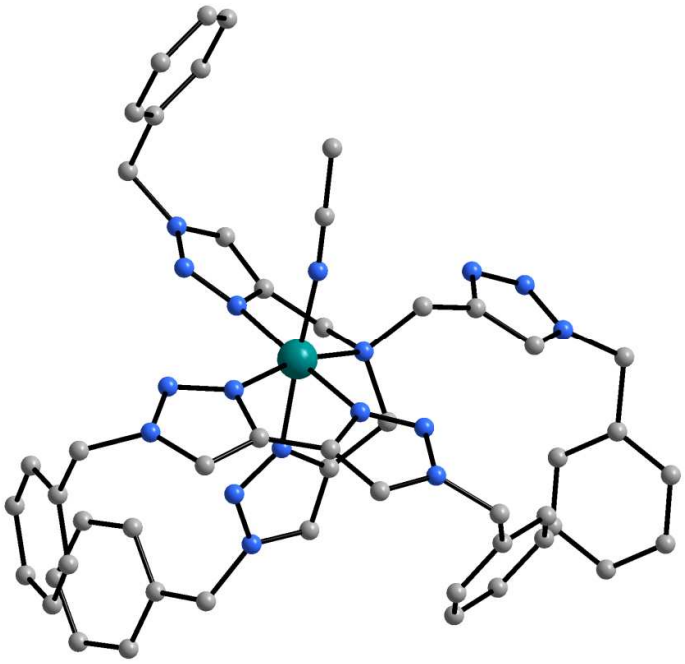

Figure S80. Optimized geometry of [**6a**$(CH_3CN)]^{2+}$ obtained by DFT calculations.

Table S8: Geometry coordinates of [6a$(CH_3CN)]^{2+}$

Ru	9.75680875906767	3.42861651883564	11.84270665279991
N	9.16951908178085	4.60658047805656	13.59120977567310
N	9.79358521065461	6.13543300275632	16.45431921434512
N	6.91581033938252	3.03026160277110	10.76747792504622
N	7.76126202526076	3.64753504186328	11.56602821922630
N	9.27552317722924	8.20963469932123	16.21497102313105
N	5.73575903550539	3.64451226320904	10.96100324553317
N	10.08923143367423	0.71559743630556	13.20708928137366
N	9.39451369662219	7.20128773710012	17.11331653905996
N	9.58733219133308	1.93380385420801	13.21710583328366
C	8.78039922419456	9.52293152403212	16.62353894034126
H	9.52106199859363	10.28151850158122	16.34057090433388
H	8.72705569533656	9.49136149844385	17.72027183048604
N	10.07110492031883	0.31131953789765	14.48729447266886

C	8.66801734340316	3.67115973883615	14.67620425415075
H	8.88038775377696	4.09008519037269	15.66873648083889
H	7.57555499591844	3.60592619603855	14.57626972500556
C	9.92422255813933	6.44942772674995	15.12552159931464
C	3.81064775324807	2.09205328063089	11.11012899543623
C	7.43236537878764	9.83231971166197	16.01131233292812
C	4.47449469268519	1.26663256708012	12.02419037876864
H	5.54656624192772	1.38155301610950	12.18713013533640
C	9.26313987333177	2.32408826019801	14.49143039069778
C	14.36339624228786	-0.92287766824567	13.66057960519166
H	14.93357608799520	-1.21606812210700	12.77813155317417
C	14.27517664561958	0.04289039062327	15.87957889111275
H	14.77677020735920	0.50154244301669	16.73262972617318
C	12.89599395692943	-0.17416844073894	15.91778826860357
H	12.32484602709273	0.11531079085348	16.80237750337580
C	1.74370935817980	0.90523895811201	11.56169250948188
H	0.67709741446213	0.76897269387560	11.37803058221230
C	5.82270618058575	4.64008836782074	11.88869588846681
H	4.96785616030207	5.23369763985317	12.18625791626594
C	10.74167139368314	-0.94612933407652	14.84735310777887
H	10.41915002245743	-1.70592501934405	14.12643770868731
H	10.37547198291426	-1.22487532931637	15.84212183016952
C	10.31306993550232	5.45178379770505	14.08936286021489
H	10.73142832134789	5.96033853368416	13.21367462601441
H	11.06670051644503	4.75862814104588	14.48059318684392
C	12.24245714749601	-0.76454588652051	14.82797381924549
C	4.92180727405907	10.44267170673462	14.91745415684703
H	3.94777449905040	10.67796324727304	14.48693113532058
C	4.55175513456772	3.12227622484685	10.28698388821426
H	4.91388249428334	2.67505788650568	9.34946973310668
H	3.90414994159233	3.97032445511318	10.03447809686729
C	9.58363264956412	1.27154873999838	15.32094760661629

H	9.50344650420721	1.13241134310062	16.39208965980276
C	2.41069816259449	0.08099892674187	12.47338109073655
H	1.86709444340409	-0.70296648704240	13.00221454660187
C	9.59006309481407	7.78402311664386	14.96901261773104
H	9.55956097187338	8.43416051208402	14.10279466318436
C	8.02073742755825	5.47617192244552	13.14978658137660
H	8.44196803180165	6.31541054045646	12.57832696169503
H	7.47574362360614	5.88387291493195	14.01228810685024
C	5.18058988511880	9.15839182953079	15.40848331034599
H	4.40759057040297	8.39001813166097	15.36600338853596
C	6.42881235262195	8.85496210094282	15.95390343056198
H	6.62255079756889	7.85140330004399	16.33752990605971
C	7.14723761171298	4.65171802481509	12.26909930720984
C	3.77591934160819	0.26884205553530	12.70695013355721
H	4.30335624112374	-0.37113335570550	13.41552761574361
C	2.44015760780349	1.91135485450414	10.88795309518179
H	1.91710227518365	2.55620167449803	10.17880748866575
C	15.01146670907148	-0.33306704951621	14.75079172812107
H	16.08911834657594	-0.16649002518898	14.72133395846104
C	12.98261565672419	-1.13425550722568	13.69835796553992
H	12.47468642816234	-1.58655665585240	12.84501351166567
C	7.17193726346978	11.11363342950731	15.51214539204203
H	7.95508430312958	11.87367502147624	15.54050313949453
C	5.91931254873098	11.41958033797446	14.97080570772800
H	5.72848890487571	12.41949865214850	14.57919452901515
H	9.55632362709899	6.06994143100493	7.43954684799376
C	9.70154821394226	5.83233026657838	8.48599597556006
N	9.78471084624344	6.78905754850128	9.44944931197016
C	9.42227733728274	8.21506765582405	9.36975069847730
H	10.26169754462237	8.80945977781471	9.74884307216629
C	8.17108906831927	8.42052080236411	10.19496985867492
C	8.23539619972663	9.07511587838016	11.43035358722107

C	7.10624347025137	9.14259916315070	12.25158571954756
H	7.15882412703625	9.65214288124917	13.21375164600724
C	5.90777870456630	8.55310494367713	11.84149637697290
H	5.03084423965418	8.60116678642885	12.48707050510154
C	5.83491766286428	7.91065188433804	10.60122029865938
H	4.89768085830497	7.46051711260810	10.27179852430820
H	9.17793774933628	9.52242246635963	11.75208192471058
C	6.96229345727259	7.84446374846199	9.78138741310515
H	6.90592144444038	7.32876448034243	8.82039177958149
H	9.27518596490346	8.44300904558090	8.30791085693258
N	9.93314015503598	6.25732000597510	10.67565192984068
N	9.94613176234205	4.95677097145660	10.50479448718801
C	9.81826319229034	4.63436838524552	9.16843420830488
C	9.73840885770525	3.22052046791834	8.92343738471134
N	9.84879314937116	2.43508341864308	10.06118455025988
N	9.64638397488299	1.17031132526570	9.77150843702245
N	9.40131465825441	1.13261360191303	8.44819486114961
C	8.86893901053756	-0.10792811816176	7.86161707048648
H	9.47909718321129	-0.93500395333154	8.24195339053301
H	9.00967098623067	-0.03117534404776	6.77747339708025
C	7.41276985375428	-0.26568374231183	8.23800300043226
C	7.05994357456318	-0.96969295684684	9.39638673844526
H	7.83840108359165	-1.44228117182902	9.99747031161078
C	5.72362918046998	-1.05328089100734	9.79006654747538
H	5.45737463874109	-1.59760832755847	10.69639213001215
C	4.72890940281305	-0.42929584937984	9.03188235180795
C	5.07503207271945	0.27361007341159	7.87399930117320
H	4.30215100656552	0.75774537392971	7.27513667747879
H	3.68681083645062	-0.48431429563036	9.34846371067479
C	6.41345851339965	0.35438622172266	7.47831862913822
H	6.68077026958705	0.90510980003462	6.57393120704594
C	9.43945222145899	2.36708913945076	7.88156230871511

H	9.24428250729590	2.53608377643741	6.82995437256937
N	11.70244938452652	3.29620638096591	12.23020005880907
C	12.80884685843322	3.10218833611992	12.52982250070444
C	14.17812034839605	2.84598864110681	12.91322513083096
H	14.81431659007855	2.78281278888422	12.01965165483438
H	14.23591109338275	1.89121134269462	13.45716701967385
H	14.55037504035193	3.65060551698155	13.56229204932957

Literature

(1) (a) Demko, Z. B.; Sharpless, K. B.; *Angew. Chem. Int. Ed.* **2002**, *41*, 2110; (b) Cwiklicki, A.; Rehse, K. *Arch. Pharm. Pharm. Med. Chem.* **2004**, *337*, 156.

(2) Hohloch, S.; Su, C.-Y.; Sarkar, B. *Eur. J. Inorg. Chem.*, **2011**, 3067.

(3) Kojima, T.; Sakamoto, T.; Matsuda, Y. *Inorg. Chem.* **2004**, *43*, 2243.

(4) Kojima, T.; Nakayama, K.; Sakaguchi, M.; Ogura, T.; Ohkubo, K.; Fukuzumi, S. *J. Am. Chem. Soc.* **2011**, *133*, 17901.